A&A 643, A138 (2020)
https://doi.org/10.1051/0004-6361/202038228

Astronomy & Astrophysics

The Villafranca catalog of Galactic OB groups

I. Systems with O2–O3.5 stars

J. Maíz Apellániz[1], P. Crespo Bellido[1,2], R. H. Barbá[3], R. Fernández Aranda[1,2], and A. Sota[4]

[1] Centro de Astrobiología, CSIC-INTA, Campus ESAC, C. Bajo del Castillo s/n, 28692 Villanueva de la Cañada, Madrid, Spain
e-mail: jmaiz@cab.inta-csic.es
[2] Departamento de Astrofísica y Física de la Atmósfera, Universidad Complutense de Madrid, 28040 Madrid, Spain
[3] Departamento de Astronomía, Universidad de La Serena, Av. Cisternas 1200 Norte, La Serena, Chile
[4] Instituto de Astrofísica de Andalucía-CSIC, Glorieta de la Astronomía s/n, 18008 Granada, Spain

Received 22 April 2020 / Accepted 15 September 2020

ABSTRACT

Context. The spectral classifications of the Galactic O-Star Spectroscopic Survey (GOSSS) and the astrometric and photometric data from *Gaia* have significantly improved our ability to measure distances and determine memberships of stellar groups (clusters, associations, or parts thereof) with OB stars. In the near future, the situation will be further improved thanks to subsequent *Gaia* data releases and new photometric and spectroscopic surveys.
Aims. We initiated a program to identify and determine the membership of Galactic stellar groups with OB stars and measure distances to them. Given the data currently available, we started with the identification and distance determinations of groups with O stars. In this paper, we concentrate on groups that contain stars with the earliest spectral subtypes.
Methods. We used GOSSS to select Galactic stellar groups with O2–O3.5 stars and the method described in paper 0 of this series, which combines *Gaia* DR2 $G + G_{\rm BP} + G_{\rm RP}$ photometry, positions, proper motions, and parallaxes to assign robust memberships and measure distances. We also included Collinder 419 and NGC 2264, the clusters cited in that paper, to generate our first list of 16 O-type Galactic stellar groups.
Results. We derived distances, determined the membership, and analyzed the structure of sixteen Galactic stellar groups with O stars, Villafranca O-001 to Villafranca O-016, including the fourteen groups with the earliest-O-type optically accessible stars known in the Milky Way. We compared our distance with previous results from the literature and establish that the best consistency is with (the small number of) VLBI parallaxes and the worst is with kinematic distances. Our results indicate that very massive stars can form in relatively low-mass clusters or even in near-isolation, as is the case for the Bajamar star in the North America nebula. This lends support to the hierarchical scenario of star formation, where some stars are born in well-defined bound clusters but others are born in associations that are unbound from the beginning: groups of newborn stars come in many shapes and sizes. We propose that HD 64 568 and HD 64 315 AB could have been ejected simultaneously from Haffner 18 (Villafranca O-012 S). Our results are consistent with a difference of ≈20 μas in the *Gaia* DR2 parallax zero point between bright and faint stars.

Key words. astrometry – catalogs – Galaxy: structure – open clusters and associations: general – stars: kinematics and dynamics – stars: early-type

1. Introduction

Traditionally, stellar clusters are defined as stellar groups with at least several tens of members and a stellar density large enough (with a threshold around 1 $M_\odot$ pc^{-3}) to keep the system in a bound state, namely, possessing a total (kinetic + potential) negative energy. According to the often-cited work of Lada & Lada (2003), most or all stars are formed in bound clusters but as they evolve, the vast majority of them become unbound as the total kinetic energy of the stars does not change very much while their potential energy becomes less negative (closer to zero) when the associated molecular gas is dispersed. In the view of Lada & Lada (2003), most clusters evolve into low-density OB associations (Ambartsumian 1958) with sizes of tens of parsecs that eventually dissolve into the Galactic disc. In an alternative view to the "most stars form in clusters" scenario, star formation is a hierarchical process that can take place in both bound and unbound clouds with a wide range of scales (Elmegreen 2010; Ward et al. 2020). In that scenario, OB associations may be born that way (the effect of nature) or they may be the consequence or gas dispersal (the effect of nurture). We note that current models have not yet provided a definitive answer as to how clusters form (Krumholz & McKee 2020).

In order to decide which of the two views is correct, it is necessary to precisely measure the total energy of stellar groups (which can be either bound stellar clusters or unbound stellar associations) but, as it often happens in astronomy, the data are not always clear for several reasons:

1. Velocities in the plane of the sky require accurate proper motions, which, until the advent of *Gaia*, were difficult to precisely measure unless the stellar group was close. Here, the limitation is the need to observe the system with a long-enough time baseline.

2. Velocities in the radial direction require (usually multi-object) spectroscopy but OB stars have a large binary and higher-order multiplicity fraction (Maíz Apellániz et al. 2019a) that can artificially inflate the velocity dispersion (Hénault-Brunet et al. 2012). This requires the spectroscopy to not only be multi-object, but also multi-epoch.

3. What counts as a group member and what does not? In sightlines with long paths across the Galactic Plane, this is far from obvious and even with good data, it cannot be completely certain for some stars.

4. Even if we solve the previous issues, stellar groups cannot be always easily divided into clusters and associations. Some stellar groups show two compact cores instead of one (double clusters, de La Fuente Marcos & de La Fuente Marcos 2009), some associations have bound cores at their centers (e.g., Maíz Apellániz 2001a), and the limits between two neighbor associations may not be well defined.

Given those limitations and considering that most stellar groups that contain OB stars (i.e., the young and massive end of the distribution) are located several kpc away and are obscured by the dust close to the Galactic Plane, a priori, it is not possible to produce a clear cut between clusters, associations, or even subassociations. In other words, lacking excellent multi-epoch multi-type data, the division into strict categories is not possible at this time for most of a reasonably large sample. For that reason, in this work, we refer to stellar groups in general, acknowledging that to some point the limits between one group and the next one will be arbitrary but, at the same time, we present our reasons why we find such a division reasonable for each particular case. The reasons may be different for one stellar group than for the next, but such a case-by-case analysis is the only way to carry out a thorough study. For stellar groups, diversity reigns and no single size fits all.

For over a decade, we have been conducting the Galactic O-Star Spectroscopic Survey (GOSSS, Maíz Apellániz et al. 2011), which has collected high-quality $R \sim 2500$ blue-violet spectroscopy for several thousand stars of spectral types O and B. The availability of the data has allowed us to produce uniform spectral classifications for a large sample of objects and correct many misclassifications in the literature. The survey has produced three major papers (Sota et al. 2011, 2014; Maíz Apellániz et al. 2016) and several others to date, of which the most recent are Maíz Apellániz et al. (2018a,b, 2019a). In the process, the GOSSS papers have become some of the most cited articles on O stars of the last decade. The data and spectral classifications from GOSSS are available from the Galactic O-Star Catalog (GOSC[1], Maíz Apellániz et al. 2004). There are several existing multi-fiber large-scale Galactic spectroscopic surveys such as *Gaia*-ESO (Gilmore et al. 2012) or LAMOST (Luo et al. 2015), but they do not have spectra for many O stars published – and this is for a variety of reasons (Blomme et al., in prep., will soon become an exception). The most significant reason is that they have complex scheduling strategies designed to satisfy many simultaneous goals, with O stars not being among their highest priorities. Therefore, even when a project like *Gaia*-ESO has observed clusters, most of them were of too-low mass or too old to contain O stars; among those that were massive and young enough, it was only in one case (Trumpler 14) that fibers could be allocated to O stars (Jackson et al. 2020). GOSSS, on the other hand, allocates over 50% of its time to O stars. Several recent single-fiber échelle surveys have also spent a significant fraction of their time observing O stars (e.g. Simón-Díaz et al. 2011; Maíz Apellániz et al. 2012; Barbá et al. 2017; Negueruela et al. 2015) and these have led to important results regarding the physical properties, multiplicity, and intervening interstellar medium (ISM) for such systems.

The *Gaia* mission (Prusti et al. 2016) produced its second data release (DR2) in April 2018 (Brown et al. 2018). *Gaia* DR2 includes five-parameter astrometry (positions, parallaxes, and proper motions) and optical photometry in the three bands G, $G_{\rm BP}$, and $G_{\rm RP}$ for over 1.3×10^9 sources. Those data constitute the largest ever collection of high-precision photometry and astrometry, allowing for a huge improvement in the identification and distance measurement of stellar groups. Soon after DR2, a large study on its application to stellar clusters was published (Cantat-Gaudin et al. 2018) and since then, several other papers have followed suit (e.g., Soubiran et al. 2018; Castro-Ginard et al. 2019, 2020; Cantat-Gaudin et al. 2019). With future data releases *Gaia* will undoubtedly keep making a huge impact on the field.

OB stars (and their descendants) are important for the study of stellar groups that contain or contained them for several reasons: (1) they irradiate the nearby ISM with UV photons, creating feedback (which can be positive or negative) for star formation within the group; (2) they inject energy into their surroundings in the form of stellar winds and supernova explosions that can make the primordial gas disperse more quickly; (3) they are the fastest polluters of the nearby ISM with the product of nuclear reactions in their interiors, thus creating the possibility of differences in chemical composition within the stellar group; (4) and they can interact with other stars and among themselves to dynamically perturb trajectories through close encounters. In summary, no other stellar type has such a large influence in the evolution of a stellar group and the presence of a single OB star may alter its evolution altogether. Therefore, to understand stellar groups (including those that had OB stars in the past but have already lost them) in general, the study of how OB stars associate with lower-mass objects is crucial. We consider whether the massive-star initial mass function (IMF) is constant or whether it depends on the environment, whether it is always populated according to the same mechanisms, and whether massive stars can form in isolation or near-isolation. Regardin the last issue, we specify that by "isolation" we mean that a massive star may be formed just by itself (possibly with one or several bound companions in a multiple system) but without belonging to a cluster or a small-scale (~3 pc) association (for the time-scales involved in star formation, material located at distances longer than ~3 pc cannot have a significant influence in the process; see Bressert et al. 2012). By "near-isolation" we mean that (usually with some effort) a group can be located around the massive star but the combined mass of the rest of the stars is so low as to have an atypical IMF with a single object having a significant fraction of the total mass.

With this paper, we have initiated an ongoing project that combines GOSSS and *Gaia* data to catalog the Galactic stellar groups that contain OB stars. The availability of these new high-quality data makes this time an opportune moment to revisit this issue in a more complete manner than previous studies. In the future, we will add information from the subsequent *Gaia* data releases and from other surveys, either photometric (e.g., GALANTE, Lorenzo-Gutiérrez et al. 2019) or spectroscopic (e.g., WEAVE, Dalton 2016). We name the catalog resulting from the project "Villafranca" after the location of the European Space Astronomy Centre (ESAC), formerly the Villafranca del Castillo Satellite Tracking Station (Vilspa), which is where the institution of three of the authors in this paper is based on. In this way, we follow the tradition of the stellar cluster community of naming catalogs after geographical locations (Berkeley, Alicante, Bochum, Escorial...) and we honor two relationships between Villafranca and the study of OB stellar groups: on the one hand, the International Ultraviolet Explorer (IUE) was part-time controlled from Vilspa between 1978 and

[1] https://gosc.cab.inta-csic.es

1996 and played an important historical role for these objects, which are among the brightest Galactic targets in the UV. On the other hand, the *Gaia* Science Data Center and Archive are located at ESAC and without *Gaia* this work could not have been possible. The zeroth paper of the series was Maíz Apellániz (2019), from now on MA19, where we describe the method used to establish the membership and determine the distance to stellar groups (see next section). In this first paper, we search for stellar groups around the optically accessible earliest Galactic O stars but we also add the two clusters in MA19 for completeness. The future papers in the series will add the rest of stellar groups with O stars but, given their large number, this should be considered a long-term project that will take a decade or so to complete, especially when we take into account the fact that new data will likely lead to new distance measurements and membership analyses of the already studied sample. Such is the curse of the devoted cataloger. If funding and human resources are available, we may also consider adding groups with B stars (but no O types) to the mix, but in that case, the sample would have to be significantly incomplete, given the much larger number of such older and/or lower mass objects.

The structure of this paper is as follows. In Sect. 2, we present the methods and data, describing how we selected the sample, determined the membership and distances, processed complementary information for some objects, and searched the literature for previous distance measurements. In Sect. 3, we analyze each of the objects in our sample, combining new and literature information. In the last section, we compare our distances with previous ones, discuss the validity of different criteria used to evaluate the membership for OB stellar groups, analyze the internal motions and the nature of the IMF for our objects, study the dependence of the *Gaia* DR2 parallax zero point on magnitude, and present our future plans.

2. Methods and data

2.1. Sample selection

The latest version of GOSC includes 594 O stars with GOSSS spectral types which, depending on how they are defined, can be collected into 200−300 stellar groups. An exact number cannot be given for the reasons given in the introduction: does a double cluster counts as a group or as two? Is a cluster within an association a separate group? Do we divide a large association such as Scorpius-Centaurus into its subassociations (Upper Centaurus Lupus, Lower Centaurus Crux, and Upper Scorpius)? If all stellar groups were well-defined clusters, a precise number could be given but that is, alas, not the case.

For this first installment of our Villafranca catalog, we started by finding all the stars in GOSC with the earliest spectral types, from O2 to O3.5, and we selected the groups, which were previously well-defined or otherwise, to which they belong. Given the diversity among stellar groups, it is necessary to go case by case to see whether all such stars are in clusters or not. As we show in the last section, the answer to that question is relevant to competing theories about the initial mass function (IMF). Such a selection based on spectral type favors the youngest and most massive groups due to the fact that in older ones, the earliest type stars would have already evolved and low-mass groups are less likely to form stars with a mass large enough to be of those spectral types at birth (but see below). We note that the most massive stars of all are not born as O-type but rather as WNh stars (Crowther et al. 2010). This point is discussed for some individual groups in the next section.

The selection criterion above yields 14 stellar groups with at least one O-type star, which we named Villafranca O-001 to Villafranca O-014, sorting them (roughly) by richness, from well-populated, concentrated, and well-defined clusters to poorly-defined clusters or stellar groups with just one or two O type-systems. Since we already analyzed two clusters with this technique in MA19, we included Villafranca O-015 and Villafranca O-016, Collinder 419, and NGC 2264, respectively, in our list. They are to be considered separately with regard to their lack of early-type O stars but as an integral part of the Villafranca catalog, as, indeed, most groups with O stars do not have such subtypes; thus, the latter will constitute the rest of the sample in subsequent articles of this series.

The sample is shown in Table 1. To alleviate the degree of arbitrariness implicit in the definition of stellar groups, we define the groups in the catalog in a "cluster scale" (sizes of a few pc), independently of their true nature as clusters, instead of in an "association scale" (sizes of 10 pc or more). In other words, we divide associations into subassociations and clusters whenever possible. However, in each case, we indicate the membership of the group to an association, where relevant. More specifically, each of the two OB associations richer in O stars in the solar neighborhood (the Carina nebula and Cygnus OB2 associations) has two stellar groups with O2–O3.5 stars. To make this clear, they are linked together in the same subsections in Sect. 3.

2.2. Distances to and membership of stellar groups

The supervised method used to determine the distances to and membership of stellar groups is the one described in MA19, which we summarize here. We start by selecting a star or stars representative of the groups from GOSSS and calculate an extinguished isochrone for a $G_{BP}-G_{RP}$ vs. G' color-magnitude diagram (CMD, see Maíz Apellániz & Weiler 2018 for a definition of G'), using the family of extinction laws of Maíz Apellániz et al. (2014) and the extinction parameters from Maíz Apellániz & Barbá (2018). We downloaded the *Gaia* DR2 data around the reference star from the archive and filtered them first by the renormalized unit weight error (RUWE), d_{CC} (see Maíz Apellániz & Weiler 2018), and σ_{ϖ_c} (the external or corrected parallax uncertainty). We then filtered the remaining stars by (a) distance r in the plane of the sky to the group center $\alpha+\delta$ in equatorial J2000 coordinates, (b) distance r_μ to a central proper motion $\mu_{\alpha*}+\mu_\delta$, and (c) position in the $G_{BP}-G_{RP}$ vs. G' CMD using as reference the previously calculated extinguished isochrone. This results in a preliminary sample with $N_{*,0}$ objects which is further culled eliminating outliers in the normalized parallax space, leaving N_* final objects. The whole process is iterated to assess the effect of changes in the selection parameters and establish the robustness of the group average parallax, ϖ_g. The final selection parameters are chosen to maximize both the cleanliness and number of the sample.

Once we have the final sample, we can calculate the group average parallax uncertainty, σ_{ϖ_g}, using Eq. (5) in Campillay et al. (2019), noting that the covariance term is usually the dominant one in the error budget. To correct for the parallax zero point and determine the final group average we use:

$$\varpi_{g,c} = \varpi_g + 0.040, \quad \sigma^2_{\varpi_{g,c}} = \sigma^2_{\varpi_g} + 0.010^2, \tag{1}$$

where the values above are given in milliarcseconds (see below for a discussion on the value of the zero point). The final group distance is then calculated using the Bayesian prior described by Maíz Apellániz (2001b, 2005) with the updated Galactic (young) disk parameters from Maíz Apellániz et al. (2008).

Table 1. Sample of Galactic O-type stellar groups in this paper.

ID	Other ID(s)	O- and WR-type stars	Spectral type	Ref.
O-001	NGC 3603	NGC 3603 HST-A1	WN6ha	C98
	RCW 57	NGC 3603 HST-B	WN6ha	C98
		NGC 3603 HST-C	WN6ha	C98
		NGC 3603 MTT 58	O2 If*/WN6 + O3 If	R13b
		NGC 3603 MTT 31	O2 V	R16
		NGC 3603 HST-48	O3.5 If*	M16
		Many others		D95,W02,M08,R12,R13a,R16
O-002	Trumpler 14	HD 93 129 Aa,Ab	O2 If* + O2 If* + OB?	M17
		HD 93 129 B	O3.5 V((f))z	M16
		HD 93 128	O3.5 V((fc))z	S14
		Many others		S14,M16
O-003	Trumpler 16 W	HD 93 162	O2.5 If*/WN6 + OB	S14
		ALS 15 210	O3.5 If* Nwk	S14
		HD 93 205	O3.5 V((f)) + O8 V	S14,TW
		HD 93 204	O5.5 V((f))	S14
O-004	Westerlund 2	V712 Car	O3 If*/WN6	TW
	RCW 49	WR 20b	WN6ha	R11
		Westerlund 2-199	O3 V	N08
		Many others		N08,R11,V13
O-005	Pismis 24	Pismis 24-1 A,B	O3.5 If*	S14
	NGC 6357 W	Pismis 24-17	O3.5 III(f*)	S14
	RCW 131 W	WR 93	WC7 + O7/9	V01
		Several others		S14,M16
O-006	Gum 35	THA 35-II-153	O3.5 If*/WN7	M16
	Majaess 133	ALS 2063	O5 Ifp	S14
		ALS 18 551	O4.5 V(n)z + O4.5 V(n)z	M16
		Several others		S14,M16
O-007	Cyg OB2-22 cluster	Cyg OB2-22 A	O3 If*	S11
	Bica 1	Cyg OB2-9	O4 If + O5.5 III(f)	M19
		Cyg OB2-22 B	O6 V((f))	S14
		Several others		S11,S14
O-008	Cyg OB2-8 cluster	Cyg OB2-7	O3 If*	S11
	Bica 2	Cyg OB2-8 C	O4.5 (fc)p var	S14
		Cyg OB2-8 A	O6 Ib(fc) + O4.5 III(fc)	M19
		Several others		S11,S14,M91
O-009	M 17	ALS 19 613 A	O2/4 V	TW
	Omega nebula	ALS 19 618 A	O4 V(n)((fc))	M16
	NGC 6618	ALS 19 617	O5 V	H08
	Sh 2-45	Several others		C78,H08
	RCW 160			
O-010	NGC 6193	HD 150 136 Aa,Ab	O3.5–4 III(f*) + O6 IV	S14
	RCW 108	HD 150 135 Aa,Ab	O6.5 V((f))z	S14
O-011	Berkeley 90	LS III +46 11	O3.5 If* + O3.5 If*	M16
	Sh 2-115	LS III +46 12	O4.5 IV(f)	M16
O-012	NGC 2467	CPD −26 2704	O7 V(n)	M16
	Sh 2-311	(†) HD 64 568	O3 V((f*))z	S14
	RCW 16	(†) HD 64 315 A,B	O5.5 V + O7 V	M16
O-012 N	Haffner 19	–		
O-012 S	Haffner 18	CPD −26 2704	O7 V(n)	M16
O-013	Sh 2-158	Sh 2-158 1	O3.5 V((f*)) + O9.5: V	M16
	NGC 7358	Sh 2-158 2	O9.5: V + B0.5: V	M16
O-014	North America nebula	Bajamar star	O3.5 III(f*) + O8:	M16
	NGC 7000	(††) HD 199 579	O6.5 V((f))z	S11
	Sh 2-117			
O-015	Collinder 419	HD 193 322 Aa,Ab	O9 Vnn + O8.5 III + B2.5: V:	T11
O-016	NGC 2264	15 Mon Aa,Ab	O7 V((f))z + B1: Vn	M20
	Sh 2-273			
O-016 N	NGC 2264 N	15 Mon Aa,Ab	O7 V((f))z + B1: Vn	M20
O-016 S	NGC 2264 S	–		

Notes. The other IDs may refer to the cluster or the associated H II region. (†)Outside region, possible runaway. (††)In nebula but chance alignment.
References. C78: Crampton et al. (1978), C98: Crowther & Dessart (1998), D95: Drissen et al. (1995), H08: Hoffmeister et al. (2008), M91: Massey & Thompson (1991), M08: Melena et al. (2008), M16: Maíz Apellániz et al. (2016), M17: Maíz Apellániz et al. (2017), M19: Maíz Apellániz et al. (2019a), M20: Maíz Apellániz & Barbá (2020), N08: Nazé et al. (2008), R11: Rauw et al. (2011), R12: Roman-Lopes (2012), R13a: Roman-Lopes (2013a), R13b: Roman-Lopes (2013b), R16: Roman-Lopes et al. (2016), S11: Sota et al. (2011), S14: Sota et al. (2014), T11: ten Brummelaar et al. (2011), TW: This work, V01: van der Hucht (2001), V13: Vargas Álvarez et al. (2013), W02: Walborn et al. (2002b).

The above supervised method is applied to calculate the distances and membership of all groups, except for one, in this paper simply by varying the region of the sky and the selection parameters. In one case, Villafranca O-014 (a stellar group defined here to be associated with the North America nebula), we followed a different strategy due to the peculiarities of that stellar group, as described below. The field sizes and filters used for each group are given in Table 2, where N_f is the number of *Gaia* DR2 sources in the field.

In addition to the strategy described in MA19, we also searched the vicinity for possible runaways from each group by looking for objects with parallaxes compatible with the distance

Table 2. Field sizes and filters applied to the O-type stellar groups and subgroups in this paper.

ID	N_f	Field	d_{CC}	α (deg)	δ (deg)	r ($''$)	$\mu_{\alpha*}$ (mas a^{-1})	μ_δ (mas a^{-1})	r_μ (mas a^{-1})	$\Delta(G_{BP}-G_{RP})$
O-001	27 873	$20' \times 20'$	<0.4	168.79	−61.26	206	−5.61	+1.97	0.44	>−0.34
O-002	14 340	$20' \times 20'$	<0.4	160.95	−59.56	166	−6.45	+2.25	0.70	>−0.69
O-003	18 441	$20' \times 20'$	<0.4	161.09	−59.73	103	−6.93	+2.61	0.73	>−1.30
O-004	60 144	$40' \times 40'$	<0.4	155.99	−57.76	400	−5.10	+2.82	0.70	>−0.65
O-005	10 374	$30' \times 30'$	<0.4	261.18	−34.21	605	−1.10	−2.20	1.40	>−1.00
O-006	48 211	$20' \times 20'$	<0.4	164.68	−61.18	200	−5.50	+2.30	0.30	>−0.90
O-007	5241	$20' \times 20'$	<0.4	308.30	+41.22	186	−2.65	−4.49	0.72	>−0.60
O-008	6136	$20' \times 20'$	<0.4	308.32	+41.31	126	−2.67	−4.15	0.50	>−0.80
O-009	5671	$20' \times 20'$	<0.4	275.12	−16.18	236	+0.10	−1.52	1.10	>−0.70
O-010	33 424	$20' \times 20'$	<0.4	250.30	−48.76	285	+1.57	−3.92	1.04	>−0.70
O-011	6513	$20' \times 20'$	<0.4	308.83	+46.84	341	−2.78	−4.31	0.50	–
O-012	25 632	$30' \times 30'$	<0.4	118.18	−26.33	390	−2.50	+2.60	0.40	>−0.15
O-012 N	25 632	$30' \times 30'$	<0.4	118.19	−26.28	200	−2.50	+2.60	0.40	>−0.15
O-012 S	25 632	$30' \times 30'$	<0.4	118.18	−26.38	200	−2.50	+2.60	0.40	>−0.15
O-013	3235	$20' \times 20'$	<0.4	348.43	+61.50	109	−3.70	−2.14	0.73	–
O-014	396 261	$120' \times 120'$	<0.4	313.96	+43.87	–	+0.01	−4.52	0.90	>+0.00
O-015	19 049	$30' \times 30'$	<0.2	304.60	+40.78	800	−2.60	−6.40	0.75	>−0.30
O-016	25 177	$60' \times 60'$	<0.2	100.25	+09.75	1500	−1.80	−3.70	1.50	>−0.20
O-016 N	25 177	$60' \times 60'$	<0.2	100.20	+09.88	540	−1.80	−3.70	1.50	>−0.20
O-016 S	25 177	$60' \times 60'$	<0.2	100.28	+09.53	540	−1.80	−3.70	1.50	>−0.20

Notes. RUWE is filtered as <1.4 and σ_{ϖ_c} as <0.1 mas in all cases. For Villafranca O-014 the coordinates correspond to those of the Bajamar star.

to the group and proper motions that point away from its center. The search has been carried out only for the brightest targets in each field, that is, possible massive runaways.

2.3. Spectral classifications and AstraLux data

We used GOSSS spectral classifications whenever possible and literature ones otherwise. In some cases, we present new GOSSS spectra and spectral classifications. The reader is referred to the GOSSS papers cited in the introduction for details on how they are obtained and processed. We also used high-resolution spectra from LiLiMaRlin (Maíz Apellániz et al. 2019b), a Library of Libraries of Massive-Star High-Resolution Spectra built by collecting data from four different surveys (CAFÉ-BEANS, Negueruela et al. 2015; IACOB, Simón-Díaz et al. 2015; NoMaDS, Maíz Apellániz et al. 2012; and OWN Barbá et al. 2010, 2017) and with additional spectra from other programs led by us and from public archives. In order to carry out spectral classification with such data, we must degrade its spectral resolution to the GOSSS value of 2500 in order to compare them with the GOSSS standards. For two dim objects, we also use OSIRIS/GTC spectra obtained with $R \sim 2000$, lower than the standard $R \sim 2500$ value. The new spectra in this paper are shown in Fig. 1.

In one case, we also present the binary data (separation, position angle, and Δm) for one star based on lucky imaging obtained with AstraLux at Calar Alto. See Maíz Apellániz (2010, 2019), Maíz Apellániz et al. (2019a) for details on AstraLux data.

2.4. Literature distances

We searched the literature for previous distance measurements to the Villafranca O-001 up through the Villafranca O-016 stellar groups and show them in Table A.1. For each measurement, we provide the distance (in pc), its uncertainty (when available), the target used (group, subgroup, individual star, or ISM object), the method used, and the reference. For groups with an associated H II region (e.g., Villafranca O-009 and M 17) we designate both as the same target in Table A.1. For simplicity, we denote methods that use a combination of spectroscopy and photometry as "spectro-photometry". Many (but not all) of our targets have *Gaia* DR2 parallax-based distances from Cantat-Gaudin et al. (2018) with very small uncertainties. As already pointed out in MA19, those uncertainties do not include the effect of the spatial covariance of the *Gaia* DR2 parallaxes (Lindegren et al. 2018), which is the dominant error source.

3. Results

The membership and distance results which constitute the main output of this paper are given in Table 3; see Maíz Apellániz (2019) for the definitions of t_ϖ, $t_{\mu_{\alpha*}}$, t_{μ_δ}, $\mu_{\alpha*,g}$, and $\mu_{\delta,g}$. The plots used to select the parameters of each group are shown in Figs. A.1–A.14. Possible runaways from each group are given in Table A.2. Each stellar group is analyzed in detail below, where we compare the *Gaia* DR2 distances with the previous measurements. We already point out here that all of our values are within one sigma of those in Cantat-Gaudin et al. (2018). See the note at the end of the previous section on the effect of the spatial covariance.

3.1. Villafranca O-001 = NGC 3603 = RCW 57

This is the densest and richest cluster in the sample. It is similar to R136, the core of 30 Doradus, in several aspects (Walborn 1973a; Moffat 1983; Moffat et al. 1994): it has three WNh stars with masses above 100 $M_\odot$ (Drissen et al. 1995; Crowther et al. 2010) and a very rich population of O stars (see the references in Table 1). One of them, NGC 3603 HST-A1, is a very massive eclipsing binary (Schnurr et al. 2008). At one point

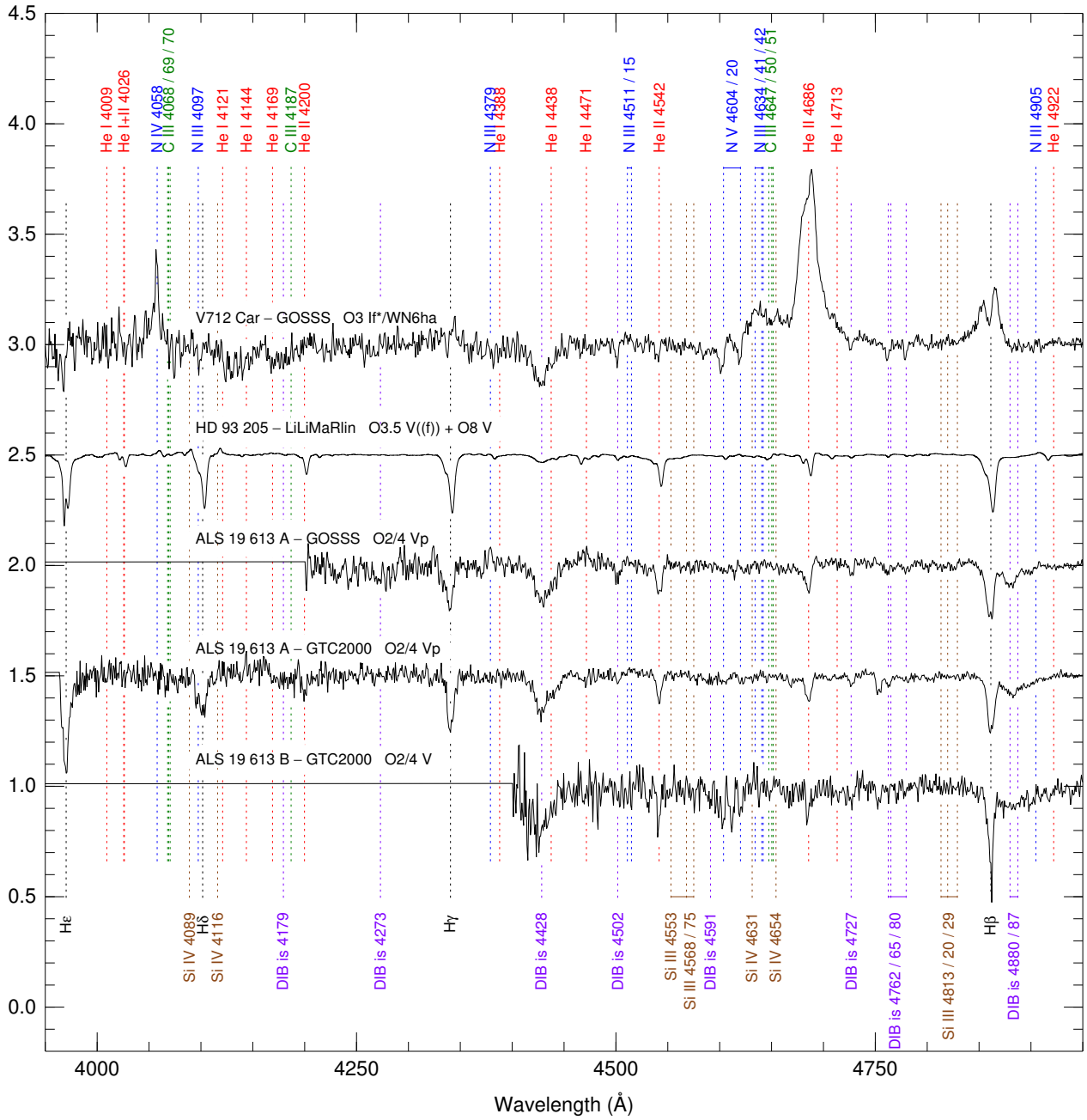

Fig. 1. New spectra in this paper.

it was thought that there were few massive stars around the cluster but recent discoveries have altered that picture (Roman-Lopes 2013a; Kalari et al. 2019; Drew et al. 2019).

There are many distance measurements to NGC 3603 (Villafranca O-001) going back to over fifty years ago; see Table A.1. Most measurements are in the 6.0−8.5 kpc range with some outliers (such as the first two measurements) and a significant scatter, making this the most distant group in our sample. The Cantat-Gaudin et al. (2018) value is significantly larger and with small uncertainties, a result of not including the spatial covariance term[2]. Our measurement of $8.0^{+2.6}_{-1.7}$ kpc is more compatible with the literature results but the error bars are large, a situation that is likely to improve with DR3 data. The cluster is not seen as a peak in the parallax distribution of Fig. A.1, where we see a nearly flat distribution of *Gaia* DR2 sources between 2 kpc and the cluster distance. If we are able to see this deep into the Galaxy in this direction, it is because this is a mostly inter-arm sightline with an exceptionally low amount of dust. Indeed, NGC 3603 is an object in the fourth quadrant at a similar distance as the Galactic center and with $A_V \sim 5$ mag, as opposed to $A_V \sim 30$ mag for the GC. Still, most of the foreground population has an even lower extinction and that is the main criterion used to differentiate the cluster stars in Fig. A.1, as the differences in proper motion are small.

The most outstanding issue regarding the distance to NGC 3603 in the literature is the extinction correction. Most papers assume a standard extinction law ($R_{5495} = 3.0-3.2$) and some detect a variable extinction across the face of the cluster.

[2] Other things being equal, the effect of the covariance term on the distance uncertainties is larger for a simultaneously more distant and rich cluster such as NGC 3603.

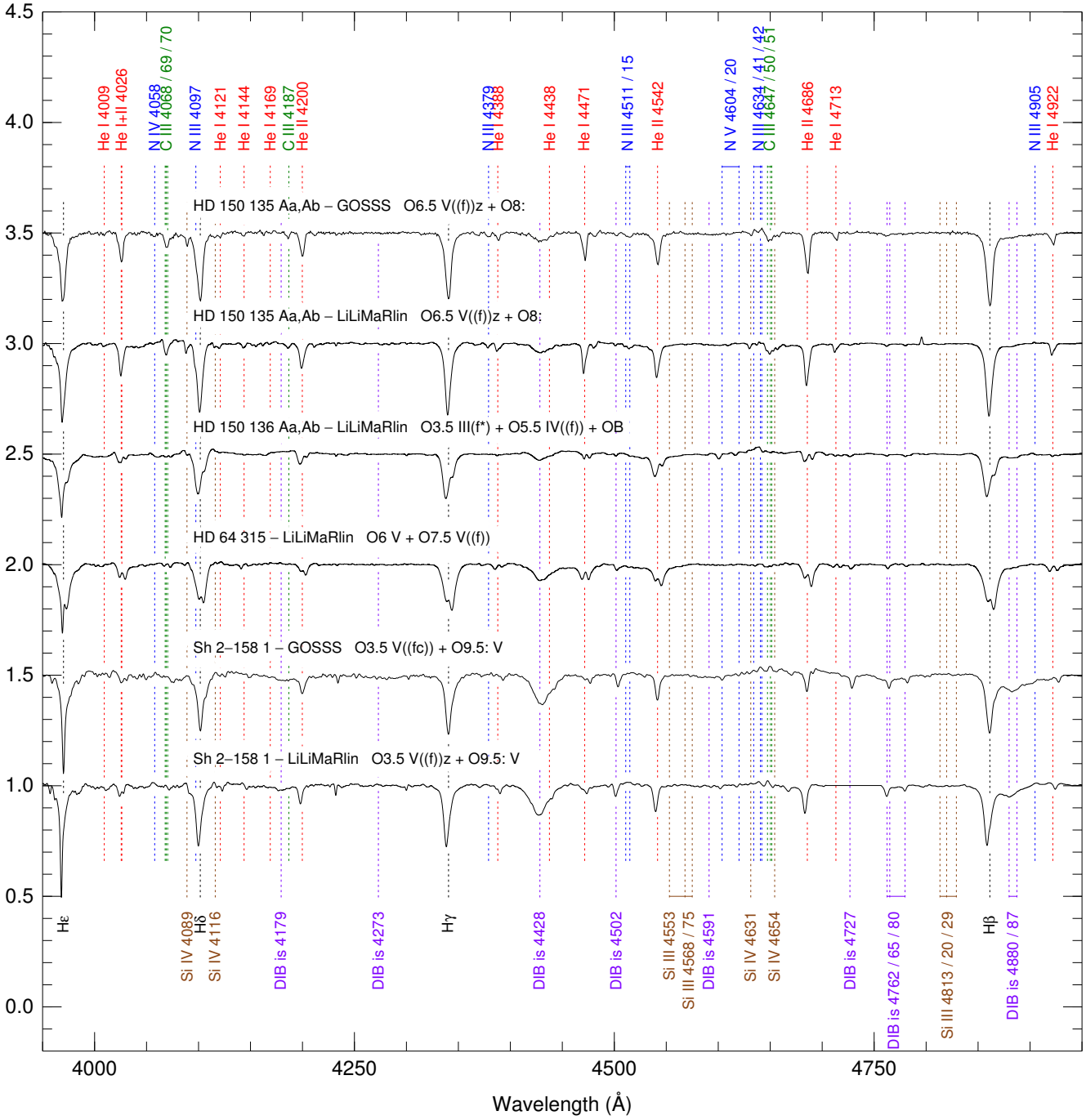

Fig. 1. continued.

Pandey et al. (2000), on the other hand, use an extinction model towards NGC 3603 with two components: a Galactic one with an assumed $R_{5495} = 3.1$ and a cluster one for which they measure $R_{5495} = 4.3$. More recently, Maíz Apellániz & Barbá (2018) measured the extinction towards four O stars in the cluster and obtained a partially consistent result with Pandey et al. (2000). The value of R_{5495} is indeed intermediate between 3.1 and 4.3 (~3.9) but the variable reddening ($E(4405-5495) = 1.2-1.4$) does not show a clear correlation with R_{5495}. We believe this issue requires further study in order to be fully resolved.

Recently, Drew et al. (2019) have searched for potential runaway stars from NGC 3603 using *Gaia* DR2 data and found nine candidates that have been likely ejected in the last million years. The field we have used for our search is smaller than theirs and we do not go as deep in magnitude but we also pick up the three candidates in the sample in common (Table A.2). In addition, we find another three bright potential candidates that may have been excluded from their list due to their slightly larger impact parameter.

3.2. The Carina nebula association: Villafranca O-002 = Trumpler 14 and Villafranca O-003 = Trumpler 16 W

The Carina nebula (NGC 3372 = RCW 53) is the site of the most intense burst of recent star formation within 3 kpc of the Sun

Table 3. Membership and distance results.

ID	$N_{*,0}$	N_*	t_ϖ	$t_{\mu_{\alpha*}}$	t_{μ_δ}	ϖ_g (mas)	$\mu_{\alpha*,g}$ (mas a^{-1})	$\mu_{\delta,g}$ (mas a^{-1})	$\varpi_{g,c}$ (mas)	d (pc)
O-001	143	137	1.13	1.97	1.65	0.074 ± 0.043	-5.551 ± 0.067	$+1.974 \pm 0.067$	0.114 ± 0.044	8000^{+2600}_{-1700}
O-002	93	91	0.88	3.98	3.29	0.387 ± 0.042	-6.540 ± 0.067	$+2.042 \pm 0.067$	0.427 ± 0.043	2430^{+290}_{-230}
O-003	20	20	0.86	2.42	1.88	0.401 ± 0.042	-7.073 ± 0.067	$+2.641 \pm 0.066$	0.441 ± 0.043	2380^{+270}_{-220}
O-004	178	174	1.05	1.89	1.76	0.188 ± 0.042	-5.190 ± 0.064	$+2.927 \pm 0.064$	0.228 ± 0.043	4730^{+1130}_{-780}
O-005	208	197	1.20	2.45	3.71	0.562 ± 0.040	-0.918 ± 0.059	-2.216 ± 0.059	0.602 ± 0.041	1690^{+130}_{-110}
O-006	99	98	1.06	1.38	1.52	0.112 ± 0.043	-5.513 ± 0.067	$+2.270 \pm 0.067$	0.152 ± 0.044	6400^{+1800}_{-1200}
O-007	82	81	0.98	2.10	1.67	0.554 ± 0.043	-2.697 ± 0.067	-4.482 ± 0.068	0.594 ± 0.044	1720^{+140}_{-120}
O-008	45	45	1.20	1.62	1.92	0.581 ± 0.043	-2.667 ± 0.067	-4.371 ± 0.067	0.621 ± 0.044	1640^{+130}_{-110}
O-009	30	30	1.15	3.26	3.12	0.587 ± 0.043	$+0.166 \pm 0.069$	-1.618 ± 0.069	0.627 ± 0.044	1630^{+130}_{-110}
O-010	115	111	1.12	2.39	3.00	0.813 ± 0.043	$+1.307 \pm 0.066$	-3.972 ± 0.066	0.853 ± 0.044	1185^{+65}_{-59}
O-011	82	79	1.22	1.67	1.38	0.287 ± 0.042	-2.840 ± 0.066	-4.316 ± 0.066	0.327 ± 0.043	2990^{+390}_{-340}
O-012	206	194	1.15	1.54	1.63	0.178 ± 0.041	-2.523 ± 0.061	$+2.586 \pm 0.061$	0.218 ± 0.042	4850^{+1160}_{-800}
O-012 N	88	87	1.14	1.41	1.18	0.164 ± 0.043	-2.544 ± 0.067	$+2.487 \pm 0.067$	0.204 ± 0.044	5190^{+1380}_{-930}
O-012 S	67	62	1.10	1.75	1.57	0.180 ± 0.043	-2.503 ± 0.067	$+2.663 \pm 0.067$	0.220 ± 0.044	4830^{+1210}_{-830}
O-013	11	11	0.95	1.96	3.95	0.316 ± 0.043	-3.708 ± 0.068	-2.214 ± 0.068	0.356 ± 0.044	2930^{+440}_{-340}
O-014	12	12	0.94	2.98	2.63	1.364 ± 0.035	-0.092 ± 0.055	-4.176 ± 0.055	1.404 ± 0.036	714^{+19}_{-18}
O-015	93	75	0.98	3.20	2.82	0.957 ± 0.034	-2.605 ± 0.048	-6.390 ± 0.048	0.997 ± 0.035	1006^{+37}_{-34}
O-016	340	286	1.12	5.15	3.56	1.354 ± 0.029	-1.885 ± 0.041	-3.716 ± 0.041	1.394 ± 0.031	719^{+16}_{-16}
O-016 N	102	99	1.04	3.99	3.25	1.357 ± 0.040	-1.716 ± 0.059	-3.705 ± 0.059	1.397 ± 0.041	719^{+22}_{-21}
O-016 S	94	90	1.19	5.15	3.43	1.350 ± 0.040	-2.077 ± 0.057	-3.788 ± 0.057	1.390 ± 0.041	722^{+22}_{-21}

(Walborn 1973b, 1995; Smith 2006a). Indeed, the stars that were used to define the spectral type O3 were in the Carina nebula (Walborn 1971). The standard division into groups has Trumpler 14, a compact very young cluster with a halo around it that makes it look like a less massive version of NGC 3603 (Ascenso et al. 2007a); Trumpler 15, an older and less massive cluster to the NE of Trumpler 14; and four additional regions, Trumpler 16, Collinder 228, Collinder 232, and Bochum 11, without a clearly defined cluster-like structure, likely making them just different parts of a larger group, the Carina nebula association (or Car OB1). In this paper, we deal with Trumpler 14 (Villafranca O-002) and the western part of Trumpler 16 (Villafranca O-003), as those are the two regions with very early O-type systems. We note that η Car, the most famous star in the nebula, is in the eastern part of Trumpler 16. The whole region is a bright H II region powered mostly by its early-O type and WR stars (Smith 2006a) but it must have experienced previous generations of massive stars, as evidenced by the existence of multiple expanding shells in the region with velocities of hundreds of km s^{-1} (Walborn 1982a; Walborn et al. 2002a). It is important to note that the extinction to the Carina nebula is surprisingly low for an object inside the Solar circle farther away than 2 kpc, as most of the space between us seems to lie in the interarm region, which was also the case for NGC 3603.

Trumpler 14 is dominated by the HD 93 129 system, a hierarchical system composed of two O2 supergiants in a centuries-long eccentric orbit (one of them with a likely short-period companion) and a farther away component (B) of spectral type O3.5 V((f))z (Maíz Apellániz et al. 2016, 2017). Inside the core there is another very early type star, HD 93 128, and many more O and early-B stars (Morrell et al. 1988; Smith 2006a; Sota et al. 2014), for a total of 91 stars detected by our method (including all the just mentioned). The halo around the cluster is extended towards the SW, where the closest remnants of the molecular cloud are located, with a pillar pointing towards the cluster core (Fig. A.2 and Tapia et al. 2003). Trumpler 14 is easily detected in both the source density and proper motion plots in Fig. A.2. A well-formed isochrone is also seen in the CMD, indicating a relatively uniform extinction ($A_V \sim 2$), with a secondary sequence to the right that could be either objects with a higher extinction or, more likely, pre-main-sequence stars (PMS) stars (Rochau et al. 2011; Damiani et al. 2017a). In the parallax histogram the peak of the overall *Gaia* DR2 density coincides with that of the cluster, likely due not only to the presence of Trumpler 14 itself but of other stars in the Carina nebula association.

Trumpler 16 W (Villafranca O-003), on the other hand, is a looser group defined by the "hot slash" star HD 93 162 and the early-O supergiant ALS 15 210 on its western side and HD 93 205 and HD 93 204 on its eastern side. No stars earlier than O4 are found in the rest of Trumpler 16 which, considering that η Car is an evolved object, points towards a small age difference between Trumpler 16 W and Trumpler 16 E. HD 93 205 (Morrell et al. 2001) is an SB2 classified in Sota et al. (2014) as O3.5 V((f)) + O8 V using a GOSSS spectrum. We have found a LiLiMaRlin epoch where the two components are well-separated in velocity and we have found the same spectral types (Fig. 1). We note that the "defiant finger" is ionized by HD 93 162 and ALS 15 210 despite its proximity in the sky to η Car (Fig. 1 in Smith et al. 2004). Trumpler 16 W does not appear as a significant overdensity in the source density plot of Fig. A.3 but its stars are clearly concentrated at the peak of the proper motion distribution, with our method having detected 20 members (including the four O stars mentioned here). It should be noted that Trumpler 16 W is crossed by the edge of the V-shaped dust lane that is one of the defining features of the H II region, with HD 93 162 and ALS 15 210 in the dust lane region (higher extinction) and with HD 93 205 and HD 93 204 outside of it (lower extinction). This likely explains not only the lack of a significant spatial

concentration of sources but also the large spread of extinctions in the CMD. We may compare this situation with the near uniform extinction of Trumpler 14. As it happened for Trumpler 14, in the parallax histogram, the peak of the overall *Gaia* DR2 density coincides with that of Trumpler 16 W. In this case, the role of the rest of the Carina nebula association is larger in achieving that aspect, given the small number of objects in the analyzed group.

Trumpler 14 and Trumpler 16 W are kinematically distinct: their differences in both declination proper motion and right ascension proper motion are large and significant at more than the 4σ level. The two systems are moving in a close-to-radial direction approaching one another, with the closest approach taking place 1 Ma from now or a bit less than that. The values of $t_{\mu_{\alpha*}}$ and t_{μ_δ} are significantly larger for Villafranca O-002, which is the likely result of a detection of the internal motions of the cluster in the *Gaia* DR2 proper motions, as expected for a true compact cluster such as Trumpler 14.

The distance to the Carina nebula and its parts has a long literature that extends over at least fifty years (see Table A.1) Before *Gaia* DR2 the most reliable result was the geometric value of Smith (2006b) of 2350 ± 50 pc based on the 3D expansion of the Homunculus nebula around η Car. The *Gaia* DR2 results from different authors (Cantat-Gaudin et al. 2018; Binder & Povich 2018; Shull & Danforth 2019; Kuhn et al. 2019; Lim et al. 2019; Zucker et al. 2020) and those cited in this paper are consistent with that value, indicating that Trumpler 14, Trumpler 16 W, and η Car are at the same or similar distance. The only discrepant *Gaia* DR2 paper is Davidson et al. (2018), which places Trumpler 14 450 ± 200 pc beyond Trumpler 16, but that work does not properly take into account the spatial correlations and systematic errors in the data. Other results in Table A.1 tend to find distances that are longer and with discrepancies between Trumpler 14 and Trumpler 16. For example, Carraro et al. (2004) finds the second one 1.5 kpc farther away than the first one and Massey & Johnson (1993) finds that Trumpler 14 is 3.61 kpc away. We believe that most of the discrepancies are due to unaccounted variations in the extinction law and to the presence of hidden binaries in the sample. As shown by Maíz Apellániz & Barbá (2018) not only is the amount of extinction variable in the Carina nebula but so is the extinction law itself, with R_{5495} being lower than 4 in some regions and higher than 6 in others (see the top left panel of Fig. 7 in that paper). As pointed out by several authors (Feinstein et al. 1973; Thé et al. 1980; Walborn 1995) errors in the value of R_{5495} lead to errors in the distance to this object. A different issue is that the values derived by Shull & Danforth (2019) using the *Gaia* DR2 data are also slightly higher (but within 1σ), something we discuss later on. The discrepant value found by Megier et al. (2009) deserves a special mention. Those authors use the ISM Ca II absorption lines and note that for Trumpler 16, they have complex kinematic profiles which they erroneously associate with circumstellar envelopes. They are actually produced by a number of expanding shells resulting from supernova (SN) explosions (Walborn 1982a; Walborn et al. 2002a), which are more prominent in Ca II than in Na I (Routly & Spitzer 1951, 1952). Given this effect, it is not a good idea to use Ca II to measure distances to stars in regions where SN explosions have already taken place unless that effect is taken into consideration in the analysis.

We find three candidate runaways ejected from Trumpler 14 (Table A.2). One of them, HDE 303 313, is a B2 V + B2 V SB2 (Alexander et al. 2016). We also find a possible runaway ejected from Trumpler 16 W.

3.3. Villafranca O-004 = Westerlund 2 = RCW 49

Westerlund 2 (Villafranca O-004) is a massive young cluster that was not identified as such until the 1960s due to its heavy extinction (Westerlund 1961), despite it being associated with the bright H II region RCW 49. It has a rich population of massive stars, including the spectroscopic binary V712 Car, which is composed of two of the most massive known stars in the Galaxy (Rauw et al. 2004). Crowther & Walborn (2011) classified the pair as O3 If*/WN6 + O3 If*/WN6. In Fig. 1, we show a GOSSS spectrum with the system caught close to conjunction (the N V $\lambda\lambda$4604,4620 lines are single) where Hβ has a P-Cygni-like profile, thus confirming the integrated spectrum is of an early Of/WN or "hot slash" nature (Sota et al. 2014). Westerlund 2 also includes a massive WNh star, WR 20b (Rauw et al. 2011).

As shown in Table A.1, the distance to Westerlund 2 has highly discrepant values in the literature, with a range that spans almost a factor of three between the minimum and the maximum. Our value lies in the middle or the range and is in reasonable agreement with the more recently published results, as most of the shorter and longer distances correspond to older papers. The extinction is higher ($A_V \sim 6$) than that of NGC 3603 despite being close to half the distance and both located in Carina. The difference is mainly caused by the sightline to NGC 3603 being mostly through interarm space, as opposed to the sightline to Westerlund 2 having a significant fraction inside the Carina-Sagittarius arm. The high extinction likely contributes to the differences in distance measured by different authors.

In the top left panel of Fig. A.4, Westerlund 2 shows its previously known core+halo structure. We identify 174 objects as cluster members, including many with early-type spectral classifications, the highest number so far in our sample. The peak in the distribution of *Gaia* DR2 is in the foreground at about ~1 kpc shorter distances. This is consistent with the high extinction to the cluster, whose stars can be easily observed only because of their high luminosity. The proper motion diagram puts Westerlund 2 at the lower left extreme of an elongated distribution that likely reflects the velocity differences along the spiral arm structure from the foreground population at the point where the sightline reaches the arm around ~2 kpc until where we get to the distance of the cluster.

We detect two possible runaways from Westerlund 2. The first one is THA 35-II-42 (also known as WR 21a), an O2 If*/WN5 star (Maíz Apellániz et al. 2016) with an early-O companion (Niemelä et al. 2008; Tramper et al. 2016) whose runaway nature was already suggested by Roman-Lopes et al. (2011). The second one is SS 215 (also known as WR 20aa), another O2 If*/WN5 star (Maíz Apellániz et al. 2016) with a runaway nature also already suggested by Roman-Lopes et al. (2011). Outside of our field of view we find WR 20c, also suggested by Roman-Lopes et al. (2011) as a star possibly ejected from the cluster, and whose *Gaia* DR2 proper motion is indeed compatible with that hypothesis. See Drew et al. (2018) for a more complete study of the possible runaways from Westerlund 2.

3.4. Villafranca O-005 = Pismis 24 = NGC 6357 W = RCW 131 W

Pismis 24 (Villafranca O-005) is a cluster with a compact core in the western part of the H II region NGC 6357 (Pišmiš 1959), which itself is likely associated with the nearby H II region NGC 6334 (Fukui et al. 2018). It has two O3.5-type systems,

Pismis 24-1 and Pismis 24-17, the first one with a supergiant luminosity classification and the second one with a giant luminosity classification (Walborn et al. 2002b; Sota et al. 2014). Pismis 24-1 is both a visual and a spectroscopic binary (Maíz Apellániz et al. 2007), with the two visual components having a small Δm, so it is likely that the system contains at least two very early type stars. However, at the present time there are no published spectral classifications in which the components are either spatially or kinematically resolved.

This is the closest cluster so far on the list and the first one under 2 kpc. There is a general good agreement between literature distances (Table A.1) except for two of the papers which use spectro-photometry (overestimates) and the four papers which give kinematic values (underestimates). This sightline is close to the direction of the Galactic center, so kinematic distances are expected to be of poor quality. Pismis 24 has a very high extinction ($A_V \sim 6$) for its short distance, a likely consequence of its location in the Carina-Sagittarius arm close to the direction of the Galactic center.

The upper left panel of Fig. A.5 shows a well-defined core with another concentration towards the south and an extended halo (this region has a complex ISM, see Cappa et al. 2011). Pismis 24-1 is not detected as a cluster member because it has no parallax or proper motions in *Gaia* DR2, but other bright objects in the cluster core such as Pismis 24-17 are. The brightest detected star is WR 93, a WC7 + O7/9 spectroscopic binary, that is the central object of a small subcluster 5′ to the east of the core. We detect 197 cluster members, even more than for Westerlund 2, due to the combination of proximity and richness. Nevertheless, the proper motion statistical tests ($t_{\mu_{\alpha*}}$ and t_{μ_δ}) are relatively high, indicating the detection of significant internal motions by *Gaia* DR2.

The proper motion panel of Fig. A.5 provides little discrimination, which is expected in a direction close to the Galactic center due to the nearly flat Galactic rotation curve. Most of the discrimination of cluster members is done using the CMD thanks to the higher extinction of the cluster compared to the field population. An important difference with previous objects in our sample is the proximity of that field population, as most of it seems to be in the foreground between a distance of 1 kpc and the cluster itself. The proportion of stars beyond 2 kpc is significantly lower than for the other groups we have analyzed so far, indicating the existence of an extinction wall at the cluster distance or slightly beyond.

We detect eight possible runaway stars from Pismis 24 (Table A.2). Of those, Pismis 24-18 is likely to be an early-type B star. See Gvaramadze et al. (2011) for a previous study on potential runaways from Pismis 24.

3.5. Villafranca O-006 = Gum 35 = Majaess 133

This is the most overlooked object in our sample, with only a few significant references in the literature (Dutra et al. 2003; Majaess 2013; Mohr-Smith et al. 2017). Its high extinction caused its discovery to be produced in the IR but it is the likely source of the visible H II region Gum 35 (Gum 1955) and its brightest stars have been studied in the visible. ALS 2067 was already classified as a "hot slash" star by Gómez & Niemelä (1987), a classification that was changed to O supergiant by Walborn & Fitzpatrick (2000) and later revised in Sota et al. (2014) to O5 Ifp. THA 35-II-153 is the earliest star in the cluster and this one is actually a "hot slash" star but its nature was only recently noticed by Maíz Apellániz et al. (2016), where its proximity to ALS 2067 was noted but it was erroneously assigned to Collinder 228. ALS 18 551 is an early O-type SB2 system also identified for the first time by Maíz Apellániz et al. (2016) but also erroneously assigned to Collinder 228 there. It was not until Mohr-Smith et al. (2017) that the relevance of this cluster was recognized.

The only previous distance measurements to Villafranca O-006 are kinematic distances between 6 and 9 kpc. A cluster at that position is clearly detected in the *Gaia* DR2 data 6.4 kpc away with relatively large uncertainties. That value makes it the second most distant target in the sample. It is close to NGC 3603 in position in the sky (2° away) and extinction ($A_V \sim 5$) and the two distance error bars overlap, so it is possible the two objects are physically associated, as suggested by Mohr-Smith et al. (2017). The cluster has a core + halo structure but the core itself has a complex, filamentary structure. Most of the field population is in the foreground, from one to several kpc closer. In the proper motion diagram of Fig. A.6, Villafranca O-006 lies at the end of an elongated structure that likely traces the foreground objects along the Carina-Sagittarius arm. The cluster is more easily distinguished from the field population by its higher extinction. A relatively large number of cluster members, 98, is identified, with THA 35-II-153 and ALS 18 551 among them – but not including ALS 2067 due to its large RUWE.

There are two possible runaways in the *Gaia* DR2 data (Table A.2). However, for objects so far away one is in dire straits determining distances for individual stars, so in this case there is a higher chance (compared to our other candidates) that they may be rejected by a subsequent analysis using better data and techniques (e.g., Tetzlaff et al. 2011). The first candidate, 2MASS J10584671−6105512, is interesting because it was classified as O8 Iabf by Maíz Apellániz et al. (2016). However, its proper motion is just outside our selection circle, so it could be just an unrelated object in this complex line of sight.

3.6. The Cygnus OB2 association: Villafranca O-007 = Cyg OB2-22 cluster = Bica 1 and Villafranca O-008 = Cyg OB2-8 cluster = Bica 2

The first six Villafranca groups are all located in the southern hemisphere and this is not a coincidence. Given our position in the Galaxy, it is easier to find massive young clusters towards the inner two Galactic quadrants than towards the two outer ones. The first two Villafranca groups in the northern hemisphere are located in Cygnus OB2, in the first quadrant but close to the second one. Cygnus OB2 is the northern OB association with the highest number of O stars and is sometimes presented as the northern equivalent of the Carina nebula association, given their relatively similar sizes, stellar contents, distances, and their symmetric positions with respect to the Galactic center (Knödlseder 2000; Comerón et al. 2002; Comerón & Pasquali 2012; Berlanas et al. 2018).

One difference that is sometimes pointed out between the Carina nebula and Cyg OB2 is the lack of significant clusters in the latter, however, that is not actually true as there are two stellar groups in Cyg OB2 that would stand out as significant clusters if they were isolated objects: namely, those around the multiple systems Cyg OB2-22 and Cyg OB2-8 (Bica et al. 2003; de La Fuente Marcos & de La Fuente Marcos 2009; Maíz Apellániz 2010), hereafter Bica 1 (Villafranca O-007) and Bica 2 (Villafranca O-008). Bica 2 includes Cyg OB2-7, the second O3 supergiant anywhere and the first object earlier than O4 in the northern hemisphere to be identified (Walborn 1973c). Bica 1 includes Cyg OB2-22 A, the second object earlier than O4 in the northern hemisphere to be identified

(Walborn et al. 2002b). Other interesting objects are Cyg OB2-9 in Bica 1, a massive highly eccentric SB2 system (Nazé et al. 2012; Maíz Apellániz et al. 2019a); Cyg OB2-8 C in Bica 2, an early-type Ofc star (Walborn et al. 2010); and Cyg OB2-8 A in Bica 2, another massive SB2 system composed of a supergiant and a giant stars. Cyg OB2-22 B is not selected by our algorithm as a member of Bica 1 due to its large RUWE but it is highly likely that it is a cluster member because of the combination of its early spectral type, small magnitude difference, and proximity to Cyg OB2-22 A (Maíz Apellániz 2010). In any case, as it was not selected by the algorithm, its *Gaia* DR2 measurements are not taken into account for the distance measurement. On the other hand, Cyg OB2-22 I (=ALS 15 161) has RUWE = 1.1 and $\varpi = 1.040 \pm 0.054$ mas, so it appears to be a foreground object.

The distance measurements to Cyg OB2 go back to the association discovery by Johnson & Morgan (1954) and cluster around a short distance of ∼1.4 kpc and a long distance of ∼1.7 kpc. The recent *Gaia* DR2 analysis by Berlanas et al. (2019) suggests that one possible explanation for this would be the existence of two subassociations: the main one, located at the long distance, and another one with only ∼10% of the stars, located at the short distance. The latter would be younger and include the four masers of Rygl et al. (2012) and the four eclipsing binaries of Kiminki et al. (2015). However, we should not discard that some results are still affected by extinction, as the column density of dust towards Cyg OB2 is at the same time very high for a group so close and highly variable, as the dust is mostly associated with the region rather than being spread uniformly along the line of sight. Our measurements for both Bica 1 and Bica 2 are compatible with the long ∼1.7 kpc distance, with a difference of less than one sigma between them. Therefore, the hypothesis of Bica et al. (2003) that they are the core of the association may remain valid if most of Cyg OB2 is at the long distance.

Both Bica 1 and Bica 2 distinguish themselves in the *Gaia* CMD as reddened sequences to the right of the low-extinction Galactic population sequence. They are also seen as density concentrations in the plane of the sky but are hard to distinguish in proper motion. The proper motions in right ascension of the two clusters are very similar while those in declination differ by a little over one sigma. The source density over the whole field is significantly lower than for the previous groups, a consequence of the larger angular distance from the Galactic center and the existence of strong extinction at short distances: Cyg OB2 is closer than the Carina nebula but the dust column is several times higher. Overall, the available information points towards Bica 1 and Bica 2 being a double cluster separated by ∼2.7 pc in the plane of the sky. We also point out that the field parallax histogram (black line in the bottom middle panels of Figs. A.7 and A.8) peaks at the same value as the clusters, a sign of the richness of the Cyg OB2 association (which increases the numbers at its parallax) and of the large amount of dust associated with it (which decreases the numbers at smaller parallaxes).

There are two possible runaways in the *Gaia* data. Cyg OB2-24 is a fast-rotating O8 Vn star (Sota et al. 2011) that appears to have been ejected from Bica 1 in the general direction of Bica 2. [MT91] 453 is a B5: V star (Kiminki et al. 2007) that may have been ejected from Bica 2 (or even Bica 1) towards the north.

3.7. Villafranca O-009 = M 17 = Omega nebula = NGC 6618 = Sh 2-45 = RCW 160

Villafranca O-009 is immersed in one of the most famous nearby H II regions, M 17, which is characterized by the highly variable and strong extinction associated with it. There are several early-O stars in the cluster. ALS 19 613 was classified as O5 V in the optical and O3–4 in the K band by Hanson et al. (1997). Hoffmeister et al. (2008) separated the A and B components and gives O4 V spectral classifications for both but indicated that the two of them are spectroscopic binaries. Both A and B (but especially the second one) are very weak targets and we have only been able to obtain relatively noisy spectra for them with GOSSS (for A) and with a reduced spectral resolution of 2000 with GTC (for both A and B) and even then with only the bluest wavelengths of the classification range (Fig. 1). Both are indeed early-type O stars, as indicated by the weak or absent He I λ4471 absorption, but the low S/N precludes an accurate classification. Other early-O stars are ALS 19 618 A and ALS 19 617.

We obtained lucky images of the core of M 17 with AstraLux on two different dates, 2012-10-02 and 2019-06-15, and measured the separation, position angle, and Δm in two filters (z and i) for ALS 19 613 A,B. We obtained a separation of $1.651 \pm 0.006''$, a position angle of $227.17 \pm 0.10°$, a Δz of 0.585 ± 0.037 mag, and a Δi of 0.894 ± 0.064 mag, with no appreciable motion in the span of almost seven years.

The distance measurements in the literature are concentrated between our value and ones ∼50% higher, with an extreme outlier that places M 17 beyond the Galactic center (Quireza et al. 2006) and three measurements around 1.3 kpc. Some of the differences may be caused by uncorrected extinction effects but others may be caused by a different location along the line of sight, as the two water maser measurements (Xu et al. 2011; Chibueze et al. 2016) give a distance around 2 kpc. Kinematic distances are overestimated, to some point expected as this sightline is close to the direction of the Galactic center. The proper motion statistical tests ($t_{\mu_{\alpha*}}$ and t_{μ_δ}) are relatively high, indicating the detection of significant internal motions by *Gaia* DR2.

The proper motion diagram in Fig. A.9 does not allow the discrimination of cluster sources easily, as expected from the small angle difference with the Galactic center. The concentration of sources and nebular emission seen towards the center (with an extension towards the east) in the top panels of Fig. A.9 is caused mostly by the lower extinction in those regions. The horizontal spread among cluster members in the CMD (bottom left panel of Fig. A.9) is another sign of the strong differential extinction. It is quite likely that the cluster is much richer in luminous OB stars than the 30 members indicated in Table 3 (Hoffmeister et al. 2008). *Gaia* DR2 resolves ALS 19 613 into A and B but their astrometric results are discrepant (and one of them with a high RUWE), so it is possible that there is cross-contamination in their data.

We detect seven possible runaways from M 17. One of them is BD −16 4826, an SB2 classified as O7 III((f)) + O9/B0 V by Maíz Apellániz et al. (2019b). Another one, NGC 6618 B-373 was classified as O8 V by Povich et al. (2009), who noted the star may be a binary based on its luminosity. A third one, 2MASS J18200299−1602068, was also classified by Povich et al. (2009) as O9 V.

3.8. Villafranca O-010 = NGC 6193 = RCW 108

NGC 6193 (Villafranca O-010) is a cluster in the Ara OB1a association that ionizes the adjacent RCW 108 H II region (Arnal et al. 1987; Baume et al. 2011). Its core is dominated by the triple system HD 150 136 Aa,Ab (Niemelä & Gamen 2005; Sánchez-Bermúdez et al. 2013; Sana et al. 2013). Sota et al. (2014) classified two of the components as O3.5–4 III(f*) + O6 IV. The other O-type system in the cluster is HD 150 135 Aa,Ab, classified in GOSSS-II as O6.5 V((f))z but note that the OWN project had previously identified it as an SB2.

We have obtained a LiLiMaRlin spectrum of HD 150 136 Aa,Ab and we have caught the system with clear double lines and a weak third component seen in He I (Fig. 1). The corresponding spectral classification is O3.5 III(f*) + O5.5 IV((f)) + OB, where the slightly earlier spectral type of the secondary can be explained by contamination from the tertiary in the GOSSS-II spectrum. We have also obtained GOSSS and LiLiMaRlin spectra of HD 150 135 Aa,Ab and in both cases we see it as an SB2 with spectral types O6.5 V((f))z + O8:.

This is the cluster in the sample that is more easily distinguished from the field population in proper motion, which can be explained by its proximity compared to most of the stars in the field. The cluster has a well defined core centered on the two O stars and the background population has a non-uniform spatial distribution centered several arcminutes to the west of the cluster core. The explanation of this effect lies in the geometry created by the destruction of the parent molecular cloud of the cluster. The ionizing radiation and stellar winds of NGC 6193 have created a cavity around it that has only partially ruptured the molecular cloud around it. The optically thicker remains are located just at the right edge and beyond the frame of the top left panel in Fig. A.10 and contain an infrared cluster (Straw et al. 1987). The only place where the cloud appears to have been completely ruptured along the line of sight is the region between the cluster core and those optically thicker remains and, indeed, there we are able to see the Galactic disc through a hole up to several times the distance to the cluster itself. The extinction to the NGC 6193 itself is relatively low. Maíz Apellániz & Barbá (2018) give a mean $E(4405-5495)$ of 0.445 for the two O stars with a high R_{5495} close to 4.0, which is typical of H II regions and suggests that a significant part of the dust affecting the line of sight is associated with the cluster itself.

The pre-*Gaia* DR2 distance measurements to NGC 6193 aggregate around 1.4 kpc but we find a value about 200 pc smaller. One possible origin for the discrepancy is the anomalous value of R_{5495}. We also tested to see whether the dark cloud to the west of the cluster that blocks most of the stars behind it is indeed at the same distance as NGC 6193. To do so, we downloaded the *Gaia* DR2 data in a $6' \times 6'$ region in the cloud and checked the parallax distribution of the sources there. Indeed, we find a steep drop in the number of sources when we get to the value of ϖ_g (compare this with the center left panel of Fig. A.10) and the few sources with smaller parallax values become significantly redder than the ones with larger values (compare this with the central panel in Fig. A.10). Therefore, we confirm that the dark cloud is associated with the cluster, as expected. This technique is a less sophisticated version of the one used by Zucker et al. (2020) to measure the distance to the molecular cloud to the south of the cluster, for which they find a slightly lower distance by 100−150 pc, indicating that other cloud may be also associated with the cluster but located slightly closer to us. We found one possible runaway from NGC 6193. Namely, 2MASS J16403254−4846296 is moving towards the west from the cluster.

3.9. Villafranca O-011 = Berkeley 90 = Sh 2-115

This cluster is dominated by two O-type systems, LS III +46 11 and LS III +46 12 (Maíz Apellániz et al. 2015a,b; Marco & Negueruela 2017) and is associated with the faint H II region Sh 2-115 (Harten & Felli 1980). The early-type nature of its two central sources was first recognized by Motch et al. (1997). LS III +46 11 is a massive near-twin binary (Maíz Apellániz et al. 2015a) and the cluster experiences a significant differential extinction (Maíz Apellániz et al. 2015b). Berkeley 90 (Villafranca O-011) is the group located at a higher Galactic latitude and at a larger physical distance from the Galactic plane in our sample.

Berkeley 90 presents a well-defined core surrounded by a halo. It does not distinguish itself well in proper motion and distance from the surrounding population, which concentrates at similar values. The most efficient separation filter is the CMD, as the local extinction affects the cluster more than the surrounding area. Therefore, it is likely that we are discarding some objects associated with the cluster but with a lower extinction.

The *Gaia* DR2 distance to Berkeley 90 of ∼3 kpc is somewhat longer than the two early estimates by Mayer & Macák (1973) and Motch et al. (1997) but consistent with the more recent values of Maíz Apellániz et al. (2015a) and Marco & Negueruela (2017), especially the former. As with most groups in this paper, our distance agrees with the Cantat-Gaudin et al. (2018) value but with a much larger uncertainty caused by the covariance term. The reason for the differences with the two early estimates lays in the incorrect spectral classifications of the two central O-type systems, the undetected binary nature of LS III +46 11, and the complex extinction (Maíz Apellániz et al. 2015b). The *Gaia* DR2 parallax of LS III +46 12 is compatible with that of the cluster, which according to the discussion in Maíz Apellániz et al. (2015a) indicates that the star is overluminous for its spectral type or that it is a yet undetected binary. We confirm that the B8 III star 2MASS J20352201+4651518, the B9 III star 2MASS J20352097+4648368, the F6 V star 2MASS J20350745+4651367, the F6 III star 2MASS J20351813+4650525, the F8 IV star 2MASS J20350955+4652199, and the G2 III star 2MASS J20351026+4651364 are foreground objects according to their parallaxes and have proper motions significantly different to that of the cluster (Marco & Negueruela 2017).

From its parallax, proper motion, and CMD position, the B0.5 V star 2MASS J20351422+4650118 (Marco & Negueruela 2017) appears to be either a background object or to have been ejected towards the south after an interaction with LS III +46 11. We also detect four additional possible objects ejected from the cluster, all with G magnitudes that would correspond to B-type stars. The first two are to the north and are bluer (likely experience less extinction) than the stars identified in the group, while the last two are to the south and are redder (likely experience more extinction) than the other group stars. This is possibly another consequence of the strong differential extinction around Berkeley 90.

3.10. Villafranca O-012 = NGC 2467 = Sh 2-311 = RCW 16

This group is a double cluster composed of a northern component (Haffner 19, Villafranca O-012 N) and a southern one (Haffner 18, Villafranca O-012 S). Its inclusion on this paper

deserves some words of explanation. There is only one confirmed O star that meets the requirements of our method, namely, CPD −26 2704 in Haffner 18, which is an O7 V(n) (Maíz Apellániz et al. 2016), making it significantly later than O4. However, there is, indeed, a star earlier than O4 associated with the cluster: HD 64 568, an O3 V((f*))z (Sota et al. 2014) that appears in the *Gaia* DR2 data as a likely runaway from Villafranca O-012, probably Haffner 18, with a flight time around 400 ka. In addition, there is another O star in the vicinity, HD 64 315 AB, classified by Maíz Apellániz et al. (2016) as O5.5 V + O7 V. HD 64 315 AB has a RUWE of 1.8 and a negative parallax, possibly due to the presence of two unresolved visible components (each one of them a binary itself, see Lorenzo et al. 2017) in the *Gaia* data, but its position in the CMD indicates that it is likely to be at a similar distance as HD 64 568 and Villafranca O-012. Interestingly, HD 64 315 AB is moving away from Haffner 18 in a direction nearly opposite to that of HD 64 568 and with a similar flight time, leading to the possibility that the two O-type systems were simultaneously ejected from the cluster. For those reasons, we consider that most likely Haffner 18, is the origin of the O3 star HD 64 568 and, thus, we include it in our sample. The Sh 2-311 H II region has a bright core close to HD 64 315 AB, its likely main ionizing source, and an extended halo. There is little Hα emission close to HD 64 568 despite its higher ionizing flux, another indication that the star is already far from its primordial cloud.

The literature distances for Villafranca O-012 (Table A.1) show a high dispersion, making it one of the objects in our sample where *Gaia* data is more useful. Indeed, there are discrepancies as to whether Haffner 18 and Haffner 19 (and other nearby regions) are at the same distance or not (e.g., Yadav et al. 2015 claims that the first one is twice as far as the second one). Our results yield a difference of less than one sigma between the two distances, indicating that it is possible that they are physically associated, but the error bars are relatively large so we cannot discard that they are not. In this case, future *Gaia* data releases may provide a more conclusive answer. For the time being, we assign a single catalog number to Haffner 18 and Haffner 19. The proper motions of the two clusters are similar, with a hint of the two approaching each other.

The double core structure is clearly seen in the top left panel of Fig. A.12. In the proper motion diagram Villafranca O-012 is located at the end of an elongated structure that likely traces the proper motion changes as a function of distance. We are able to see a long way through this sightline, placed in a low extinction hole towards the outer galaxy (this is the target located at a larger Galactocentric radius in our sample). Maíz Apellániz & Barbá (2018) measured $A_V = 1.388 \pm 0.018$ for HD 64 568 and higher values for the other two stars, indicating there is little dust in the sightline and that the internal contribution is significant. The *Gaia* CMD gives a higher average extinction (as well as a larger dispersion in its values) for the southern cluster.

We obtained a LiLiMaRlin spectrum of HD 64 315 AB. The spectral type we derive from it is O6 V + O7.5 V((f)), that is, the spectral types for both the primary and secondary are later by half a spectral type than in the GOSSS result. In addition to the two cases already mentioned (HD 64 568 and HD 64 315 AB) there are another five possible runaways from Villafranca O-012. As for the other groups, they are listed in Table A.2.

3.11. Villafranca O-013 = Sh 2-158 = NGC 7538

This group is a poorly defined cluster embedded in the bright H II region Sh 2-158. The majority of the ionizing photons originate in the primary star of the central binary system Sh 2-158 1 with a small contribution from the late-type O star Sh 2-158 2 (Maíz Apellániz et al. 2016). A third bright object near the two, Tyc 4279-01349-1 is actually a foreground K star (Wynn-Williams et al. 1974). Differential extinction is very strong and is likely to be hiding additional cluster members, especially to the south.

In GOSSS-III, we classified Sh 2-158 1 as O3.5 V((f)) + O9.5: V. In Fig. 1 we present two new spectra of this object, one from GOSSS and the other one from LiLiMaRlin, selected from several tens we have obtained with those projects. The primary is classified as O3.5 V and the secondary as O9.5: V in all three cases. The suffix of the primary changes between spectra as a consequence of the varying strength of C III λ4650 in emission and He II λ4686 in absorption. We also observe rapid velocity changes from night to night in our spectra, a sign that this spectroscopic binary has a short period. One possibility is that the two stars are close enough for the object to be an eclipsing or ellipsoidal variable and that the suffix changes are being caused by different cross sections of the stars being exposed. We checked the photometry in the ASAS-SN project (Kochanek et al. 2017) and we found no signs of eclipses.

It is difficult to distinguish Villafranca O-013 from the surrounding population, which is mostly located at distances similar to that of the cluster. Its proper motion is somewhat more negative in RA but its most differentiating characteristic is its higher extinction, which is associated with the cluster and H II region. This is clearly the poorest stellar cluster so far in our sample, with only eleven confirmed members. One reason why we do not detect more cluster members in the *Gaia* DR2 data is that the presence of strong nebulosity that contaminates G_{BP} and G_{RP} pushes some d_{CC} values above our selection threshold.

The literature values in Table A.1 can be divided in two types: high kinematic distances and low values similar to the one found using our method. In this case it is clear that the kinematic values are wrong, pointing to a possible peculiar velocity of the cluster, as it is not close to the Galactic center or anticenter. Both O-type systems are among the eleven confirmed members.

There are five possible runaways from Villafranca O-013 in the *Gaia* DR2 data from the positions and proper motions. The brightest one is red and bright, so it is either a luminous, highly extinguished OB star or a fast-moving red giant coincidentally at the distance of the cluster. The other four candidates are bluer and with positions in the CMD consistent with being B stars. One of them, [MO2001] 77, is listed as an object with Hα emission by Mikami & Ogura (2001).

3.12. Villafranca O-014 = North America nebula = NGC 7000 = Sh 2-117

The North America nebula is one of the most famous ionized nebulae in the sky and also one of the closest and largest (in angular size) ones. It is located to the east of the Pelican nebula and the two of them are thought to be a single H II region obscured at its center by a molecular cloud with the shape of the Atlantic Ocean and Gulf of Mexico (the latter part is called L935) that gives the North America nebula its distinct shape and name (Reipurth & Schneider 2008; Zhang et al. 2014).

The ionizing star of the North America nebula was unknown until Comerón & Pasquali (2005) used 2MASS photometry and visible + infrared spectroscopy to identify a highly reddened early-O object and give it a preliminary spectral type of O5 V,

noting that they could not exclude an earlier spectral subtype. Maíz Apellániz et al. (2016) observed it as part of GOSSS, discovered it is an SB2 with spectral types O3.5 III(f*) + O8:, and named it Bajamar star based on its location with respect to the nebula[3].

The literature on the distance to the North America nebula is long and goes back to the 1950s (Table A.1). Previous results yielded wildly varying distances from 150 pc to 2 kpc, in good part due to the different assumptions about the ionizing source which, as mentioned above, was not identified until 2005. For example, Neckel et al. (1980) gave the shortest distance above based on the identification of a star (2MASS J20535282+4424015) as the ionizing source but that object is actually a late-type object that *Gaia* DR2 places at a distance of about 2 kpc. The more recent, pre-*Gaia* results yielded distances that cluster around 500−600 pc and were mostly based on detecting the blocking effect of the molecular clouds on the background stars. A similar technique using *Gaia* DR2 (Zucker et al. 2020) yields significantly longer distances around 800 pc (with slightly different values for different parts of the molecular cloud). An analysis of the stars in the nearby Pelican nebula with *Gaia* DR2 (Bhardwaj et al. 2019) gives also a longer distance of 858 ± 56 pc.

The Bajamar star has a *Gaia* DR2 $\varpi = 1.473 \pm 0.097$ mas, which after applying the same zero point and prior as for the rest of the targets in this paper leads to a distance of 675^{+47}_{-42} pc. That distance places it between the pre-*Gaia* results and the *Gaia* ones for the molecular cloud (which have a significant spread for different parts) and the Pelican nebula. This confirms that it is the main ionizing source of the region and makes it the only massive star earlier than O4 within 1 kpc, significantly closer than HD 150 136 Aa,Ab, which is the second such star in terms of distance to the Sun.

The question now is what about the stellar group that the Bajamar star belongs to? Comerón & Pasquali (2005) already noted the isolation of the star. They used a search radius of half a degree and determined there were no companions earlier than B2 V. Damiani et al. (2017b) searched for X-ray sources and found no concentration of young low mass stars, specifically stating that "Unlike most star-forming regions, this most massive star appears isolated even in X-ray images". On this basis, we used a conservative approach in downloading from the *Gaia* archive a very large area of $2° \times 2°$ around $\alpha = 314.55°$, $\delta = +44.14°$. The top-left panel of Fig. A.14 shows that the *Gaia* source density traces the shape of North America well, which indicates that the molecular cloud stands in front of the vast majority of the stars in the field and that the ionized gas is optically thin, allowing us to see well beyond its location. Indeed, this is what can be seen in the panels where parallax is plotted, where the source density increases up to ≈3 kpc. Those circumstances preclude the functioning of our standard method, as the alleged group would be a minor contaminant and it would be strongly affected by extinction, with the possible exception of some stars that could be present on the near side of the molecular cloud. Furthermore, using a circular aperture around the Bajamar star soon starts including the region of the southeastern part of the United States, where the source density is much higher.

To estimate the distance to the North America nebula, we adjust the method in two ways: we substitute the circular aperture by an ad-hoc narrow polygonal aperture that traces the core of the molecular cloud (effectively shielding most of the background population) and we establish a G' magnitude cut at 18.5. Also, we use HD 199 579 as our reference star for the isochrone, as the Bajamar star is not included in Maíz Apellániz & Barbá (2018). The resulting sample consists of the 12 stars in Table 4. The sample is clearly separated in proper motion from the field population, as expected from the difference in distance. The Bajamar star is the most extinguished object among the 12, which could be partly a selection effect (low-mass objects with that extinction would be dimmer than $G' = 18.5$) but cannot tell the whole story, as BA stars with its extinction should still be detected. The distance to Villafranca O-014 from the 12 stars is 714^{+19}_{-16} pc, which is within one sigma of the distance to the Bajamar star, and indicates that pre-*Gaia* measurements from the last two decades in general underestimated the distance to the nebula by 10−30%. With that distance, the second and third stars in Table 4 have *Gaia* DR2 + 2MASS photometry roughly consistent with being extinguished MS B-type stars embedded in the Gulf of Mexico + Atlantic Ocean molecular cloud (but we cannot discard them being of late spectral type due to the intrinsic color-reddening degeneracy for *Gaia* colors). We note, however, that both stars are considerably far away in the plane of the sky from the Bajamar star (9 pc and 6 pc, respectively) so they cannot be part of the same bound cluster. Instead, they are just stars being born from the same extended cloud.

Table 4. *Gaia* DR2-selected stars in Villafranca O-014.

Gaia DR2 ID	ϖ (mas)	Other ID
2 162 889 493 831 375 488	1.473 ± 0.097	Bajamar star
2 162 977 317 322 486 144	1.334 ± 0.054	–
2 162 091 866 866 267 008	1.211 ± 0.084	–
2 162 128 013 311 282 304	1.458 ± 0.065	–
2 162 967 421 717 817 984	1.430 ± 0.080	–
2 162 965 531 932 197 504	1.372 ± 0.112	–
2 162 121 244 442 829 568	1.379 ± 0.104	–
2 162 902 413 092 613 248	1.317 ± 0.134	–
2 162 963 019 373 410 432	1.206 ± 0.143	–
2 162 123 198 648 385 024	1.433 ± 0.152	–
2 162 910 930 018 064 512	1.298 ± 0.138	–
2 162 909 108 944 432 256	1.262 ± 0.165	–

Previous works (e.g., Laugalys et al. 2006; Straižys & Laugalys 2008; Armond et al. 2011; Damiani et al. 2017b) have suggested that some stars may be associated with the North America and Pelican nebulae. Here we discuss these candidates based on their *Gaia* DR2 data:

– HD 199 579 is an O6.5 V((f))z star (Sota et al. 2011) with a faint B-type companion (Williams et al. 2001) that was proposed in the past as the ionizing source of the region (Sharpless & Osterbrock 1952). Its parallax (1.0633 ± 0.0589 mas) puts it beyond the nebula and its proper motion also differs from those in Villafranca O-014.

– V1057 Cyg is an FU Ori star whose parallax (1.0864 ± 0.0388 mas) places it a distance similar to that of HD 199 579 but with quite a different proper motion.

– V2493 Cyg, on the other hand, has a parallax (ϖ = 1.2973 ± 0.0313 mas) that is consistent with that of the 12 stars

[3] As Comerón & Pasquali (2005) put it, "just East of the Florida Peninsula", where they meant east in the geographical sense, not in the astronomical one. We note that Bajamar, meaning low tide in Spanish, was the original name given to the Bahamas.

identified in Villafranca O-014 and the only reason why it was previously discarded was that its proper motion being slightly outside the proper motion circle. Therefore, it is another likely member.

– V1539 Cyg, LkHA 186, and LkHA 188 are three stars in a situation similar to that of V2493 Cyg, so they are additional likely members of Villafranca O-014. Indeed, those four objects are in the same region in the Gulf of Mexico and they are the brightest members of the closest structure to a cluster in the region, which also includes *Gaia* DR2 2 162 128 013 311 282 304, one of the objects in Table 4.

– On the other hand, LkHA 187 and LkHA 189, despite it being in the same region of the Gulf of Mexico, have parallaxes that put them beyond the nebula. Their proper motions are also closer to those of the (more distant) field population.

– Objects 1, 4, 7, and 9 from Straižys & Laugalys (2008), who suspected these could be extinguished O stars, have *Gaia* DR2 parallaxes with relatively large uncertainties but they all appear to be significantly beyond Villafranca O-014.

For Villafranca O-014, it is a complicated undertaking to search for runaways in the same manner as for the rest of the sample as there is no defined center to run away from. For the sake of completeness, we searched in the low-extinction regions of the field for bright stars with parallaxes compatible with that of the North America nebula. Here are the most significant cases:

– HD 200 102 is a sixth-magnitude star with a Simbad classification of G1 Ib in the upper-midwest United States part of the nebula. It has a proper motion significantly different from those of the stars in Table 4 moving towards the NW, which combined with its spectral type (which suggests a non-coeval age with an early-O star) points towards being a field star.

– V354 Cyg is listed as a long period variable in Simbad and is located in the southwestern United States part of the nebula. Its proper motion points away from the Gulf of Mexico so it could be an ejected PMS star.

– Simbad gives a spectral classification of K4 III for Tyc 3179-00416-1, which is located in the Central America region of the nebula and moving southward away from the Gulf of Mexico. Therefore, this is another potentially ejected PMS star.

– Another interesting case is Tyc 3179-00023-1, located close to the previous one, but moving away from the Caribbean Sea or Atlantic Ocean regions, possibly even the location of the Bajamar star. Simbad gives a spectral type of B9 IV, so if it is a young runaway it would be already close to the main sequence.

– Tyc 3179-01439-1 is located near the Yucatan peninsula but moving towards the Gulf of Mexico instead of away from it, so it is likely a field star. Simbad gives a classification of A4 V.

– ALS 11 602 is near the edge of the field, close to the Pelican nebula. Its parallax and its proper motion are similar to those of the stars in Table 4, and it is a B2 Vn star, according to Straižys et al. (1999), so it is a likely member of the association, albeit a distant one from the Bajamar star.

– Finally, [SKV93] 2-72 is close to the previous object but has a very different proper motion. It is a fast moving object and its proper motion traces back to a region close to the Bajamar star, making it another possible runaway star. Straizys et al. (1993) classify it as K0 III-IV.

In summary, the Bajamar star seems to be a genuine case of a massive binary star born in near-isolation i.e. with only a small number of intermediate- and low-mass stars around it. There are other stars being born from the same molecular cloud but they are considerably less massive and not bound to the Bajamar star in a cluster-like fashion. What we call Villafranca O-014 in this paper is a poor stellar association instead and the North America and Pelican nebulae have no clearly defined, concentrated cluster despite being significantly larger (in size and number of ionizing photons) than other nearby H II regions such as the Orion nebula or NGC 2264, whose central clusters are well -established.

Following the submission of this paper to the journal, an independent analysis of the North America and Pelican nebulae using *Gaia* DR2 data was published and the referee dutifully pointed us to it (Kuhn et al. 2020). Most of the results in that paper agree with what we present here but there are some small differences, which we go on to discuss below.

First, the authors set into doubt the fact that the Bajamar star is a double-lined spectroscopic binary on the basis of a single-epoch spectroscopic observation. We obtained multi-epoch spectroscopy of the system and we can indeed confirm that the absorption lines move as we would expect for such a binary. We are currently working on a paper with an orbit for the system. Regarding the distance, Kuhn et al. (2020) find a mean parallax for their group E (objects in the Gulf of Mexico) of 1.27 ± 0.02 mas, which can be compared to our non-zero-point-corrected value of 1.354 ± 0.029 mas. Their value for the dispersion apparently does not include the spatial covariance term (their Sect. 7.4) but including it would leave the difference between our two results at a two-sigma level. Finally, the paper suggests that the Bajamar star may have originated from the region of the Pelican nebula (their group D) and they calculate that it is moving away from there with a relative velocity of 6.6 ± 0.5 km s^{-1}. That scenario is plausible (the plane-of-the-sky travel time would be 1−2 Ma) but we note that it is far below the standard threshold for runaway stars and that some refer to such objects as "walkaway stars" (Renzo et al. 2019). We note that Kuhn et al. (2020) place their group D beyond their group E and that the parallax for the Bajamar star places it even closer albeit with a relatively large uncertainty. Hopefully, future *Gaia* releases will shed some light into these (relatively small) distance discrepancies. In any case, if the walkaway scenario from group D were true, it would not change our basic conclusion, as the Bajamar star would still be the only O-type system in the region and we would still have a case of a very massive star formation in near-isolation.

3.13. Villafranca O-015 = Collinder 419

This cluster was studied in MA19. Here, we summarize those authors findings. As previously mentioned in this paper, we include it here as one of the (many future) members of the Villafranca catalog of groups with O stars even though it has no objects of the O2–3.5 subtypes. Collinder 419 (Villafranca O-015) is a relatively unstudied cluster in Cygnus dominated by the O-type system HD 193 322. It is quite poor, as MA19 confirmed only 75 members, and can be described as a small concentration around the O-type system surrounded by an asymmetric halo. It is much better defined in proper motion than in position, as it sits in front of a rich background Galactic population at a distance of 2−5 kpc. The cluster experiences low extinction and MA19 derives a distance of $1.006^{+0.037}_{-0.034}$ kpc. HD 193 322 is a complex system with at least two O stars, but of a late subtype compared to the much earlier types present in Villafranca O-001 to Villafranca O-014.

Furthermore, MA19 noted the existence of a late-type giant, 2MASS J20175763+4044373, with a parallax compatible with that of Collinder 419 and a peculiar NE-SW motion, which indicated a possible ejection from a high-extinction region to the NE. Here, we list in Table A.2 another five stars with similar

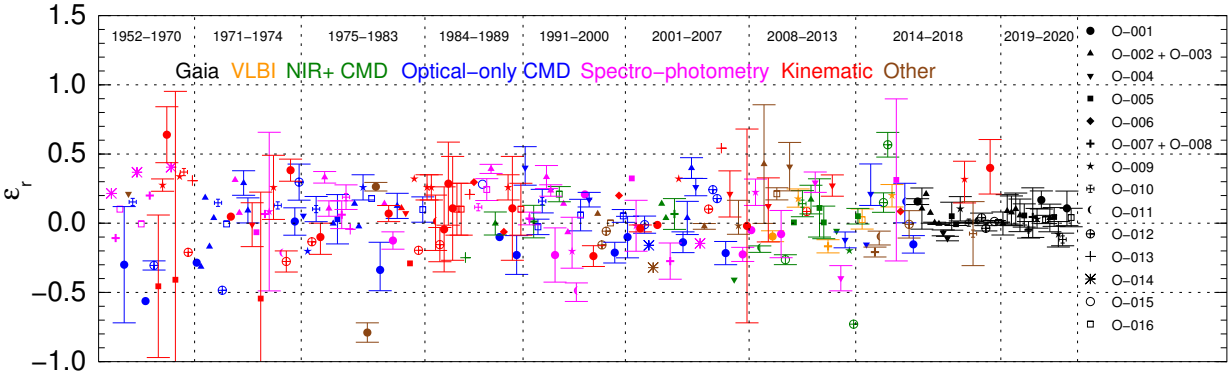

Fig. 2. Fractional distance difference of the literature distance measurements, d, with respect to the values reported in this paper, d_r. Colors are used to encode the method used and symbols to encode the group. Symbols without error bars correspond to measurements without uncertainties and those with error bars reflect only the uncertainty in d and not in d_r.

parallaxes and an anomalous motion in the opposite direction and away from Collinder 419. They could be runaways from the cluster or they might constitute an independent moving group.

3.14. Villafranca O-016 = NGC 2264 = Sh 2-273

This object was also studied in MA19. Here, we provide a summary of those results. As previously mentioned, we include it here as one of the (many future) members of the Villafranca catalog of groups with O stars even though it has no objects of the O2–3.5 subtypes. NGC 2264 (Villafranca O-016) is a well-known cluster and a favorite target of amateur astronomers due to its associated H II region. It has a double-cluster structure, with the northern core centered around the O-type multiple system, 15 Mon, and the southern core around the Cone nebula, with possibly even more embedded cores. It is a richer cluster than Collinder 419, with 286 members confirmed by MA19, and also clearly defined in terms of proper motions. The molecular cloud associated with the H II region acts as a screen blocking the background population, located at much longer distances that the value of 719 ± 16 pc determined by MA19, with no significant differences in distance between the two cores. The interesting new finding from Zucker et al. (2020) reports distances to the associated molecular clouds that are consistent with our distance result but with the clouds around the edges somewhat closer to us than the one located at the same position as the cluster core. This would be consistent with the cluster having carved a hole on the near side of the molecular cloud that lets us see the cluster with little extinction and the cloud still blocking the view of the background. NGC 2264 appears to be very young, as indicated by the H II region and its associated structures, the embedded cores, and the z suffix in the O7 V((f))z spectral classification of 15 Mon Aa. We note that since the publication of MA19, 15 Mon has been spectroscopically separated into its Aa and Ab components by Maíz Apellániz & Barbá (2020).

We have also searched for possible runaways for this object and detected two (Table A.2). In both cases, their proper motions indicate a more likely ejection from the northern core than from the southern one.

4. Analysis and future work

4.1. Comparison with previous distances

In this paper, we presented *Gaia* DR2 distances to 16 stellar groups with O stars, Villafranca O-001 to Villafranca O-016. Two of those (Villafranca O-012 and Villafranca O-016) are double clusters located at the same distance (within our measurement errors) and another two pairs (Villafranca O-002 + Villafranca O-003 and Villafranca O-007 + Villafranca O-008) have been analyzed separately; nonetheless, we have also determined they are also likely to be physically related, so a common single distance can be adopted for each pair (besides the long list of references in the corresponding subsections and in Table A.1, the interested reader can find additional information on such physical associations in Turner & Moffat 1980; Piatti et al. 2010; Hur et al. 2012; Reiter & Parker 2019). This leaves us with a total of 14 distances to stellar groups d_r (or pairs of them) for which we have collected 226 literature distances d (i.e., an average of 16.1 measurements per stellar group)[4]. In this subsection, we analyze the accuracy of the literature distances according to different parameters. In Fig. 2, we plot the fractional distance difference $\varepsilon = (d - d_r)/\max(d, d_r)$ in chronological order using colors and symbols to encode methods and groups, respectively[5]. Of the 226 literature distances, 145 have uncertainty measurements and for those we have computed the uncertainty for the difference $d - d_r$, $\sigma_t = \sqrt{\sigma_d^2 + \sigma_{d_r}^2}$, and calculated the normalized deviation of the literature distance from our value $d_n = (d - d_r)/\sigma_t$, which encodes not only the accuracy of the literature values but also of their uncertainty estimates. In Table 5, we display the basic statistics of ε and d_n (average, standard deviation, and number of measurements) as a function of publication year range, stellar group, method, and first author. Ideally, both averages should be zero for unbiased measurements, σ_ε should be as low as possible for a better precision of the average distance, and σ_{d_n} should be close to 1 for independent measurements with correctly estimated uncertainties.

An overall feature of Table 5 is that positive values for $\overline{\varepsilon}$ and $\overline{d_n}$ dominate over negative ones. Therefore, our distances tend to be shorter than the literature values. The difference is small when compared to other *Gaia* DR2 results, for which ε is just $3 \pm 7\%$ overall and $1 \pm 6\%$ for the Cantat-Gaudin et al. (2018) values, showing the extent of the small effect of sample selection and different parallax zero points. We also note that σ_{d_n}

[4] We exclude from the sample the kinematic distance to M17 by Quireza et al. (2006) because it is an extreme outlier that distorts the analysis.

[5] We define ε with the maximum of d and d_r in the denominator to avoid outliers in the resulting distribution caused by one value being many times greater than the other.

Table 5. Distance statistics as a function of year range, stellar group, method, and first author.

Type	$\overline{\varepsilon}$	σ_ε	N_ε	$\overline{d_n}$	σ_{d_n}	N_{d_n}
Year range						
1952–1970	0.06	0.34	20	0.63	2.32	6
1971–1974	0.00	0.25	25	0.74	1.43	10
1975–1983	0.01	0.23	29	0.40	3.70	15
1984–1989	0.10	0.18	23	1.04	1.74	16
1991–2000	0.03	0.21	24	0.44	1.84	16
2001–2007	0.03	0.22	29	0.00	1.48	16
2008–2013	0.01	0.26	25	0.28	2.08	19
2014–2018	0.07	0.16	34	0.37	1.26	30
2019–2020	0.04	0.07	17	0.42	0.68	17
Group						
O-001	–0.10	0.18	18	–0.31	0.51	11
O-002 + O-003	0.11	0.15	41	1.30	1.58	23
O-004	0.07	0.23	20	0.66	1.18	14
O-005	–0.05	0.25	16	0.10	0.50	12
O-006	0.13	0.15	4	–	–	0
O-007 + O-008	–0.03	0.14	12	–0.57	1.23	9
O-009	0.13	0.18	22	1.31	1.37	17
O-010	0.11	0.13	12	0.14	0.25	7
O-011	–0.12	0.21	7	–0.83	1.57	6
O-012	–0.05	0.28	21	0.34	1.73	10
O-013	0.10	0.28	11	0.41	1.83	6
O-014	0.01	0.33	20	–0.25	3.91	14
O-015	0.01	0.27	3	–2.46	3.99	2
O-016	0.08	0.08	19	1.20	1.44	14
Method						
Gaia	0.03	0.07	34	0.30	0.57	32
VLBI	0.03	0.16	5	0.34	1.71	5
NIR+ CMD	–0.02	0.26	21	0.42	2.32	13
Optical-only CMD	0.01	0.22	54	0.33	1.43	31
Spectro-photometry	0.06	0.22	43	0.61	2.17	22
Kinematic	0.09	0.25	52	0.77	1.36	31
Other	–0.01	0.29	17	0.02	4.46	11
First author						
Binder	0.05	0.08	4	0.41	0.55	4
Becker	–0.05	0.29	8	–	–	0
Carraro	0.08	0.35	4	1.04	2.47	4
Cantat-Gaudin	0.01	0.06	11	0.07	0.32	11
Fich	0.05	0.14	6	0.42	1.07	6
Georgelin	0.08	0.32	10	0.48	1.83	5
Humphreys	0.17	0.12	4	1.50	1.75	4
Kuhn	0.06	0.03	5	0.54	0.15	5
Moffat	0.09	0.19	5	0.59	1.40	3
Massey	0.23	0.14	4	2.05	1.43	3
Russeil	0.10	0.23	5	–0.18	1.21	3
Shaver	0.01	0.22	6	0.27	–	1
Stark	0.19	0.09	6	1.20	0.99	6
Thé	0.00	0.13	4	–	–	0
Walborn	0.11	0.12	6	–	–	0
Zucker	0.00	0.09	5	0.16	0.62	5

Notes. For the latter, only those with four or more measurements are listed.

is lower than 1 for *Gaia* DR2 results, as the measurements are not independent.

The evolution with time shows no significant change of $\overline{\varepsilon}$, indicating that overall distances have not been getting shorter or longer. However, there is an evolution related to the dispersion. The highest value is for results older than fifty years. Then comes a long period with little change in the dispersion, which is only significantly reduced when the *Gaia* DR2 results appeared. We could ascribe that to the superior quality of *Gaia* DR2 results but we should keep in mind that the comparison is not undertaken among independent data, so the final verdict should come from a future confirmation. Comparing different methods results in few differences. The Very Long Baseline Interferometry (VLBI) parallaxes have a lower dispersion than other non-*Gaia* methods but run into the problem of the sources not being necessarily at the same distance as the group. Using the near infrared (NIR, with or without the optical) to build CMDs does not provide a significant advantage over optical-only equivalents. Spectrophotometry and, especially, kinematic distances overestimate (on average) distances more than other methods but in all cases the dispersion is significantly larger than $\overline{\varepsilon}$.

Using the average of the literature values as a distance to a group produces a result that is, at worst, 13% off from our value. The best predictor of how large the dispersion in the literature measurements is comes from the richness of the group: those with few stars or with low contrast with the field population (i.e., Villafranca O-012 to Villafranca O-014) have a larger scatter than concentrated clusters with many stars (e.g., NGC 3603 or Trumpler 14) or those that are easily differentiated from the field population (e.g., NGC 6193 or NGC 2244). As for individual first authors, those that use primarily *Gaia* DR2 distances (Binder, Cantat-Gaudin, Kuhn, and Zucker) have values of $\overline{\varepsilon}$ close to zero and low values of σ_ε, as expected. There are significant differences among the rest of first authors. Fich, Thé, and Walborn produce the best-quality results. At the other extreme, the distances by Becker, Carraro, and Georgelin yield the largest dispersions, and those by Humphreys, Stark, and especially Massey, produce the largest overestimates.

4.2. Identifying group members

Many group-finding algorithms (e.g., Cantat-Gaudin et al. 2018) give a large weight to proper motions in the identification of members of a stellar group. The results in this paper indicate that proper motions are, indeed, quite useful for that task when the distance is less than 1.5 kpc but for higher values, they become less so, as the differences in proper motion decrease as distance increases. For massive young clusters, such as the ones we analyze here, giving more weight to the CMD is recommended, as the extinction usually associated with the cluster allows for a better discrimination. This is not necessarily a general result, as astrometry with better precision may increase the distance range at which proper motions are good discriminants and as older groups should not have a significant associated extinction, but it appears to be true under the circumstances described here. We plan to test this hypothesis in future papers.

Even though we did not use them here, radial velocities are another potential discriminant for group membership, especially as the only dependence of their quality with distance is that given by S/N and their values do not tend to zero at infinity as proper motions do. Ongoing multifiber ground-based surveys and future *Gaia* DR2 data releases should be useful in this respect. We note, however, two important caveats. O and B stars (especially the former) have few useful lines for radial velocities in the Calcium triplet region used by the *Gaia* RVS instrument, so for those stars, we need to resort to ground-based surveys. Also, a large fraction of OB stars are spectroscopic binaries, so single-epoch spectroscopy will not do the job correctly.

Finally, we point to a problem in the *Gaia* photometric data: G is obtained from PSF fitting of image-like data (actually, one coordinate is spatial and the other one is temporal as the spacecraft sweeps the sky) but G_{BP} and G_{RP} are obtained through aperture photometry of slitless spectrophotometric data. This makes

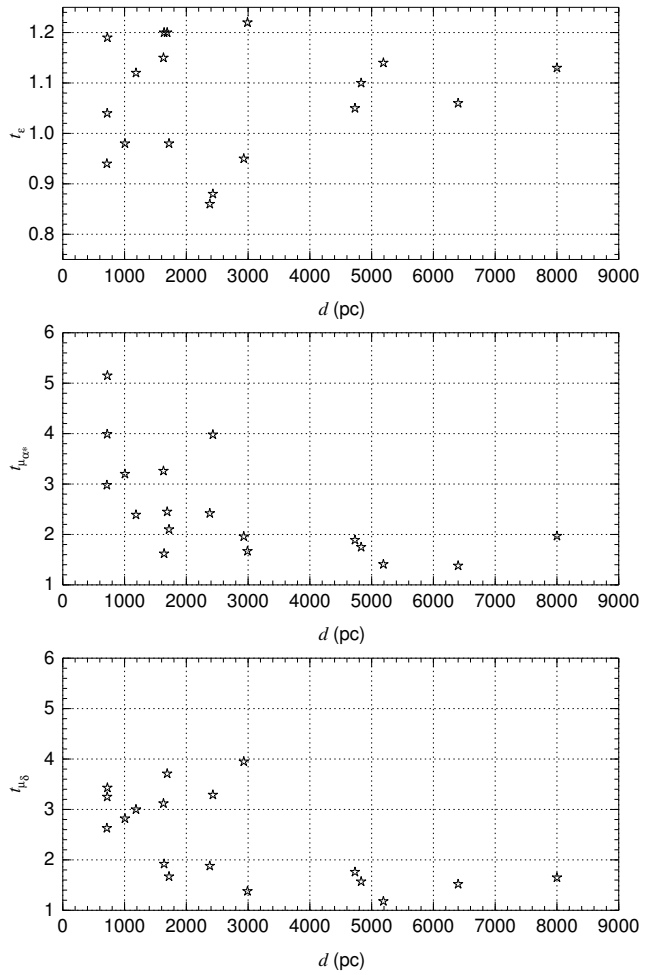

Fig. 3. Statistical tests t_ϖ, $t_{\mu_{\alpha*}}$, and t_{μ_δ} as a function of distance for the groups in this paper including Villafranca O-012 N, Villafranca O-012 S, Villafranca O-016 N, and Villafranca O-016 S separately.

the latter two quite sensitive to stellar crowding and nebular contamination. In some stellar groups (disperse and with no nebulosity) the effect is small, but in others, such as Villafranca O-013, it is not and causes our algorithm to reject many stars based on the d_{CC} criterion. This is one case where ground-based photometric surveys such as GALANTE can complement the *Gaia* data and improve on the sample selection. In addition, *Gaia* DR2 (and the future EDR3) provides little information on the spectral energy distribution (SED) to the left of the Balmer jump, given the low sensitivity of G_{BP} at those wavelengths (Maíz Apellániz & Weiler 2018), and that part of the SED is crucial for correctly measuring the effective temperature of OB stars without resorting to expensive spectroscopy (Maíz Apellániz & Sota 2008; Maíz Apellániz et al. 2014). That is another aspect where ground-based surveys can complement *Gaia* with a *u*-like filter. In principle, *Gaia* DR3 should help with this issue when it releases the G_{BP}-associated spectrophotometry but we note that there may be some calibration issues for a significant number of OB stars given the combination of the G_{BP} sensitivity profile and the reddened character of most of the Galactic OB SEDs (Weiler et al. 2020).

4.3. Internal motions

In Fig. 3, we plot the statistical tests t_ϖ, $t_{\mu_{\alpha*}}$, and t_{μ_δ} as a function of distance for the groups studied here, and t_ϖ shows no trend with distance and the values cluster around 1, indicating the sample selection process works well and the final result should have few contaminants (non-group members). The plots for the proper motion statistical tests are different. All values are above 1, indicating that there are likely internal group motions affecting the stellar proper motions. A trend with distance is also clear: for distances longer than 4 kpc the two proper motion tests stay below 2 while for shorter distances the two tests (especially $t_{\mu_{\alpha*}}$) increase as we move towards zero. This is an effect of the proper motions being inversely proportional to the distance and shows that *Gaia* DR2 is limited in the detection of internal proper motions. The two exceptions to the trend are Pismis 24 and, especially, Trumpler 14. The likely explanation is that those two are the most massive compact clusters in our sample within 4 kpc.

4.4. Richness and the IMF

What is the relationship between the richness of a cluster, defined as the concentration of many stars in a small volume, and its initial mass function (IMF)? In the view of Kroupa (2004), the IMF is universal but the mass of a cluster correlates with the maximum stellar mass, as clusters of small mass will not be able to form very massive stars. Therefore, as Weidner & Kroupa (2006) put it, "10^4 clusters of mass $10^2\,M_\odot$ will not produce the same IMF as one cluster with a mass of $10^6\,M_\odot$", implying that the second option should have a larger proportion of massive stars. A corollary of this hypothesis is that massive stars should not be able to form in isolation and that any such object found without nearby massive companions should be a runaway (Gvaramadze et al. 2012).

There are several observational facts that seem to contradict that hypothesis. The first one is that massive stars are seen in associations (Ambartsumian 1958), which agrees with star formation being a hierarchical process that happens in both bound and unbound clouds with a wide range of scales (Elmegreen 2010). Associations can be rich in massive stars even if they do not have well-defined clusters in them and they can be scaled up to large masses, with two objects with structures as different as 30 Dor and NGC 604 having formed similar numbers of massive stars (Maíz Apellániz 2001a). One past critique of this has been that associations form as clusters that lose their gas rapidly and disperse until we see them as unbound structures. However, this critique has been disproven with modern data for the northern association with the largest number of O stars (Wright et al. 2014, the title of the paper says it clearly: "Cygnus OB2 was always an association") and the results in this paper confirm that: Cyg OB2 retains a double core, each with a normal velocity dispersion as determined from the proper motions (see previous subsection) and no abnormal relative velocity between them, in line with the Wright et al. (2016) analysis that reveals no global expansion pattern.

Another contradictory observational fact is the existence of massive stars that appear to be truly isolated while not being runaways. Bressert et al. (2012) found 15 such objects in 30 Dor, for which they noted they could not be line-of-sight runaways based on their radial velocities. A second study (Platais et al. 2018) discarded the possibility that most of them could be plane-of-the-sky runaway stars, indicating they are true cases of isolated massive-star formation. Of course, 30 Dor is 50 kpc away and even though Bressert et al. (2012) used HST images to try to discard the existence of a multiple system or mini-cluster around their targets, the spatial resolution at that distance could not rule that out. In this paper, however, we present the case of the

Bajamar star, which is located almost two orders of magnitude closer than 30 Doradus and, furthermore, with a primary of the earliest type in comparison to any of the Bressert et al. (2012) objects. It is located near the center of the molecular cloud from which it appears to have been born, it shows only a small relative velocity with respect to its natal cloud (Kuhn et al. 2020), and there are no other ejected O stars in the vicinity seen in the *Gaia* DR2 data. It is a short-period spectroscopic binary with approximate masses (as estimated from their spectral types) of $\gtrsim$50 $M_\odot$ and ~25 $M_\odot$, there is no cluster around it, and the few relatively nearby association members are at most of intermediate mass. Therefore, it is a true counterexample to the hypothesis that massive stars (or massive binary systems) cannot form in relative isolation.

Another attempt at salvaging the Weidner & Kroupa (2006) hypothesis is the idea that very massive stars can exist in not so massive clusters because they form by collisions resulting from three-body interactions after the formation of the cluster (Oh & Kroupa 2018). Such three-body encounters indeed take place in clusters and this is one of the two classic mechanisms that produce O-type runaways (Poveda et al. 1967; Hoogerwerf et al. 2001; Maíz Apellániz et al. 2018b). However, for a runaway to be produced in such a way one needs a very compact cluster to start with, as otherwise there is little chance that the three-body interaction will take place. No such cluster exists in the case of the Bajamar star in the North America nebula, so that is not the way that system could have formed. We note that in that case, we would also have to explain that what we currently have is a short-period spectroscopic binary, implying that at least four stars should have been involved in the interaction (the two progenitors of the primary, the secondary, and the ejected star). We already made some of these points regarding LS III +46 11 and LS III +46 12 in Berkeley 90 in Maíz Apellániz et al. (2015a). With the results in this paper and the non-detection of ejected O stars from the cluster, we confirm that Berkeley 90 is an example of a low-mass cluster with two very massive systems and no other O stars that does not have the high stellar density at its core required for mergers from three-body interactions to be likely. Finally, we point to the case of Villafranca O-013, which is rather similar to Berkeley 90 but with an even poorer stellar density at its core: one very massive spectroscopic system, another O star, no other good candidates for being massive stars above 15 $M_\odot$, and no massive runaways. In summary, the results in this paper clearly point in the direction that massive stars can form in near-isolation or in relatively low-mass clusters and that star formation is a hierarchical process.

A corollary to this conclusion is that a fixed criterion to search for a stellar group around an O star cannot be established, as we had already anticipated in the sample selection subsection above. If the star(s) is (are) immersed in a rich cluster, the task is easy. If it is not, and a poorer cluster exists, one may still be detect the cluster if the contrast with the field population is high enough. As a third option, if a cluster is not seen, the star may be located in an association but identifying its members may be hard if it extends over a large region of the sky. Finally, there is the chance that the O star is isolated or nearly so, which could be caused by [a] being a runaway, in which case we would need to analyze its kinematics to search for an origin in a known stellar group; or by [b] having truly formed in near-isolation, in which case we can develop an ad-hoc method to see if any lower-mass stars can be detected in the vicinity with comparable distances and kinematics.

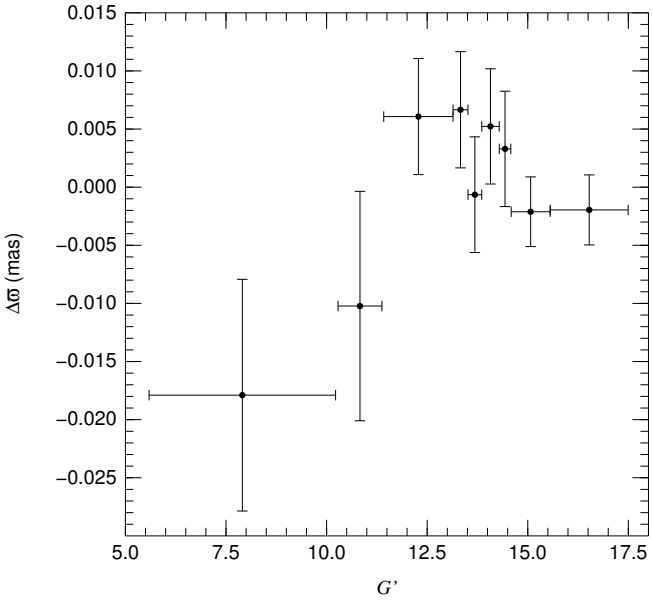

Fig. 4. Difference between individual stellar parallaxes and the group parallax as a function of G' for the stars in Villafranca O-001 to Villafranca O-013 plus Villafranca O-015 and Villafranca O-016. The data have been binned to see the effect as a function of magnitude. The horizontal error bars show the extent of G' magnitudes binned and the vertical error bars show the weighted standard deviation of the mean using as inputs the values with the external uncertainties.

4.5. The Gaia DR2 parallax zero point

Lindegren et al. (2018) presented the astrometric results from *Gaia* DR2 and detected the existence of a parallax zero point of $\approx$30 μas in the sense that *Gaia* DR2 parallaxes are too small and that is the value that should be added to correct for the zero point. To establish that value, Lindegren et al. (2018) used a sample of quasars, which in general are faint sources compared to typical *Gaia* DR2 sources. Other authors (Riess et al. 2018; Zinn et al. 2019; Khan et al. 2019; Chan & Bovy 2020) have found that for brighter (stellar) sources the zero point is $\approx$50 μas. Given the variability, in this work we used a zero point of 40 ± 10 μas, as already mentioned above.

Our data give us the opportunity of studying the magnitude dependence of the parallax zero point in a relative sense. We do that by plotting in Fig. 4 the difference between the stellar parallax of the members of all the groups in our sample (excluding the special case of Villafranca O-014) and the group parallax itself as a function of G'. The data are binned in magnitude to reduce the uncertainties but we note that the binning covers larger ranges for bright stars due to their relative scarcity. Even though the error bars are relatively large, the results are consistent with a difference of $\approx$20 μas between bright and dim stars found by other authors. The transition takes place around G' between 11 and 12.

We think this effect is the reason for the small difference in the distance to Trumpler 14 and Trumpler 16 between our results and those of Shull & Danforth (2019). Most of our stars in those groups are in the dim range as defined above while those authors use objects mostly in the bright region. They also apply a parallax zero point of 30 μas while we use one of 40 μas. Both differences move their distances towards higher values.

4.6. Future work

In the future, we will continue using *Gaia* to analyze more Galactic stellar groups with O stars and, if the resources allow it, extend the catalog to groups without them but with B stars. We will also revise the results once the early third data release becomes available in late 2020, as currently expected. Later on, we will also incorporate the new types of output from *Gaia* DR3 such as the spectrophotometry. The larger sample will allow us to study the spatial distribution of the groups containing O stars.

In addition to *Gaia* data, we will also incorporate results from GALANTE (Maíz Apellániz et al. 2019c; Lorenzo-Gutiérrez et al. 2019), a photometric survey that is imaging the northern Galactic Plane in seven narrow- and intermediate-band filters using the JAST/T80 telescope at Javalambre, Teruel, Spain. Each single-CCD-chip field has a size of 2 square degrees with a pixel size of 0.″55. The filter set has been especially tailored to measure the effective temperatures and extinction of OB stars and the survey includes different exposure times to achieve a large dynamic range. GALANTE will be used as a complement to *Gaia* data to study the Villafranca groups. The survey will be extended to the southern Galactic Plane in the future using the T-80S telescope at Cerro Tololo, Chile. GALANTE will allow us to overcome one of the limitations of *Gaia*, the photometric study of crowded and nebular regions, where the results for G are reliable but those for $G_{\rm BP}$ and $G_{\rm RP}$ are not. In turn, that will allow us to study extinction variations and derive the IMF more accurately.

Finally, we will keep obtaining new spectroscopy using GOSSS and adding new data to our optical+NIR high-resolution spectroscopic database LiLiMaRlin (Maíz Apellániz et al. 2019b) to characterize the stars in the Villafranca stellar groups. To those surveys, we will add WEAVE (Dalton 2016), a multi-fiber instrument that will be mounted at the *William Herschel* Telescope at La Palma, Spain in 2020. One of the WEAVE projects, SCIP (Stellar, Circumstellar, and Interstellar Physics), will obtain intermediate-resolution spectroscopy of a large number of OB stars in stellar groups in the northern Galactic Plane and their results will be used to improve our knowledge of their membership.

Acknowledgements. We dedicate this paper to the memory of Nolan R. Walborn, of whom the first and third authors were postdoctoral researchers and who sparked their interest in several of these stellar groups. We thank Danny Lennon for useful discussions on this topic. J.M.A. and A.S. acknowledge support from the Spanish Government Ministerio de Ciencia through grants AYA2016-75 931-C2-2-P and PGC2018-095 049-B-C22. R.H.B. acknowledges support from DIDULS Project 18 143 and the ESAC visitors program. This work has made use of data from the European Space Agency (ESA) mission *Gaia* (`https://www.cosmos.esa.int/gaia`), processed by the *Gaia* Data Processing and Analysis Consortium (DPAC, `https://www.cosmos.esa.int/web/gaia/dpac/consortium`). Funding for the DPAC has been provided by national institutions, in particular the institutions participating in the *Gaia* Multilateral Agreement. Additionally, this paper includes data obtained with the MPG/ESO 2.2 m Telescope at the Observatorio de La Silla, Chile; the 2.5 m du Pont Telescope at the Observatorio de Las Campanas, Chile; the 10 m *Hobby-Eberly* Telescope at McDonald Observatory, Texas, USA; the 4.2 m *William Herschel* Telescope and the 10.4 m Gran Telescopio Canarias at the Observatorio del Roque de los Muchachos, La Palma, Spain; and the 2.2 m Telescope at the Centro Astronómico Hispano Andaluz, Almería, Spain. We thank the staff at those observatories for their support. This research has made extensive use of the SIMBAD and VizieR databases, operated at CDS, Strasbourg, France.

References

Alexander, M. J., Hanes, R. J., Povich, M. S., & McSwain, M. V. 2016, AJ, 152, 190
Ambartsumian, V. A. 1958, Rev. Mod. Phys., 30, 944
Armandroff, T. E., & Herbst, W. 1981, AJ, 86, 1923
Armond, T., Reipurth, B., Bally, J., & Aspin, C. 2011, A&A, 528, A125
Arnal, M., Levato, H., García, B., & Morrell, N. 1987, Rev. Mex. Astron. Astrofís., 14, 423
Ascenso, J., Alves, J., Vicente, S., & Lago, M. T. V. T. 2007a, A&A, 476, 199
Ascenso, J., Alves, J., Beletsky, Y., & Lago, M. T. V. T. 2007b, A&A, 466, 137
Avedisova, V. S., & Palous, J. 1989, Bull. Astron. Inst. Czechoslov., 40, 42
Balser, D. S., Rood, R. T., Bania, T. M., & Anderson, L. D. 2011, ApJ, 738, 27
Barbá, R. H., Gamen, R. C., Arias, J. I., et al. 2010, Rev. Mex. Astron. Astrofís. Ser. Conf., 38, 30
Barbá, R. H., Gamen, R., Arias, J. I., & Morrell, N. I. 2017, in The Lives and Death-Throes of Massive Stars, IAU Symp., 329, 89
Baume, G., Carraro, G., Comeron, F., & de Elía, G. C. 2011, A&A, 531, A73
Baxter, E. J., Covey, K. R., Muench, A. A., et al. 2009, AJ, 138, 963
Becker, W., & Fenkart, R. 1963, Z. Astrophys., 56, 257
Becker, W., & Fenkart, R. 1971, A&AS, 4, 241
Benaglia, P., Koribalski, B., Peri, C. S., et al. 2013, A&A, 559, A31
Berlanas, S. R., Herrero, A., Comerón, F., et al. 2018, A&A, 612, A50
Berlanas, S. R., Wright, N. J., Herrero, A., Drew, J. E., & Lennon, D. J. 2019, MNRAS, 484, 1838
Bhardwaj, A., Panwar, N., Herczeg, G. J., Chen, W. P., & Singh, H. P. 2019, A&A, 627, A135
Bica, E., Bonatto, C., & Dutra, C. M. 2003, A&A, 405, 991
Binder, B. A., & Povich, M. S. 2018, ApJ, 864, 136
Bressert, E., Bastian, N., Evans, C. J., et al. 2012, A&A, 542, A49
Brown, A. G. A., Vallenari, A., Prusti, T., et al. 2018, A&A, 616, A1
Cambrésy, L., Beichman, C. A., Jarrett, T. H., & Cutri, R. M. 2002, AJ, 123, 2559
Campillay, A. R., Arias, J. I., Barbá, R. H., et al. 2019, MNRAS, 484, 2137
Cantat-Gaudin, T., Jordi, C., Vallenari, A., et al. 2018, A&A, 618, A93
Cantat-Gaudin, T., Krone-Martins, A., Sedaghat, N., et al. 2019, A&A, 624, A126
Cappa, C. E., Barbá, R. H., Duronea, N. U., et al. 2011, MNRAS, 415, 2844
Carraro, G., & Munari, U. 2004, MNRAS, 347, 625
Carraro, G., Romaniello, M., Ventura, P., & Patat, F. 2004, A&A, 418, 525
Carraro, G., Turner, D., Majaess, D., & Baume, G. 2013, A&A, 555, A50
Castro-Ginard, A., Jordi, C., Luri, X., Cantat-Gaudin, T., & Balaguer-Núñez, L. 2019, A&A, 627, A35
Castro-Ginard, A., Jordi, C., Luri, X., et al. 2020, A&A, 635, A45
Caswell, J. L., & Haynes, R. F. 1987, A&A, 171, 261
Cersosimo, J. C., Muller, R. J., Figueroa Vélez, S., et al. 2007, ApJ, 656, 248
Chan, V. C., & Bovy, J. 2020, MNRAS, 493, 4367
Chibueze, J. O., Kamezaki, T., Omodaka, T., et al. 2016, MNRAS, 460, 1839
Chini, R., Elsaesser, H., & Neckel, T. 1980, A&A, 91, 186
Comerón, F., & Pasquali, A. 2005, A&A, 430, 541
Comerón, F., & Pasquali, A. 2012, A&A, 543, A101
Comerón, F., Pasquali, A., Rodighiero, G., et al. 2002, A&A, 389, 874
Crampton, D., Georgelin, Y. M., & Georgelin, Y. P. 1978, A&A, 66, 1
Crowther, P. A., & Dessart, L. 1998, MNRAS, 296, 622
Crowther, P. A., & Walborn, N. R. 2011, MNRAS, 416, 1311
Crowther, P. A., Schnurr, O., Hirschi, R., et al. 2010, MNRAS, 408, 731
Dalton, G. 2016, in Multi-Object Spectroscopy in the Next Decade: Big Questions, Large Surveys, and Wide Fields, eds. I. Skillen, M. Balcells, & S. Trager, ASP Conf. Ser., 507, 97
Dame, T. M. 2007, ApJ, 665, L163
Damiani, F., Klutsch, A., Jeffries, R. D., et al. 2017a, A&A, 603, A81
Damiani, F., Pillitteri, I., & Prisinzano, L. 2017b, A&A, 602, A115
Davidson, K., Helmel, G., & Humphreys, R. M. 2018, Res. Notes Am. Astron. Soc., 2, 133
de La Fuente Marcos, R., & de La Fuente Marcos, C. 2009, A&A, 500, L13
de Pree, C. G., Nysewander, M. C., & Goss, W. M. 1999, AJ, 117, 2902
Dieter, N. H. 1967, ApJ, 150, 435
Drew, J. E., Herrero, A., Mohr-Smith, M., et al. 2018, MNRAS, 480, 2109
Drew, J. E., Monguió, M., & Wright, N. J. 2019, MNRAS, 486, 1034
Drissen, L., Moffat, A. F. J., Walborn, N. R., & Shara, M. M. 1995, AJ, 110, 2235
Dutra, C. M., Bica, E., Soares, J., & Barbuy, B. 2003, A&A, 400, 533
Elmegreen, B. G. 2010, IAU Symp., 266, 3
Fang, M., van Boekel, R., King, R. R., et al. 2012, A&A, 539, A119
Feinstein, A. 1983, Ap&SS, 96, 293
Feinstein, A., Marraco, H. G., & Muzzio, J. C. 1973, A&AS, 12, 331
Feldbrugge, P. T. M., & van Genderen, A. M. 1991, A&AS, 91, 209
Fich, M., & Blitz, L. 1984, ApJ, 279, 125
Fitzgerald, M. P. 1987, MNRAS, 229, 227
Fitzgerald, M. P., & Moffat, A. F. J. 1974, AJ, 79, 873
Forte, J. C. 1978, AJ, 83, 1199
Fukui, Y., Kohno, M., Yokoyama, K., et al. 2018, PASJ, 70, S41
Furukawa, N., Dawson, J. R., Ohama, A., et al. 2009, ApJ, 696, L115

Gamen, R. C., Barbá, R., Rubio, M., Méndez, R. A., & Minniti, D. 2006, Rev. Mex. Astron. Astrofís., 26, 72
Georgelin, Y. P., & Georgelin, Y. M. 1970, A&A, 6, 349
Georgelin, Y. M., Georgelin, Y. P., & Roux, S. 1973, A&A, 25, 337
Georgelin, Y. M., Russeil, D., Amram, P., et al. 2000, A&A, 357, 308
Gilmore, G., Randich, S., Asplund, M., et al. 2012, The Messenger, 147, 25
Gómez, D. O., & Niemelä, V. S. 1987, MNRAS, 224, 641
Goss, W. M., Radhakrishnan, V., Brooks, J. W., & Murray, J. D. 1972, ApJS, 24, 123
Gum, C. S. 1955, Mem. R. Astron. Soc., 67, 155
Gvaramadze, V. V., Kniazev, A. Y., Kroupa, P., & Oh, S. 2011, A&A, 535, A29
Gvaramadze, V. V., Weidner, C., Kroupa, P., & Pflamm-Altenburg, J. 2012, MNRAS, 424, 3037
Hanson, M. M. 2003, ApJ, 597, 957
Hanson, M. M., Howarth, I. D., & Conti, P. S. 1997, ApJ, 489, 698
Harten, R., & Felli, M. 1980, A&A, 89, 140
Hénault-Brunet, V., Gieles, M., Evans, C. J., et al. 2012, A&A, 545, L1
Herbig, G. H. 1958, ApJ, 128, 259
Herbst, W., & Havlen, R. J. 1977, A&AS, 30, 279
Hoffmeister, V. H., Chini, R., Scheyda, C. M., et al. 2008, ApJ, 686, 310
Hoogerwerf, R., de Bruijne, J. H. J., & de Zeeuw, P. T. 2001, A&A, 365, 49
Hron, J. 1987, A&A, 176, 34
Humphreys, R. M. 1978, ApJS, 38, 309
Hur, H., Sung, H., & Bessell, M. S. 2012, AJ, 143, 41
Hur, H., Park, B.-G., Sung, H., et al. 2015, MNRAS, 446, 3797
Jackson, R. J., Jeffries, R. D., Wright, N. J., et al. 2020, MNRAS, 496, 4701
Johnson, H. M. 1973, ApJ, 182, 497
Johnson, H. L., & Morgan, W. W. 1954, ApJ, 119, 344
Kalari, V. M., Vink, J. S., de Wit, W. J., Bastian, N. J., & Méndez, R. A. 2019, A&A, 625, L2
Kaltcheva, N. T., & Golev, V. K. 2012, PASP, 124, 128
Kamezaki, T., Imura, K., Omodaka, T., et al. 2014, ApJS, 211, 18
Khan, S., Miglio, A., Mosser, B., et al. 2019, A&A, 628, A35
Kharchenko, N. V., Piskunov, A. E., Schilbach, E., Röser, S., & Scholz, R.-D. 2013, A&A, 558, A53
Kiminki, D. C., Kobulnicky, H. A., Kinemuchi, K., et al. 2007, ApJ, 664, 1102
Kiminki, D. C., Kobulnicky, H. A., Vargas Álvarez, C. A., Alexander, M. J., & Lundquist, M. J. 2015, ApJ, 811, 85
Knödlseder, J. 2000, A&A, 360, 539
Kochanek, C. S., Shappee, B. J., Stanek, K. Z., et al. 2017, PASP, 129, 104502
Kroupa, P. 2004, New Astron. Rev., 48, 47
Krumholz, M. R., & McKee, C. F. 2020, MNRAS, 494, 624
Kuhn, M. A., Hillenbrand, L. A., Sills, A., Feigelson, E. D., & Getman, K. V. 2019, ApJ, 870, 32
Kuhn, M. A., Hillenbrand, L. A., Carpenter, J. M., & Avelar Menendez, A. R. 2020, ApJ, 899, 128
Lada, C. J., & Lada, E. A. 2003, ARA&A, 41, 57
Laugalys, V., & Straižys, V. 2002, Balt. Astron., 11, 205
Laugalys, V., Straižys, V., Vrba, F. J., et al. 2006, Balt. Astron., 15, 483
Lim, B., Nazé, Y., Gosset, E., & Rauw, G. 2019, MNRAS, 490, 440
Lima, E. F., Bica, E., Bonatto, C., & Saito, R. K. 2014, A&A, 568, A16
Lindegren, L., Hernández, J., Bombrun, A., et al. 2018, A&A, 616, A2
Lodén, L. O. 1966, Arkiv for Astronomi, 4, 65
Lorenzo, J., Simón-Díaz, S., Negueruela, I., et al. 2017, A&A, 606, A54
Lorenzo-Gutiérrez, A., Alfaro, E. J., Maíz Apellániz, J., et al. 2019, MNRAS, 486, 966
Luo, A. L., Zhao, Y.-H., Zhao, G., et al. 2015, Res. Astron. Astrophys., 15, 1095
Mahy, L., Gosset, E., Manfroid, J., et al. 2018, A&A, 616, A75
Maíz Apellániz, J. 2001a, ApJ, 563, 151
Maíz Apellániz, J. 2001b, AJ, 121, 2737
Maíz Apellániz, J. 2005, in The Three-Dimensional Universe with Gaia, eds. C. Turon, K. S. O'Flaherty, & M. A. C. Perryman, ESA Spec. Publ., 576, 179
Maíz Apellániz, J. 2010, A&A, 518, A1
Maíz Apellániz, J. 2019, A&A, 630, A119
Maíz Apellániz, J., & Barbá, R. H. 2018, A&A, 613, A9
Maíz Apellániz, J., & Barbá, R. H. 2020, A&A, 636, A28
Maíz Apellániz, J., & Weiler, M. 2018, A&A, 619, A180
Maíz Apellániz, J., & Sota, A. 2008, Rev. Mex. Astron. Astrofís. Ser. Conf., 33, 44
Maíz Apellániz, J., Walborn, N. R., Galué, H. Á., & Wei, L. H. 2004, ApJS, 151, 103
Maíz Apellániz, J., Walborn, N. R., Morrell, N. I., Niemelä, V. S., & Nelan, E. P. 2007, ApJ, 660, 1480
Maíz Apellániz, J., Alfaro, E. J., & Sota, A. 2008, ArXiv e-prints [arXiv:0804.2553]
Maíz Apellániz, J., Sota, A., Walborn, N. R., et al. 2011, in Highlights of Spanish Astrophysics VI, eds. M. R. Zapatero Osorio, J. Gorgas, & J. Maíz Apellániz, 467
Maíz Apellániz, J., Pellerin, A., Barbá, R. H., et al. 2012, in Astronomical Society of the Pacific Conference Series, eds. L. Drissen, C. Robert, N. St-Louis, & A. F. J. Moffat, 465, 484
Maíz Apellániz, J., Evans, C. J., Barbá, R. H., et al. 2014, A&A, 564, A63
Maíz Apellániz, J., Negueruela, I., Barbá, R. H., et al. 2015a, A&A, 579, A108
Maíz Apellániz, J., Alfaro, E. J., Arias, J. I., et al. 2015b, in Highlights of Spanish Astrophysics VIII, eds. A. J. Cenarro, F. Figueras, & C. Hernández-Monteagudo, 603
Maíz Apellániz, J., Sota, A., Arias, J. I., et al. 2016, ApJS, 224, 4
Maíz Apellániz, J., Sana, H., Barbá, R. H., Le Bouquin, J.-B., & Gamen, R. C. 2017, MNRAS, 464, 3561
Maíz Apellániz, J., Barbá, R. H., Simón-Díaz, S., et al. 2018a, A&A, 615, A161
Maíz Apellániz, J., Pantaleoni González, M., Barbá, R. H., et al. 2018b, A&A, 616, A149
Maíz Apellániz, J., Trigueros Páez, E., Negueruela, I., et al. 2019a, A&A, 626, A20 (MONOS I)
Maíz Apellániz, J., Trigueros Páez, E., Jiménez Martínez, I., et al. 2019b, in Highlights on Spanish Astrophysics X, eds. B. Montesinos, A. Asensio Ramos, & F. Buitrago, 420
Maíz Apellániz, J., Alfaro, E. J., Barbá, R. H., et al. 2019c, in Highlights on Spanish Astrophysics X, eds. B. Montesinos, A. Asensio Ramos, & F. Buitrago, 346
Majaess, D. 2013, Ap&SS, 344, 175
Marco, A., & Negueruela, I. 2017, MNRAS, 465, 784
Massey, P., & Johnson, J. 1993, AJ, 105, 980
Massey, P., & Thompson, A. B. 1991, AJ, 101, 1408
Massey, P., DeGioia-Eastwood, K., & Waterhouse, E. 2001, AJ, 121, 1050
Mayer, P., & Macák, P. 1973, Bull. Astron. Inst. Czechoslov., 24, 50
Megier, A., Strobel, A., Galazutdinov, G. A., & Krełowski, J. 2009, A&A, 507, 833
Melena, N. W., Massey, P., Morrell, N. I., & Zangari, A. M. 2008, AJ, 135, 878
Melnick, J., & Grosbol, P. 1982, A&A, 107, 23
Melnick, J., Tapia, M., & Terlevich, R. 1989, A&A, 213, 89
Mendoza V., E. E., & Gómez, T. 1980, MNRAS, 190, 623
Mikami, T., & Ogura, K. 2001, Ap&SS, 275, 441
Miller, J. S. 1968, ApJ, 151, 473
Moffat, A. F. J. 1974, A&A, 35, 315
Moffat, A. F. J. 1983, A&A, 124, 273
Moffat, A. F. J., & Vogt, N. 1973, A&AS, 10, 135
Moffat, A. F. J., & Vogt, N. 1975, A&AS, 20, 125
Moffat, A. F. J., Shara, M. M., & Potter, M. 1991, AJ, 102, 642
Moffat, A. F. J., Drissen, L., & Shara, M. M. 1994, ApJ, 436, 183
Mohr-Smith, M., Drew, J. E., Napiwotzki, R., et al. 2017, MNRAS, 465, 1807
Moreno, M. A., & Chavarría-K., C. 1986, A&A, 161, 130
Moreno-Corral, M. A., Chavarría-K. C., & de Lara, E. 2002, Rev. Mex. Astron. Astrofís., 38, 141
Morrell, N. I., García, B., & Levato, H. 1988, PASP, 100, 1431
Morrell, N. I., Barbá, R. H., Niemelä, V. S., et al. 2001, MNRAS, 326, 85
Moscadelli, L., Reid, M. J., Menten, K. M., et al. 2009, ApJ, 693, 406
Motch, C., Haberl, F., Dennerl, K., Pakull, M., & Janot-Pacheco, E. 1997, A&A, 323, 853
Nazé, Y., Rauw, G., & Manfroid, J. 2008, A&A, 483, 171
Nazé, Y., Mahy, L., Damerdji, Y., et al. 2012, A&A, 546, A37
Neckel, T. 1978, A&A, 69, 51
Neckel, T., Harris, A. W., & Eiroa, C. 1980, A&A, 92, L9
Negueruela, I., Maíz Apellániz, J., Simón-Díaz, S., et al. 2015, in Highlights of Spanish Astrophysics VIII, eds. A. J. Cenarro, F. Figueras, & C. Hernández-Monteagudo, 524
Neri, L. J., Chavarría-K., C., & de Lara, E. 1993, A&AS, 102, 201
Nielbock, M., Chini, R., Jütte, M., & Manthey, E. 2001, A&A, 377, 273
Niemelä, V. S., & Gamen, R. C. 2005, MNRAS, 356, 974
Niemelä, V. S., Gamen, R. C., Barbá, R. H., et al. 2008, MNRAS, 389, 1447
Nürnberger, D. E. A., Bronfman, L., Yorke, H. W., & Zinnecker, H. 2002, A&A, 394, 253
Ogura, K., & Ishida, K. 1976, PASJ, 28, 35
Oh, S., & Kroupa, P. 2018, MNRAS, 481, 153
Pandey, A. K., Ogura, K., & Sekiguchi, K. 2000, PASJ, 52, 847
Park, B.-G., Sung, H., Bessell, M. S., & Kang, Y. H. 2000, AJ, 120, 894
Pérez, M. R., The, P. S., & Westerlund, B. E. 1987, PASP, 99, 1050
Piatti, A. E., Bica, E., & Claria, J. J. 1998, A&AS, 127, 423
Piatti, A. E., Clariá, J. J., & Ahumada, A. V. 2010, PASP, 122, 516
Pišmiš, P. 1959, Boletin de los Observatorios Tonantzintla y Tacubaya, 2, 37
Pišmiš, P., & Moreno, M. A. 1976, Rev. Mex. Astron. Astrofís., 1, 373
Platais, I., Lennon, D. J., van der Marel, R. P., et al. 2018, AJ, 156, 98
Poveda, A., Ruiz, J., & Allen, C. 1967, Boletin de los Observatorios Tonantzintla y Tacubaya, 4, 86
Povich, M. S., Stone, J. M., Churchwell, E., et al. 2007, ApJ, 660, 346
Povich, M. S., Churchwell, E., Bieging, J. H., et al. 2009, ApJ, 696, 1278

Prusti, T., de Bruijne, J. H. J., Brown, A. G. A., et al. 2016, A&A, 595, A1
Puga, E., Marín-Franch, A., Najarro, F., et al. 2010, A&A, 517, A2
Quireza, C., Rood, R. T., Bania, T. M., Balser, D. S., & Maciel, W. J. 2006, ApJ, 653, 1226
Ramírez-Tannus, M. C., Poorta, J., Bik, A., et al. 2020, A&A, 633, A155
Rastorguev, A. S., Glushkova, E. V., Dambis, A. K., & Zabolotskikh, M. V. 1999, Astron. Lett., 25, 595
Rauw, G., De Becker, M., Nazé, Y., et al. 2004, A&A, 420, L9
Rauw, G., Sana, H., & Nazé, Y. 2011, A&A, 535, A40
Reddish, V. C., Lawrence, L. C., & Pratt, N. M. 1966, Publ. R. Obs. Edinb., 5, 111
Reipurth, B., & Schneider, N. 2008, Star Formation and Young Clusters in Cygnus (ASP), 4, 36
Reiter, M., & Parker, R. J. 2019, MNRAS, 486, 4354
Renzo, M., Zapartas, E., de Mink, S. E., et al. 2019, A&A, 624, A66
Riess, A. G., Casertano, S., Yuan, W., et al. 2018, ApJ, 861, 126
Roberts, L. C., Gies, D. R., Parks, J. R., et al. 2010, AJ, 140, 744
Rochau, B., Brandner, W., Stolte, A., et al. 2011, MNRAS, 418, 949
Roman-Lopes, A. 2012, MNRAS, 427, L65
Roman-Lopes, A. 2013a, MNRAS, 435, L73
Roman-Lopes, A. 2013b, MNRAS, 433, 712
Roman-Lopes, A., Barbá, R. H., & Morrell, N. I. 2011, MNRAS, 416, 501
Roman-Lopes, A., Franco, G. A. P., & Sanmartim, D. 2016, ApJ, 823, 96
Routly, P. M., & Spitzer, L., Jr. 1951, AJ, 56, 138
Routly, P. M., & Spitzer, L., Jr. 1952, ApJ, 115, 227
Russeil, D. 2003, A&A, 397, 133
Russeil, D., Adami, C., & Georgelin, Y. M. 2007, A&A, 470, 161
Russeil, D., Zavagno, A., Adami, C., et al. 2012, A&A, 538, A142
Russeil, D., Adami, C., Bouret, J. C., et al. 2017, A&A, 607, A86
Rygl, K. L. J., Brunthaler, A., Sanna, A., et al. 2012, A&A, 539, A79
Sagar, R., & Joshi, U. C. 1983, MNRAS, 205, 747
Sagar, R., Munari, U., & de Boer, K. S. 2001, MNRAS, 327, 23
Sana, H., Le Bouquin, J.-B., Mahy, L., et al. 2013, A&A, 553, A131
Sánchez-Bermúdez, J., Schödel, R., Alberdi, A., et al. 2013, A&A, 554, L4
Schnurr, O., Casoli, J., Chené, A.-N., Moffat, A. F. J., & St-Louis, N. 2008, MNRAS, 389, L38
Sharpless, S., & Osterbrock, D. 1952, ApJ, 115, 89
Shaver, P. A., McGee, R. X., Newton, L. M., Danks, A. C., & Pottasch, S. R. 1983, MNRAS, 204, 53
Sher, D. 1965, MNRAS, 129, 237
Shull, J. M., & Danforth, C. W. 2019, ApJ, 882, 180
Simón-Díaz, S., Castro, N., García, M., & Herrero, A. 2011, IAU Symp., 272, 310
Simón-Díaz, S., Negueruela, I., Maíz Apellániz, J., et al. 2015, in Highlights of Spanish Astrophysics VIII, eds. A. J. Cenarro, F. Figueras, & C. Hernández-Monteagudo, 576
Smith, N. 2006a, MNRAS, 367, 763
Smith, N. 2006b, ApJ, 644, 1151
Smith, N., Barbá, R. H., & Walborn, N. R. 2004, MNRAS, 351, 1457
Sota, A., Maíz Apellániz, J., Walborn, N. R., et al. 2011, ApJS, 193, 24
Sota, A., Maíz Apellániz, J., Morrell, N. I., et al. 2014, ApJS, 211, 10
Soubiran, C., Cantat-Gaudin, T., Romero-Gómez, M., et al. 2018, A&A, 619, A155
Stark, A. A. 1984, ApJ, 281, 624
Stark, A. A., & Brand, J. 1989, ApJ, 339, 763
Straižys, V., & Laugalys, V. 2008, Balt. Astron., 17, 143
Straižys, V., Corbally, C. J., & Laugalys, V. 1999, Balt. Astron., 8, 355
Straizys, V., Goldberg, E. P., Meistas, E., & Vansevicius, V. 1989, A&A, 222, 82
Straizys, V., Kazlauskas, A., Vansevicius, V., & Cernis, K. 1993, Balt. Astron., 2, 171
Straw, S., Hyland, A. R., Jones, T. J., et al. 1987, ApJ, 314, 283
Sung, H., & Bessell, M. S. 2004, AJ, 127, 1014
Sung, H., Bessell, M. S., & Lee, S.-W. 1997, AJ, 114, 2644
Tadross, A. L. 2008, MNRAS, 389, 285
Tapia, M., Roth, M., Marraco, H., & Ruiz, M. T. 1988, MNRAS, 232, 661
Tapia, M., Roth, M., Vázquez, R. A., & Feinstein, A. 2003, MNRAS, 339, 44
ten Brummelaar, T. A., O'Brien, D. P., Mason, B. D., et al. 2011, AJ, 142, 21
Tetzlaff, N., Neuhäuser, R., & Hohle, M. M. 2011, MNRAS, 410, 190
Thé, P. S., & Vleeming, G. 1971, A&A, 14, 120
Thé, P. S., Bakker, R., & Antalova, A. 1980, A&AS, 41, 93
Torres-Dodgen, A. V., Carroll, M., & Tapia, M. 1991, MNRAS, 249, 1
Tramper, F., Sana, H., Fitzsimons, N. E., et al. 2016, MNRAS, 455, 1275
Turner, D. G., & Moffat, A. F. J. 1980, MNRAS, 192, 283
van den Bergh, S. 1978, A&A, 63, 275
van der Hucht, K. A. 2001, New Astron. Rev., 45, 135
Vargas Álvarez, C. A., Kobulnicky, H. A., Bradley, D. R., et al. 2013, AJ, 145, 125
Vazquez, R. A., & Feinstein, A. 1992, A&AS, 92, 863
Walborn, N. R. 1971, ApJ, 167, L31
Walborn, N. R. 1973a, ApJ, 182, L21
Walborn, N. R. 1973b, ApJ, 179, 517
Walborn, N. R. 1973c, ApJ, 180, L35
Walborn, N. R. 1982a, ApJS, 48, 145
Walborn, N. R. 1982b, AJ, 87, 1300
Walborn, N. R. 1995, Rev. Mex. Astron. Astrofís. Ser. Conf., 2, 51
Walborn, N. R., & Fitzpatrick, E. L. 2000, PASP, 112, 50
Walborn, N. R., Danks, A. C., Vieira, G., & Landsman, W. B. 2002a, ApJS, 140, 407
Walborn, N. R., Howarth, I. D., Lennon, D. J., et al. 2002b, AJ, 123, 2754
Walborn, N. R., Sota, A., Maíz Apellániz, J., et al. 2010, ApJ, 711, L143
Walker, M. F. 1956, ApJ, 124, 668
Ward, J. L., Kruijssen, J. M. D., & Rix, H.-W. 2020, MNRAS, 495, 663
Weidner, C., & Kroupa, P. 2006, MNRAS, 365, 1333
Weiler, M., Carrasco, J. M., Fabricius, C., & Jordi, C. 2020, A&A, 637, A85
Wenger, T. V., Balser, D. S., Anderson, L. D., & Bania, T. M. 2018, ApJ, 856, 52
Westerlund, B. 1961, Arkiv for Astronomi, 2, 419
Whiteoak, J. B. 1963, MNRAS, 125, 105
Williams, A. M., Gies, D. R., Bagnuolo, W. G., Jr., et al. 2001, ApJ, 548, 425
Wilson, T. L., Mezger, P. G., Gardner, F. F., & Milne, D. K. 1970, A&A, 6, 364
Wright, N. J., Parker, R. J., Goodwin, S. P., & Drake, J. J. 2014, MNRAS, 438, 639
Wright, N. J., Bouy, H., Drew, J. E., et al. 2016, MNRAS, 460, 2593
Wynn-Williams, C. G., Becklin, E. E., & Neugebauer, G. 1974, ApJ, 187, 473
Xu, Y., Moscadelli, L., Reid, M. J., et al. 2011, ApJ, 733, 25
Yadav, R. K., Pandey, A. K., Sharma, S., et al. 2015, New Astron., 34, 27
Zeidler, P., Sabbi, E., Nota, A., et al. 2015, AJ, 150, 78
Zhang, S., Xu, Y., & Yang, J. 2014, AJ, 147, 46
Zinn, J. C., Pinsonneault, M. H., Huber, D., & Stello, D. 2019, ApJ, 878, 136
Zucker, C., Speagle, J. S., Schlafly, E. F., et al. 2020, A&A, 633, A51

Appendix A: Additional tables and figures

In this appendix, we present additional material: a list of the existing literature distances for the stellar groups in this paper, the plots used to analyze the *Gaia* DR2 results for Villafranca O-001 to Villafranca O-014 (see MA19 for the equivalent plots for Villafranca O-015 and Villafranca O-016), and a list of the candidate runaways detected.

Table A.1. Literature distances.

ID	Distance (pc)	Target	Description	Ref.
O-001	9490^{+190}_{-210}	NGC 3603	*Gaia* DR2 parallax, no covariance term	C18
	7600	NGC 3603	Visible spectro-photometry	M08
	6900^{+600}_{-600}	NGC 3603	Visible CMD	S04
	7900	H II gas	Kinematic distance	R03
	7700^{+200}_{-200}	H II gas	Kinematic distance	N02
	7200^{+1200}_{-1200}	NGC 3603	Visible CMD	S01
	6300^{+600}_{-600}	NGC 3603	Visible CMD	P00a
	6100^{+600}_{-600}	H II gas	Kinematic distance	d99
	10 100	NGC 3603	Visible spectro-photometry	C98
	7200	NGC 3603	Visible CMD	M89
	8600^{+500}_{-500}	H II gas	Kinematic distance	S83a
	7000^{+500}_{-500}	NGC 3603	Visible spectro-photometry	M83
	5300^{+1600}_{-1200}	NGC 3603	Visible CMD	M82
	7200^{+800}_{-1000}	H II gas	Kinematic distance	v78
	8100^{+800}_{-800}	NGC 3603	Visible CMD	M74
	8400	H II gas	Kinematic distance	G72
	5720	NGC 3603	Visible CMD	B71
	3500	NGC 3603	Visible CMD	S65
O-002 + O-003	2500^{+250}_{-250}	Molecular clouds	*Gaia* DR2 parallax	Z20
	2400^{+200}_{-200}	Car OB1	*Gaia* DR2 parallax	L19
	2640^{+310}_{-250}	Trumpler 14	*Gaia* DR2 parallax	K19
	2610^{+310}_{-250}	Trumpler 16	*Gaia* DR2 parallax	K19
	2680^{+310}_{-310}	Trumpler 14	*Gaia* DR2 parallax	S19
	2550^{+300}_{-300}	Trumpler 16	*Gaia* DR2 parallax	S19

Notes. The specific target and a brief description of the method is given. Note that "spectro-photometry" indicates a combination of spectroscopic and photometric methods. For simplicity, random and systematic uncertainties have been combined.

References. A81: Armandroff & Herbst (1981), A89: Avedisova & Palous (1989), A07: Ascenso et al. (2007b), B63: Becker & Fenkart (1963), B71: Becker & Fenkart (1971), B03: Bica et al. (2003), B09: Baxter et al. (2009), B11a: Baume et al. (2011), B11b: Balser et al. (2011), B13: Benaglia et al. (2013), B18: Binder & Povich (2018), B19a: Berlanas et al. (2019), B19b: Bhardwaj et al. (2019), C05: Comerón & Pasquali (2005), C78: Crampton et al. (1978), C80: Chini et al. (1980), C87: Caswell & Haynes (1987), C98: Crowther & Dessart (1998), C02: Cambrésy et al. (2002), C04a: Carraro et al. (2004), C04b: Carraro & Munari (2004), C07: Cersosimo et al. (2007), C13: Carraro et al. (2013), C16: Chibueze et al. (2016), C18: Cantat-Gaudin et al. (2018), D67: Dieter (1967), d99: de Pree et al. (1999), D07: Dame (2007), D17: Damiani et al. (2017b), D18: Davidson et al. (2018), F73: Feinstein et al. (1973), F74: Fitzgerald & Moffat (1974), F78: Forte (1978), F83: Feinstein (1983), F84: Fich & Blitz (1984), F87: Fitzgerald (1987), F91: Feldbrugge & van Genderen (1991), F09: Furukawa et al. (2009), F12: Fang et al. (2012), G70: Georgelin & Georgelin (1970), G72: Goss et al. (1972), G73: Georgelin et al. (1973), G00: Georgelin et al. (2000), G06: Gamen et al. (2006), G11: Gvaramadze et al. (2011), H58: Herbig (1958), H77: Herbst & Havlen (1977), H78: Humphreys (1978), H87: Hron (1987), H97: Hanson et al. (1997), H03: Hanson (2003), H08: Hoffmeister et al. (2008), H12: Hur et al. (2012), H15: Hur et al. (2015), J54: Johnson & Morgan (1954), J73: Johnson (1973), K12: Kaltcheva & Golev (2012), K13: Kharchenko et al. (2013), K14: Kamezaki et al. (2014), K15: Kiminki et al. (2015), K19: Kuhn et al. (2019), L66: Lodén (1966), L02: Laugalys & Straižys (2002), L06: Laugalys et al. (2006), L14: Lima et al. (2014), L17: Lorenzo et al. (2017), L19: Lim et al. (2019), M68: Miller (1968), M73a: Mayer & Macák (1973), M73b: Moffat & Vogt (1973), M74: Moffat (1974), M75: Moffat & Vogt (1975), M80: Mendoza V. & Gómez (1980), M82: Melnick & Grosbol (1982), M83: Moffat (1983), M86: Moreno & Chavarría-K. (1986), M88: Morrell et al. (1988), M89: Melnick et al. (1989), M91a: Moffat et al. (1991), M91b: Massey & Thompson (1991), M93: Massey & Johnson (1993), M97: Motch et al. (1997), M01: Massey et al. (2001), M02: Moreno-Corral et al. (2002), M08: Melena et al. (2008), M09a: Megier et al. (2009), M09b: Moscadelli et al. (2009), M15: Maíz Apellániz et al. (2015a), M17a: Mohr-Smith et al. (2017), M17b: Marco & Negueruela (2017), M18: Mahy et al. (2018), N78: Neckel (1978), N80: Neckel et al. (1980), N01: Nielbock et al. (2001), N02: Nürnberger et al. (2002), N93: Neri et al. (1993), O76: Ogura & Ishida (1976), P76: Pišmiš & Moreno (1976), P87: Pérez et al. (1987), P98: Piatti et al. (1998), P00a: Pandey et al. (2000), P00b: Park et al. (2000), P07: Povich et al. (2007), P10: Puga et al. (2010), Q06: Quireza et al. (2006), R66: Reddish et al. (1966), R99: Rastorguev et al. (1999), R03: Russeil (2003), R07: Russeil et al. (2007), R10: Roberts et al. (2010), R11: Rauw et al. (2011), R12a: Russeil et al. (2012), R12b: Rygl et al. (2012), R17: Russeil et al. (2017), R20: Ramírez-Tannus et al. (2020), S52: Sharpless & Osterbrock (1952), S65: Sher (1965), S83a: Shaver et al. (1983), S83b: Sagar & Joshi (1983), S84: Stark (1984), S89a: Stark & Brand (1989), S89b: Straizys et al. (1989), S93: Straizys et al. (1993), S97: Sung et al. (1997), S01: Sagar et al. (2001), S04: Sung & Bessell (2004), S06: Smith (2006b), S19: Shull & Danforth (2019), T71: Thé & Vleeming (1971), T80: Thé et al. (1980), T88: Tapia et al. (1988), T91: Torres-Dodgen et al. (1991), T03: Tapia et al. (2003), T08: Tadross (2008), v78: van den Bergh (1978), V92: Vazquez & Feinstein (1992), V13: Vargas Álvarez et al. (2013), W56: Walker (1956), W61: Westerlund (1961), W63: Whiteoak (1963), W70: Wilson et al. (1970), W73a: Walborn (1973b), W73b: Walborn (1973c), W82: Walborn (1982b), W95: Walborn (1995), W18: Wenger et al. (2018), X11: Xu et al. (2011), Y15: Yadav et al. (2015), Z15: Zeidler et al. (2015), Z20: Zucker et al. (2020).

Table A.1. continued.

ID	Distance (pc)	Target	Description	Ref.
O-002 + O-003 (continued)	2690^{+400}_{-400}	Car OB1	*Gaia* DR2 parallax	B18
	305	Trumpler 14	*Gaia* DR2 parallax	D18
	2600	Trumpler 16	*Gaia* DR2 parallax	D18
	2414^{+9}_{-9}	Trumpler 14	*Gaia* DR2 parallax, no covariance term	C18
	2395^{+12}_{-11}	Trumpler 16	*Gaia* DR2 parallax, no covariance term	C18
	2900^{+300}_{-300}	Trumpler 14 + Trumpler 16	Visible + NIR CMD	H12
	4200^{+1800}_{-1800}	Trumpler 16	Ca II ISM lines	M09a
	2350^{+50}_{-50}	η Car	Geometric distance from Homunculus expansion	S06
	2500^{+300}_{-300}	Trumpler 14	Visible CMD	C04a
	4000^{+300}_{-300}	Trumpler 16	Visible CMD	C04a
	2800	Trumpler 14	Visible + NIR CMD	T03
	2500	Trumpler 16	Visible + NIR CMD	T03
	2580	Car OB1	Statistical parallaxes	R99
	2800	Car OB1	Visible spectro-photometry with $R_{5495} = 3.0$	W95
	2250	Car OB1	Visible spectro-photometry with $R_{5495} = 4.0$	W95
	3610^{+300}_{-300}	Trumpler 14	Visible spectro-photometry	M93
	3150^{+130}_{-130}	Trumpler 16	Visible spectro-photometry	M93
	3960^{+130}_{-130}	Trumpler 14	Visible spectro-photometry	M88
	2400^{+200}_{-200}	Car OB1	Visible + NIR CMD	T88
	2750^{+250}_{-250}	Trumpler 14	Visible CMD	F83
	2700	H II gas	Kinematic distance	S83a
	2800	Trumpler 16	Visible spectro-photometry	W82
	2800	Car OB1	Visible CMD with $R_{5495} = 3.3$	T80
	2350	Car OB1	Visible CMD with $R_{5495} = 4.0$	T80
	3600^{+150}_{-150}	Trumpler 14	Visible spectro-photometry	H78
	2690^{+150}_{-150}	Trumpler 16	Visible spectro-photometry	H78
	2400	Car OB1	Visible CMD	F78
	3500	Trumpler 14	Visible spectro-photometry	W73a
	2600	Trumpler 16	Visible spectro-photometry	W73a
	3390^{+300}_{-300}	Trumpler 14 + Trumpler 16	Visible CMD with $R_{5495} = 3.0$	F73
	2650^{+240}_{-240}	Trumpler 14 + Trumpler 16	Visible CMD with $R_{5495} = 4.0$	F73
	1650	Trumpler 14	Visible CMD	B71
	2950	Trumpler 16	Visible CMD	B71
	2000	Trumpler 14	Visible CMD	T71
	2500	Trumpler 16	Visible CMD	T71
O-004	4400^{+100}_{-100}	Westerlund 2	*Gaia* DR2 parallax	B18
	4208^{+74}_{-80}	Westerlund 2	*Gaia* DR2 parallax, no covariance term	C18
	4000	Westerlund 2	Visible CMD	Z15
	6000^{+1300}_{-500}	Westerlund 2	Visible CMD	H15
	6500^{+500}_{-500}	Molecular clouds	Kinematic distance	B13
	4469	Westerlund 2	Visible + NIR CMD	K13
	2850^{+430}_{-430}	Westerlund 2	Visible spectro-photometry	C13
	4160^{+270}_{-270}	Westerlund 2	Visible CMD	V13
	6698^{+512}_{-475}	Westerlund 2	Visible spectro-photometry	K12
	8000^{+1400}_{-1400}	Three EBs	Spectroscopic eclipsing binaries	R11
	5400^{+1100}_{-1400}	Molecular clouds	Kinematic distance	F09
	6000^{+1000}_{-1000}	Molecular clouds	Kinematic distance	D07
	2800	Westerlund 2	NIR CMD	A07
	6400^{+400}_{-400}	Westerlund 2	Visible CMD	C04b
	5700^{+300}_{-300}	Westerlund 2	Visible CMD	P98
	7900^{+1200}_{-1000}	Westerlund 2	Visible CMD	M91a
	5100	H II gas	Kinematic distance	S83a
	5000	Westerlund 2	Visible CMD	M75
	4680^{+750}_{-750}	H II gas	Kinematic distance	G73
	6000	Westerlund 2	Association with spiral arm	W61

Table A.1. continued.

ID	Distance (pc)	Target	Description	Ref.
O-005	1770^{+120}_{-120}	NGC 6357	*Gaia* DR2 parallax	R20
	1790^{+150}_{-150}	Pismis 24	*Gaia* DR2 parallax	K19
	1780^{+180}_{-180}	NGC 6357	*Gaia* DR2 parallax	B18
	1678^{+18}_{-16}	NGC 6357	*Gaia* DR2 parallax, no covariance term	C18
	2460^{+1440}_{-1440}	Pismis 24	Visible spectro-photometry	R17
	1780^{+100}_{-100}	NGC 6357	NIR CMD	L14
	1900^{+400}_{-400}	NGC 6357	Visible + NIR CMD	R12a
	1700^{+200}_{-200}	Pismis 24	Visible + NIR CMD	F12
	1700	Pismis 24	Visible + NIR CMD	G11
	2500	Pismis 24	Visible spectro-photometry	M01
	1200	H II gas	Kinematic distance	S83a
	1740^{+310}_{-310}	NGC 6357 + NGC 6334	Visible CMD	N78
	1580	NGC 6357	Visible spectro-photometry	J73
	770^{+1300}_{-1300}	H II gas	Kinematic distance	G73
	1000^{+2300}_{-2300}	H II gas	Kinematic distance	W70
	920^{+870}_{-870}	H II gas	Kinematic distance	D67
O-006	7000	H II gas	Kinematic distance	M17a
	8000	H II gas	Kinematic distance	G00
	6000	H II gas	Kinematic distance	A89
	9100	H II gas	Kinematic distance	C87
O-007 + O-008	1600^{+100}_{-100}	Cyg OB2	*Gaia* DR2 parallax	L19
	1760^{+370}_{-261}	Cyg OB2	*Gaia* DR2 parallax, foreground group at 1350^{+210}_{-160} pc	B19a
	1330^{+60}_{-60}	Four EBs	Spectroscopic eclipsing binaries	K15
	1400^{+80}_{-80}	Four masers	VLBI parallaxes	R12b
	1220^{+220}_{-220}	Cyg OB2	Visible spectro-photometry	H03
	1800^{+200}_{-200}	Bica 1 + 2	NIR CMD	B03
	1740^{+80}_{-80}	Cyg OB2	Visible spectro-photometry	M91b
	1700^{+200}_{-200}	Cyg OB2	Visible + NIR CMD	T91
	1790^{+180}_{-180}	Cyg OB2	Visible spectro-photometry	H78
	1800	Cyg OB2	Visible spectro-photometry	W73b
	2100	Cyg OB2	Visible spectro-photometry	R66
	1500	Cyg OB2	Visible spectro-photometry	J54
O-009	1500^{+150}_{-150}	Molecular clouds	*Gaia* DR2 parallax	Z20
	1680^{+130}_{-110}	M 17	*Gaia* DR2 parallax	K19
	1820^{+160}_{-160}	M 17	*Gaia* DR2 parallax	B18
	2390^{+310}_{-410}	H II gas	Kinematic distance	W18
	2040^{+160}_{-170}	One maser	VLBI parallax	C16
	1308	M 17	Visible + NIR CMD	K13
	1980^{+140}_{-120}	One maser	VLBI parallax	X11
	2100^{+200}_{-200}	M 17	Visible + NIR spectro-photometry	H08
	1600^{+300}_{-100}	M 17	Luminosity budget	P07
	14 550	H II gas	Kinematic distance	Q06
	2400	H II gas	Kinematic distance	R03
	1600^{+300}_{-300}	M 17	Visible + NIR spectro-photometry	N01
	1300^{+400}_{-200}	M 17	Visible + NIR spectro-photometry	H97
	2200^{+200}_{-200}	Molecular clouds	Kinematic distance	S89a
	2200^{+200}_{-200}	Molecular clouds	Kinematic distance	F84
	2200^{+200}_{-200}	Molecular clouds	Kinematic distance	S84
	2400	H II gas	Kinematic distance	S83a
	2200^{+200}_{-200}	M 17	Visible CMD	C80
	1300	M 17	Visible CMD	O76
	1780^{+1020}_{-1020}	M 17	Visible spectro-photometry	J73
	2200^{+510}_{-510}	H II gas	Kinematic distance	G73
	2460	H II gas	Kinematic distance	G70
	2250^{+100}_{-100}	H II gas	Kinematic distance	D67

Table A.1. continued.

ID	Distance (pc)	Target	Description	Ref.
O-010	1046^{+54}_{-54}	Southern molecular cloud	*Gaia* DR2 parallax	Z20
	1190^{+4}_{-4}	NGC 6193	*Gaia* DR2 parallax, no covariance term	C18
	1096^{+274}_{-274}	HD 150 136	Spectroastrometric orbit	M18
	1380^{+130}_{-130}	NGC 6193	Visible + NIR CMD	B11a
	1410^{+120}_{-120}	NGC 6193	Visible CMD	V92
	1340	Ara OB1	Visible spectro-photometry	F87
	1460^{+130}_{-130}	Ara OB1a	Visible spectro-photometry	H78
	1320^{+120}_{-120}	Ara OB1	Visible CMD	H77
	1360	NGC 6193	Visible CMD	M73b
	1390	NGC 6193	Visible CMD	B71
	1880	H II gas	Kinematic distance	G70
	1400	Ara OB1	Visible CMD	W63
O-011	3016^{+41}_{-36}	Berkeley 90	*Gaia* DR2 parallax, no covariance term	C18
	3500^{+500}_{-500}	Berkeley 90	Visible CMD	M17b
	2670^{+150}_{-150}	Berkeley 90	CHORIZOS analysis of LS III +46 11 and LS III +46 12	M15
	2430^{+70}_{-70}	Berkeley 90	NIR CMD	T08
	1500^{+200}_{-200}	LS III +46 11	Visible spectro-photometry	M97
	3000^{+600}_{-600}	Molecular clouds	Kinematic distance	F84
	2320	LS III +46 12	Visible spectro-photometry	M73a
O-012	5050^{+170}_{-160}	Haffner 19	*Gaia* DR2 parallax, no covariance term	C18
	4673^{+92}_{-92}	Haffner 18	*Gaia* DR2 parallax, no covariance term	C18
	4810^{+480}_{-480}	Two EBs	Spectroscopic eclipsing binaries	L17
	5700^{+400}_{-400}	Haffner 19	Visible + NIR CMD	Y15
	$11\,200^{+1000}_{-1000}$	Haffner 18	Visible + NIR CMD	Y15
	1313	Villafranca O-012	Visible + NIR CMD	K13
	5300	H II gas	Kinematic distance	B11b
	5400	H II gas	Kinematic distance	Q06
	6400	Haffner 19	Visible CMD	G06
	5900	Haffner 18	Visible CMD	G06
	4800^{+300}_{-300}	Haffner 19	Visible CMD	M02
	4090	Haffner 19	Statistical parallaxes	R99
	4570	Haffner 18	Statistical parallaxes	R99
	4100^{+600}_{-600}	Molecular clouds	Kinematic distance	F84
	3900	H II gas	Kinematic distance	S83a
	4200	H II gas	Kinematic distance	P76
	6900^{+900}_{-900}	Villafranca O-012	Visible CMD	F74
	3510^{+370}_{-370}	H II gas	Kinematic distance	G73
	2500	Villafranca O-012	Visible CMD	B71
	3830	H II gas	Kinematic distance	G70
	3370^{+160}_{-160}	Villafranca O-012	Visible CMD	L66
O-013	4880^{+1000}_{-920}	H II gas	Kinematic distance	W18
	2700^{+500}_{-500}	Villafranca O-013	NIR spectro-photometry	P10
	2650^{+120}_{-110}	Two masers	VLBI parallaxes	M09b
	2270^{+150}_{-150}	Villafranca O-013	Visible spectro-photometry	R07
	6400	H II gas	Kinematic distance	Q06
	2200	Villafranca O-013	NIR CMD	M86
	3700	H II gas	Kinematic distance	M86
	2800^{+900}_{-900}	Molecular clouds	Kinematic distance	F84
	2800	Two stars	Visible spectro-photometry	C78
	4750^{+380}_{-380}	H II gas	Kinematic distance	G73
	4230	H II gas	Kinematic distance	G70

Table A.1. continued.

ID	Distance (pc)	Target	Description	Ref.
O-014	800^{+100}_{-100}	Molecular clouds	*Gaia* DR2 parallax	Z20
	858^{+56}_{-56}	Pelican nebula stars	*Gaia* DR2 parallax	B19b
	605^{+45}_{-45}	Molecular clouds	Visible CMD	D17
	700^{+500}_{-500}	North America nebula	Kinematic distance	C07
	560^{+60}_{-60}	Molecular clouds	Visible CMD	L06
	610	Bajamar star	Visible + NIR spectro-photometry	C05
	600	Molecular clouds	Visible CMD	L02
	485	Molecular clouds	Star counts	C02
	550^{+140}_{-140}	Molecular clouds	Visible spectro-photometry	S93
	800^{+300}_{-300}	Molecular clouds	Kinematic distance	S89a
	550^{+100}_{-100}	Molecular clouds	Visible CMD	S89b
	1000^{+300}_{-300}	Molecular clouds	Kinematic distance	S84
	800^{+300}_{-300}	Molecular clouds	Kinematic distance	F84
	970^{+30}_{-30}	Molecular clouds	Star counts	A81
	150^{+50}_{-50}	2MASS J20535282+4424015	Stellar parameters estimation	N80
	1200	HD 199 579	Visible spectro-photometry	M68
	1980^{+400}_{-400}	H II gas	Kinematic distance	D67
	1130	HD 199 579	Visible spectro-photometry	B63
	500^{+300}_{-300}	Molecular clouds	Visible CMD	H58
	910	HD 199 579	Visible spectro-photometry	S52
O-015	1019^{+7}_{-6}	Collinder 419	*Gaia* DR2 parallax, no covariance term	C18
	741^{+36}_{-36}	Collinder 419	Visible + NIR CMD	R10
	1400	Collinder 419	Visible CMD	H87
O-016	750^{+50}_{-50}	Molecular clouds	*Gaia* DR2 parallax	Z20
	738^{+23}_{-21}	NGC 2244	*Gaia* DR2 parallax, no covariance term	K19
	723^{+2}_{-2}	NGC 2244	*Gaia* DR2 parallax	C18
	738^{+57}_{-50}	Two masers	VLBI parallaxes	K14
	913^{+40}_{-40}	NGC 2244	$v \sin i$ and rotation periods	B09
	759^{+35}_{-35}	NGC 2244	Visible CMD	P00b
	720	NGC 2244	Statistical parallaxes	R99
	764^{+87}_{-87}	NGC 2244	Visible CMD	S97
	910^{+50}_{-50}	NGC 2244	Visible + NIR CMD	N93
	700^{+40}_{-40}	NGC 2244	Visible CMD	F91
	800^{+150}_{-150}	Molecular clouds	Kinematic distance	S89a
	950^{+75}_{-75}	NGC 2244	Visible spectro-photometry	P87
	800^{+150}_{-150}	Molecular clouds	Kinematic distance	S84
	800^{+150}_{-150}	Molecular clouds	Kinematic distance	F84
	798^{+73}_{-73}	NGC 2244	Visible CMD	S83b
	875	NGC 2244	Visible CMD	M80
	715	NGC 2244	Visible CMD	B71
	715	NGC 2244	Visible spectro-photometry	B63
	800	NGC 2244	Visible spectro-photometry	W56

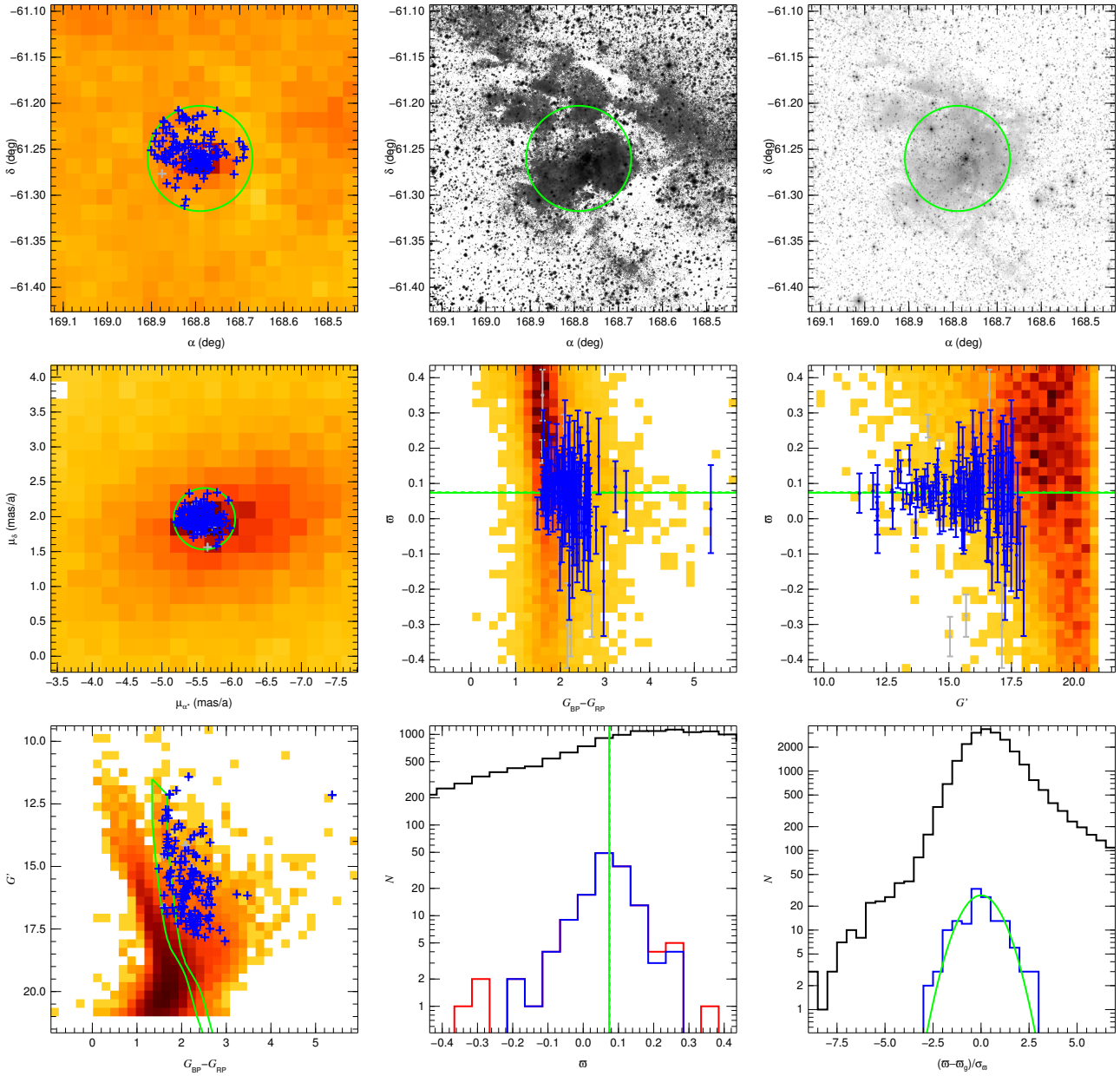

Fig. A.1. NGC 3603 (Villafranca O-001) *Gaia* DR2 distances and membership results. *Top row (left to right)*: source density diagram, DSS2 red image, and 2MASS *J* image. *Middle row (left to right)*: proper motions, color-parallax, and magnitude-parallax diagrams. *Bottom row (left to right)*: color-magnitude diagram, parallax histogram, and normalized-parallax histogram. In all diagrams, a heat-type scale (increasing as white-yellow-orange-red-black) is used to indicate the total *Gaia* DR2 density in a linear scale (except in the CMD, where a log scale is used). In the first four panels, the green circle indicates the coordinates or proper motion constraints. In the CMD the green lines show the reference extinguished isochrone (*right*) and the displaced isochrone used as constraint (*left*), joined at the top by the extinction trajectory. In all diagrams, the blue symbols indicate the objects used in the final sample and the gray symbols those rejected by the normalized parallax criterion. The plotted parallax uncertainties are the external ones. In the parallax histogram, black indicate the total *Gaia* DR2 density, red the sample prior to the application of the normalized parallax criterion, and blue the final sample, while the two green vertical lines delineate the weighted-mean parallax: dotted for $\varpi_{g,0}$ and solid for ϖ_g. Black and blue have the same meaning in the normalized parallax histogram, where the green line shows the expected normal distribution.

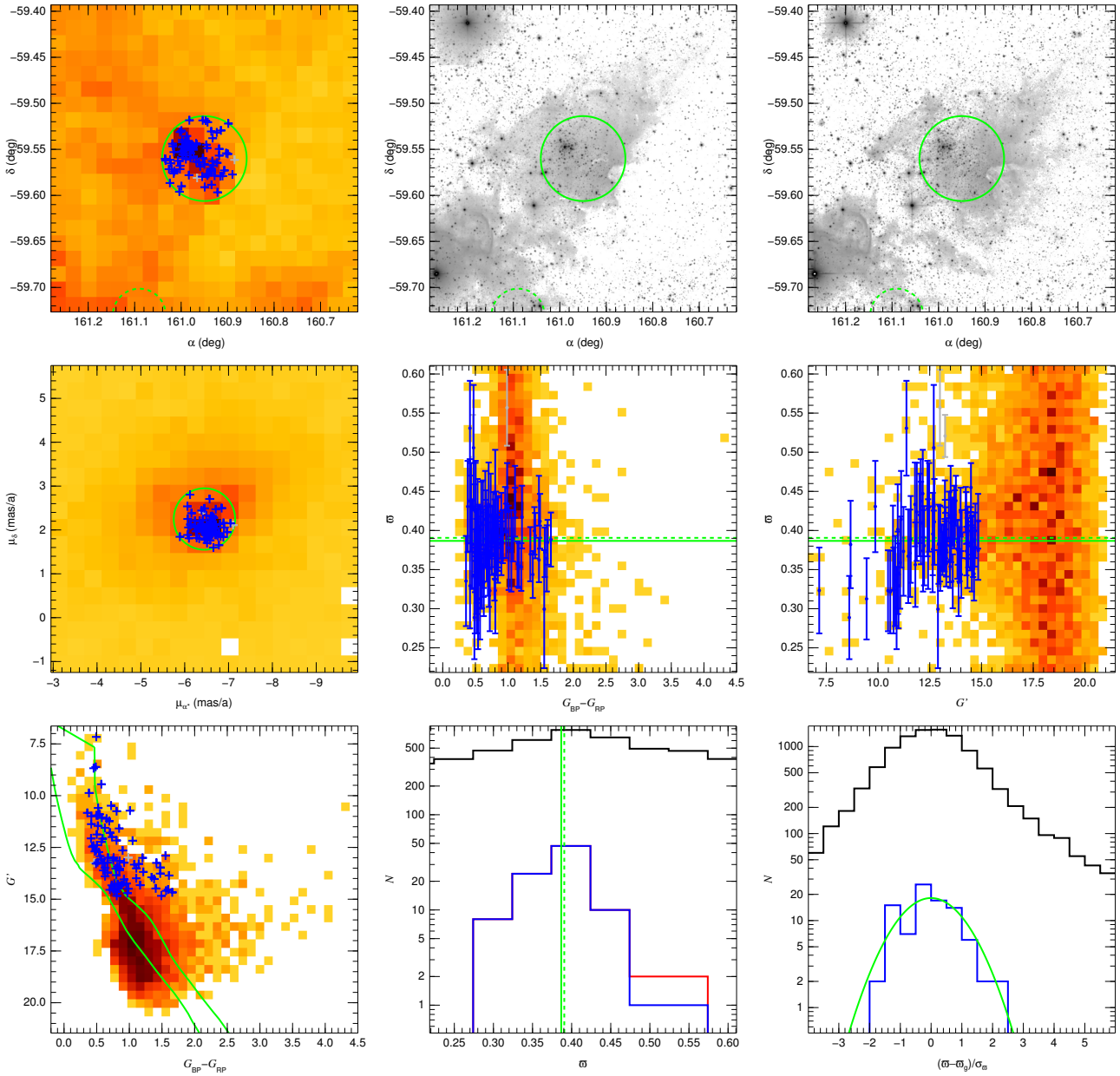

Fig. A.2. Same as Fig. A.1 for Trumpler 14 (Villafranca O-002) but with the 2MASS *J* image in the top center panel and the 2MASS *K* image in the top right one. The partial dashed green circle in the top three panels shows the position of the neighbor Trumpler 16 W (Villafranca O-003).

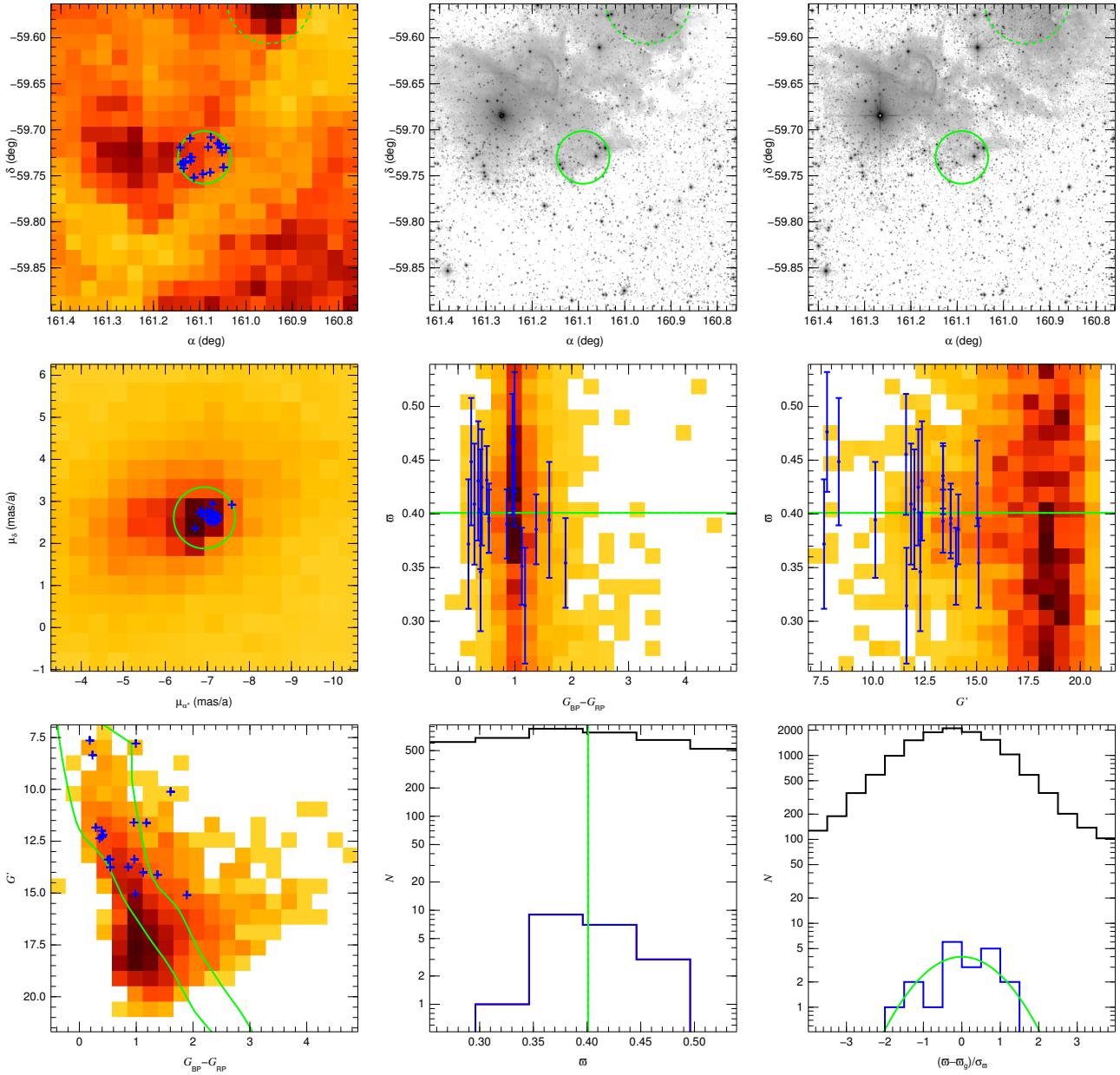

Fig. A.3. Same as Fig. A.2 for Trumpler 16 W (Villafranca O-003) The partial dashed green circle in the top three panels shows the position of the neighbor Trumpler 14 (Villafranca O-002).

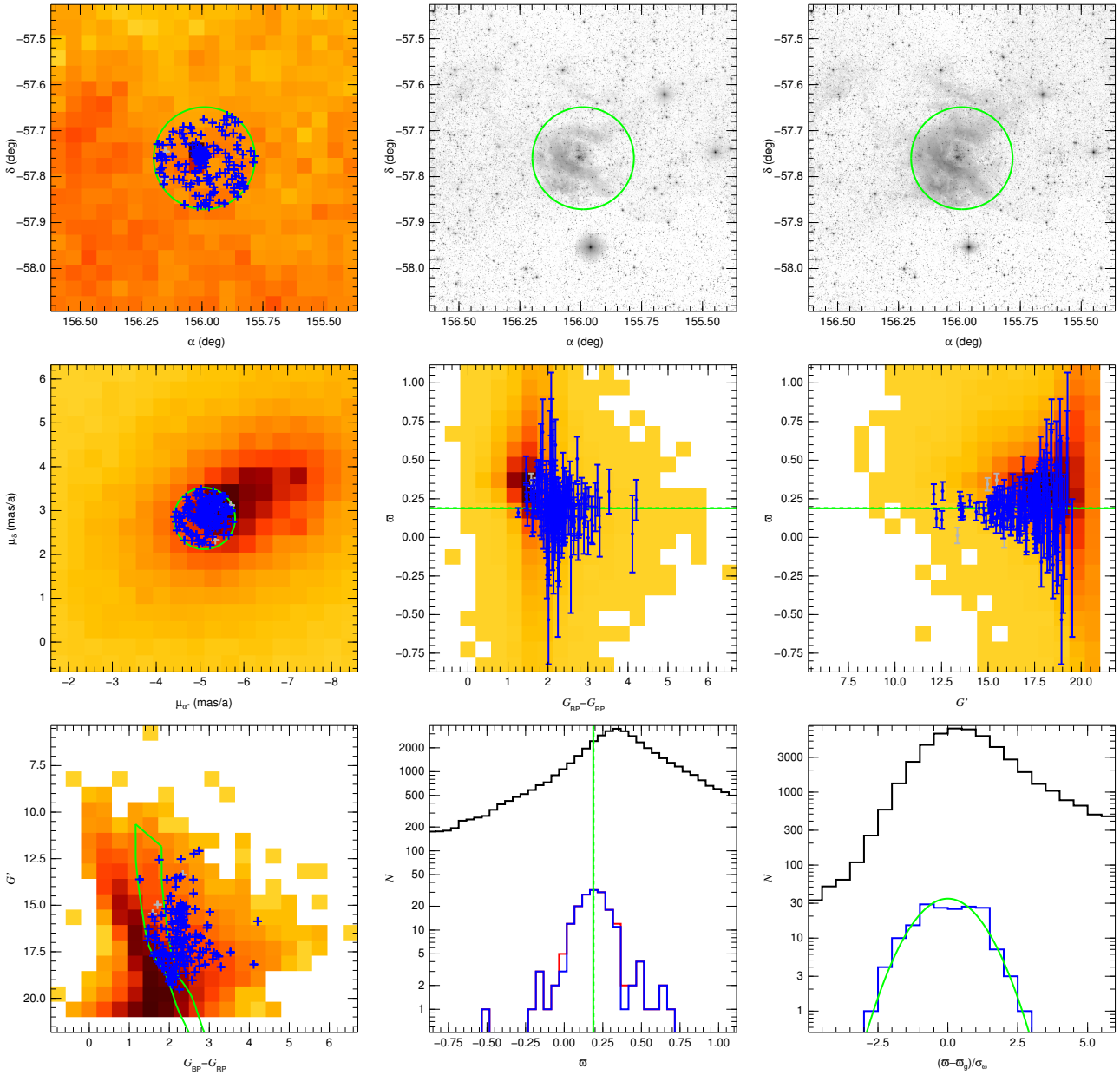

Fig. A.4. Same as Fig. A.1 for Westerlund 2 (Villafranca O-004) but with the 2MASS *J* image in the top center panel and the 2MASS *K* image in the top-right one.

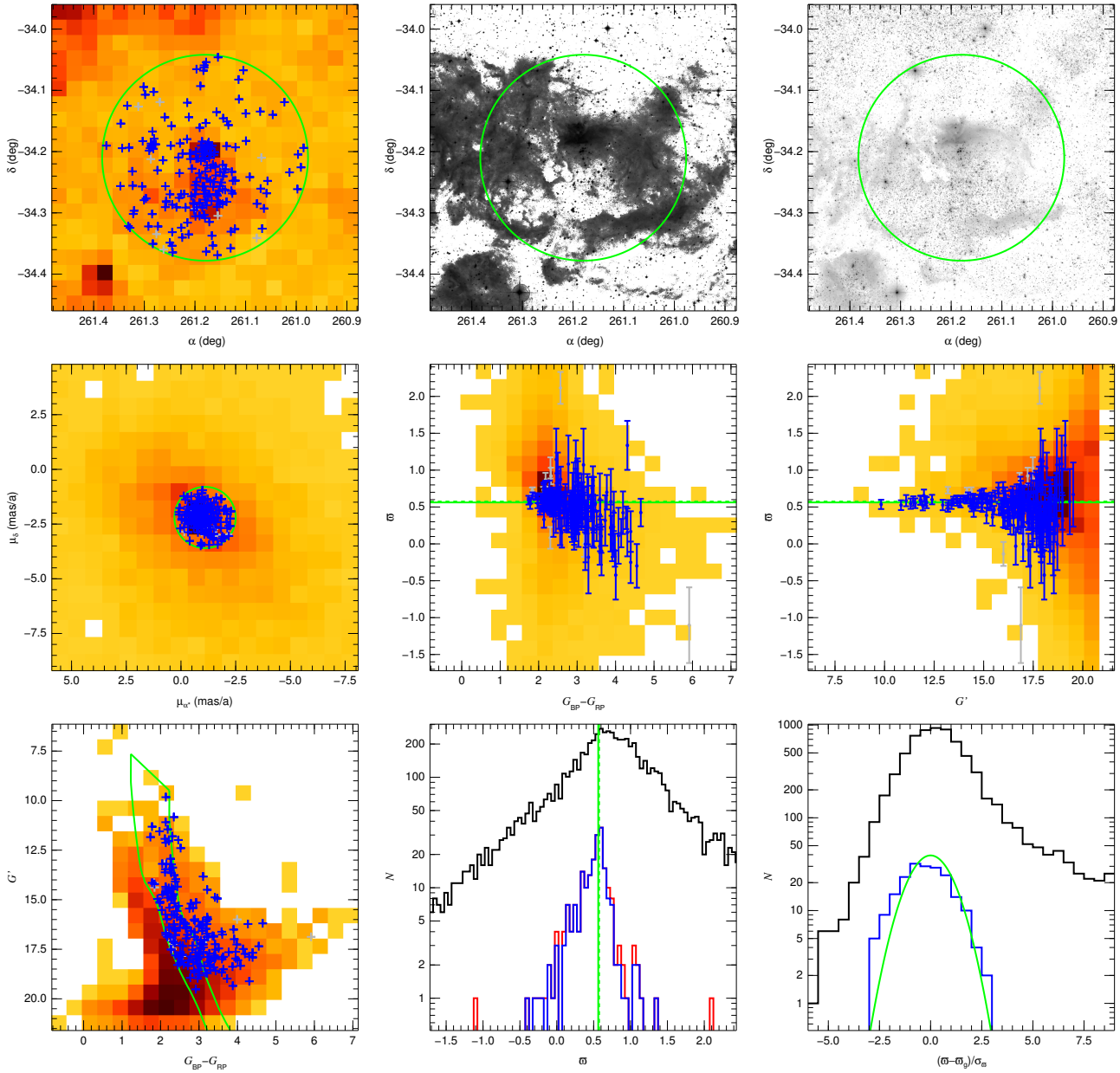

Fig. A.5. Same as Fig. A.1 for Pismis 24 (Villafranca O-005).

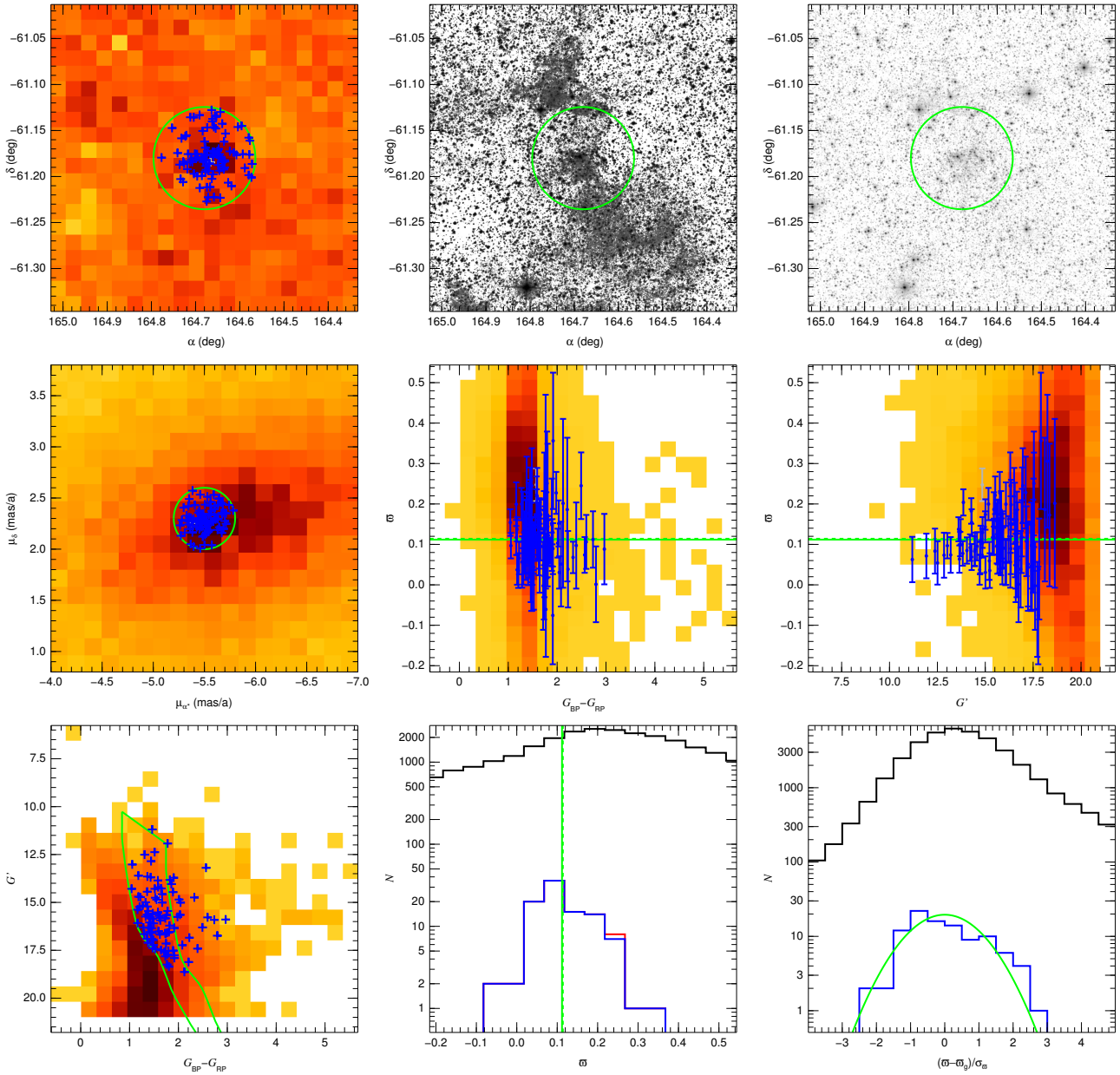

Fig. A.6. Same as Fig. A.1 for Villafranca O-006.

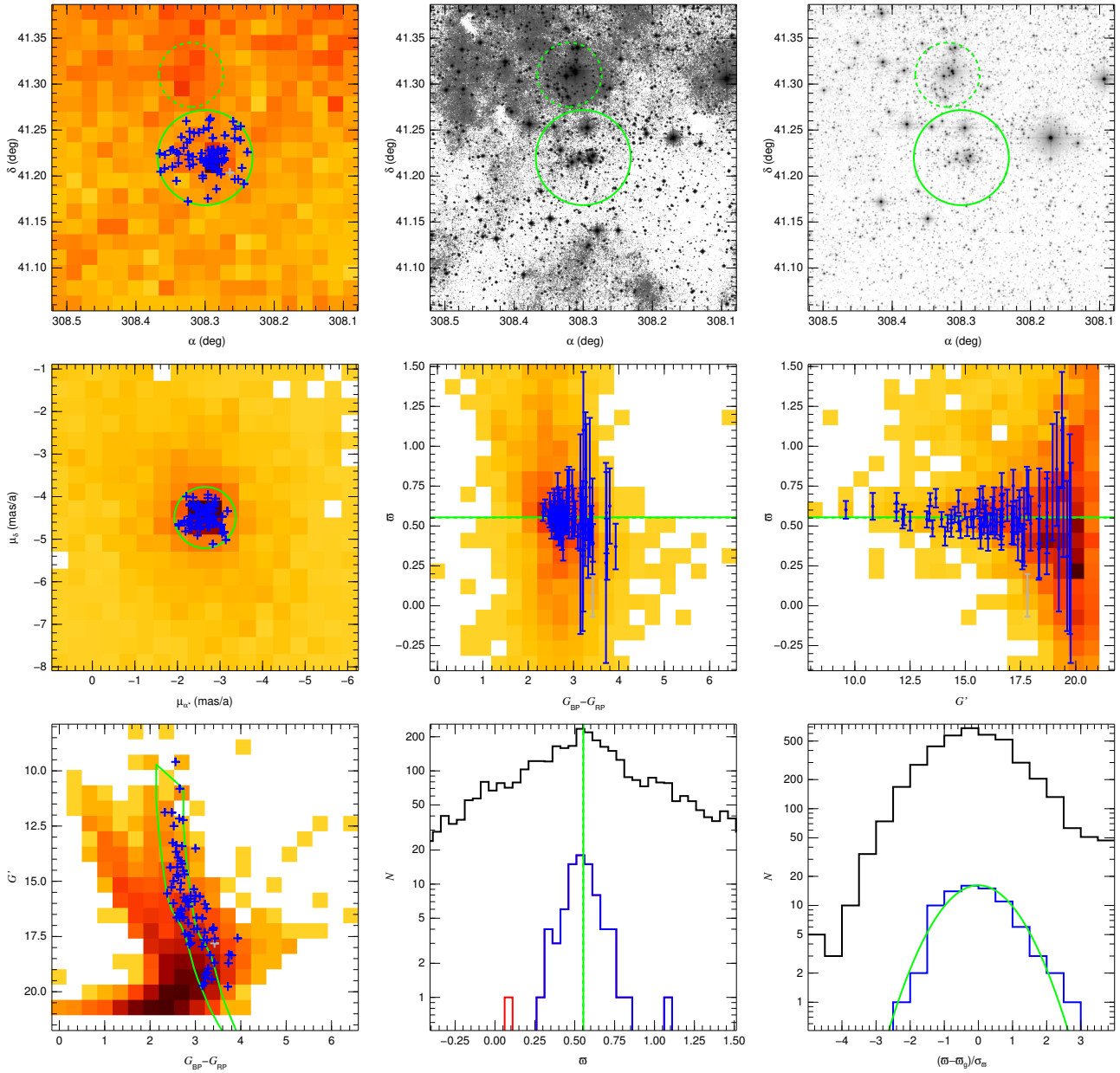

Fig. A.7. Same as Fig. A.1 for Bica 1 (Villafranca O-007). The dashed green circle in the top three panels shows the position of the neighbor Bica 2 (Villafranca O-008).

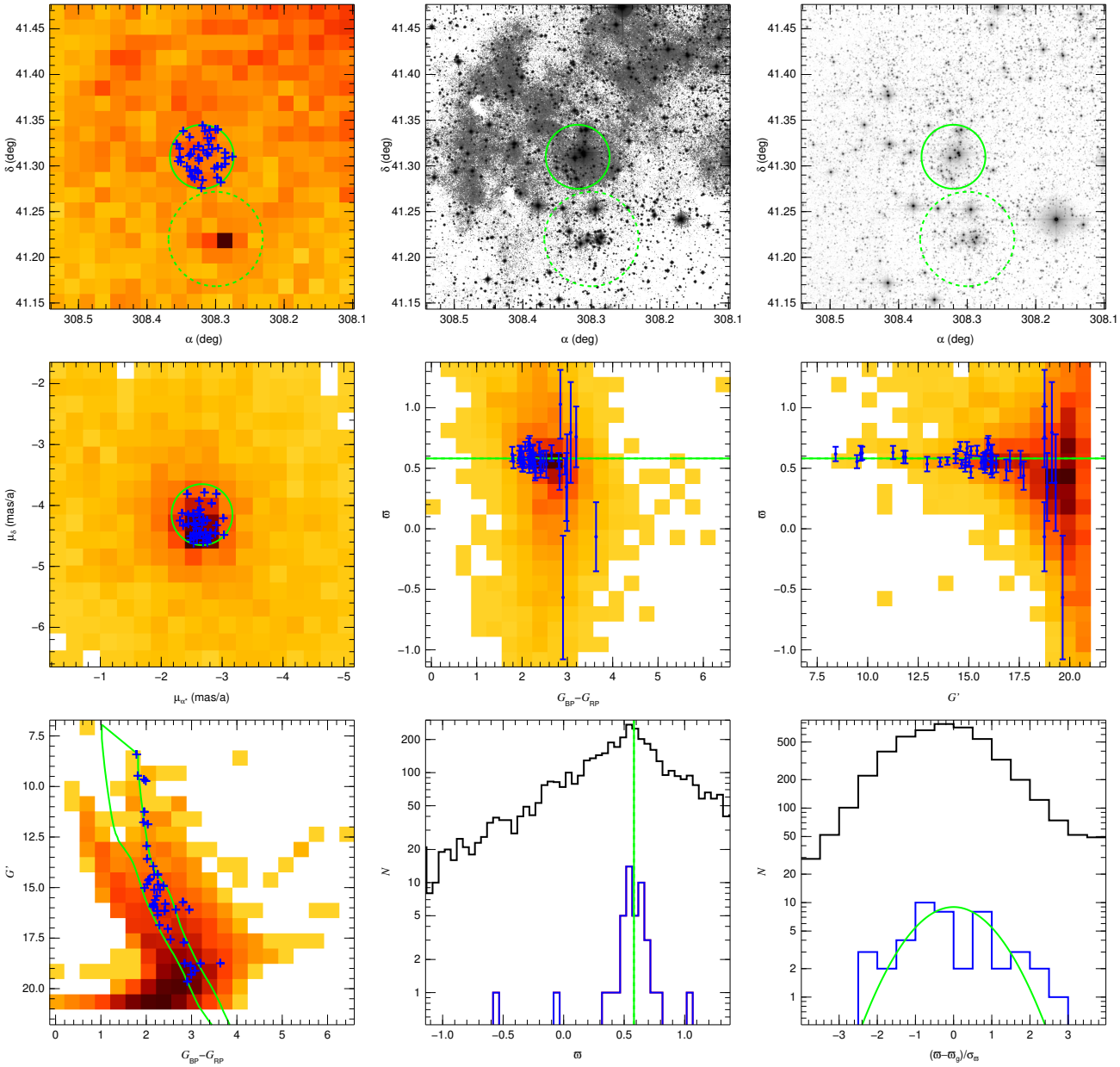

Fig. A.8. Same as Fig. A.7 for Bica 2 (Villafranca O-008). The dashed green circle in the top three panels shows the position of the neighbor Bica 1 (Villafranca O-007).

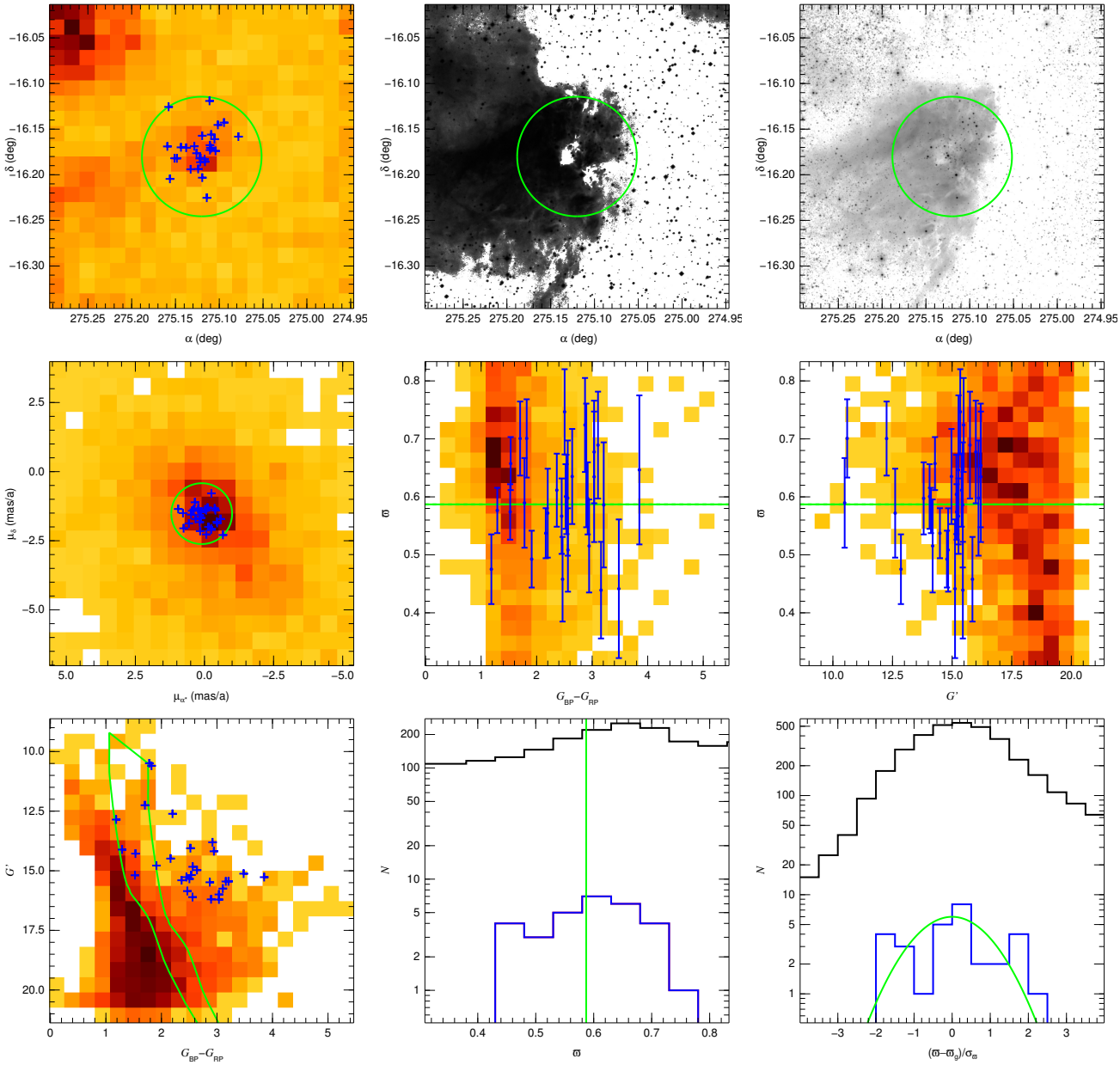

Fig. A.9. Same as Fig. A.1 for M 17 (Villafranca O-009).

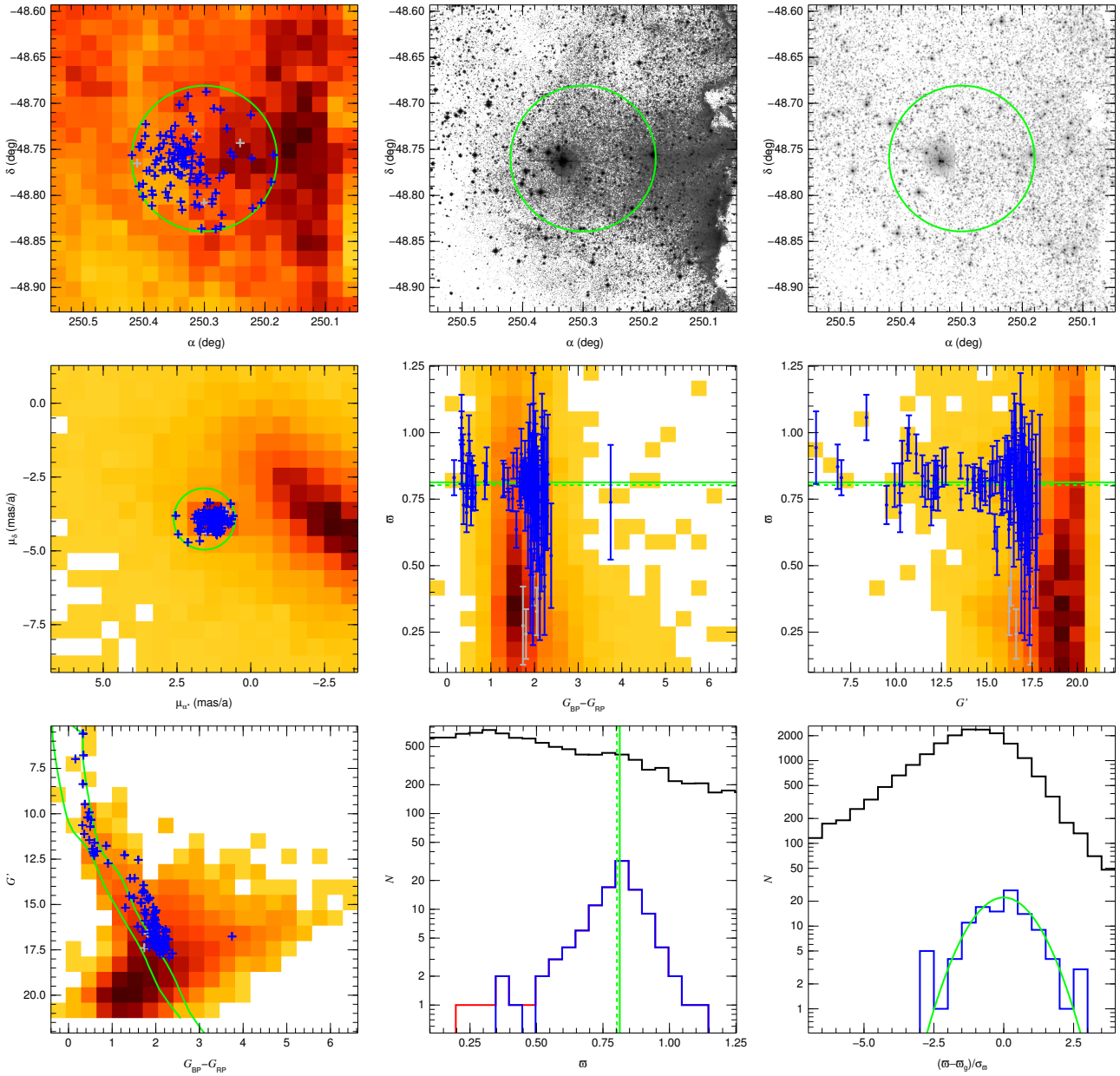

Fig. A.10. Same as Fig. A.1 for NGC 6193 (Villafranca O-010).

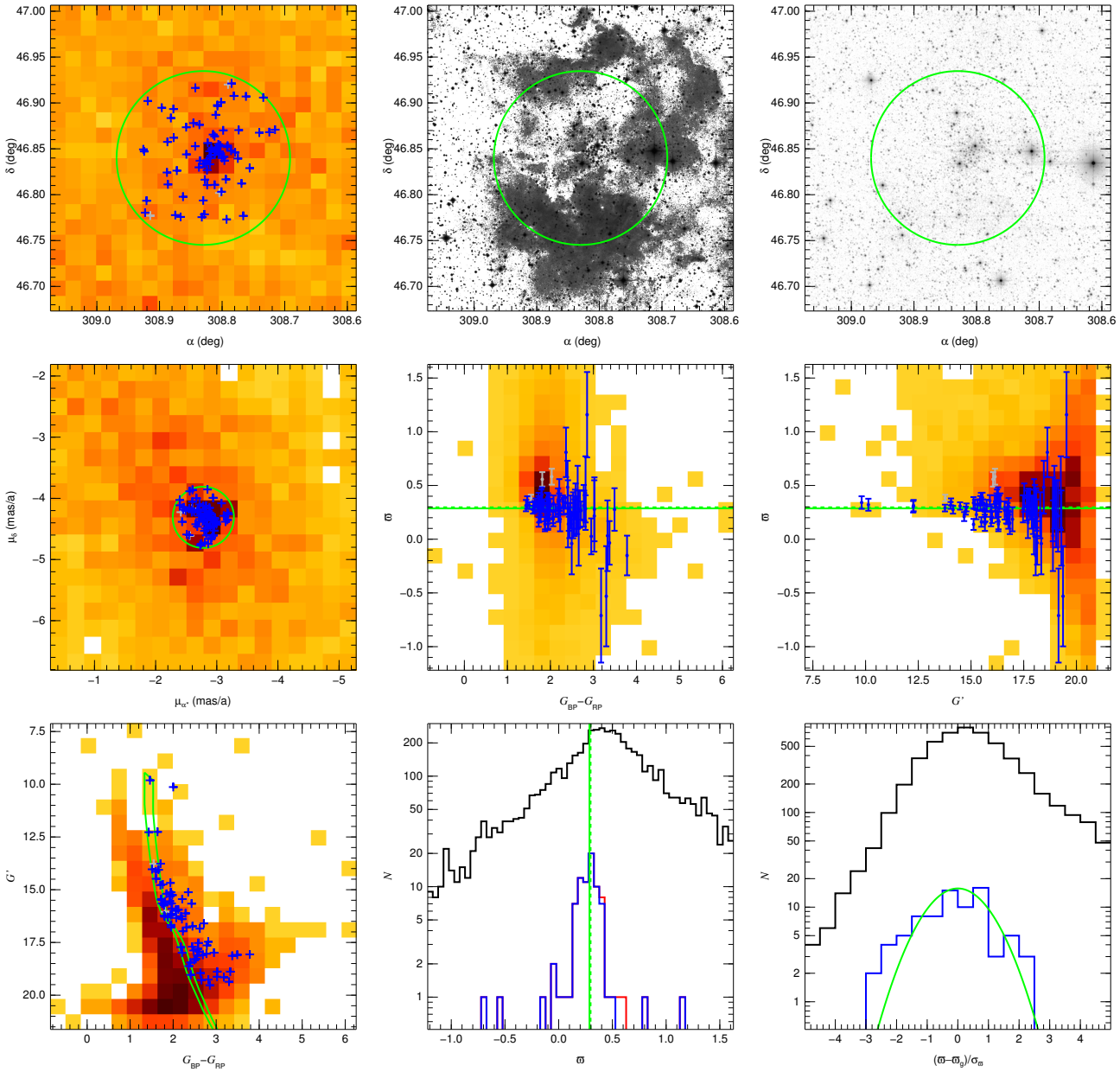

Fig. A.11. Same as Fig. A.1 for Berkeley 90 (Villafranca O-011).

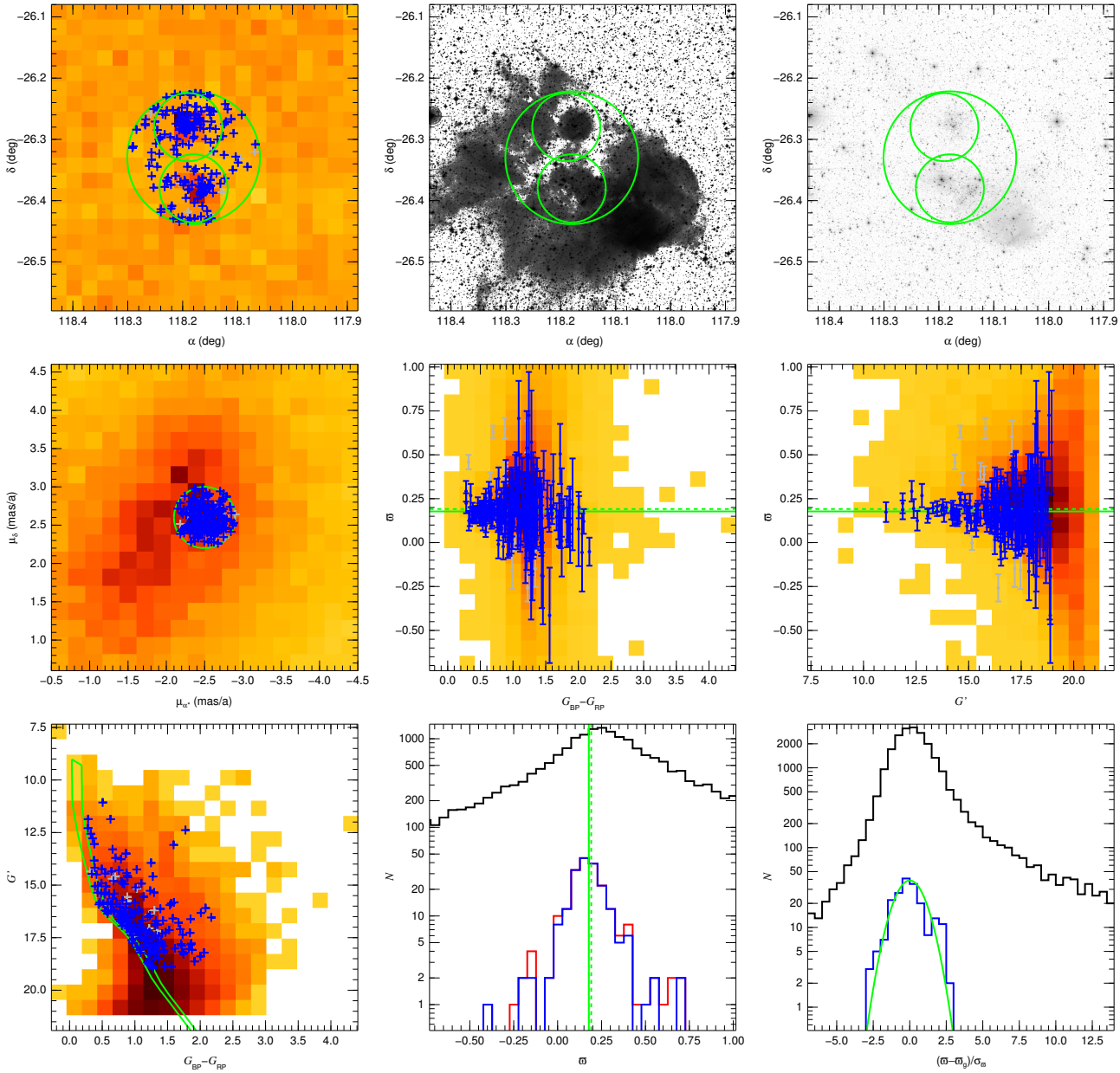

Fig. A.12. Same as Fig. A.1 for Villafranca O-012. The two small green circles in the top panels correspond to the Haffner 18 (Villafranca O-O12 S) and Haffner 19 (Villafranca O-012 N) subgroups.

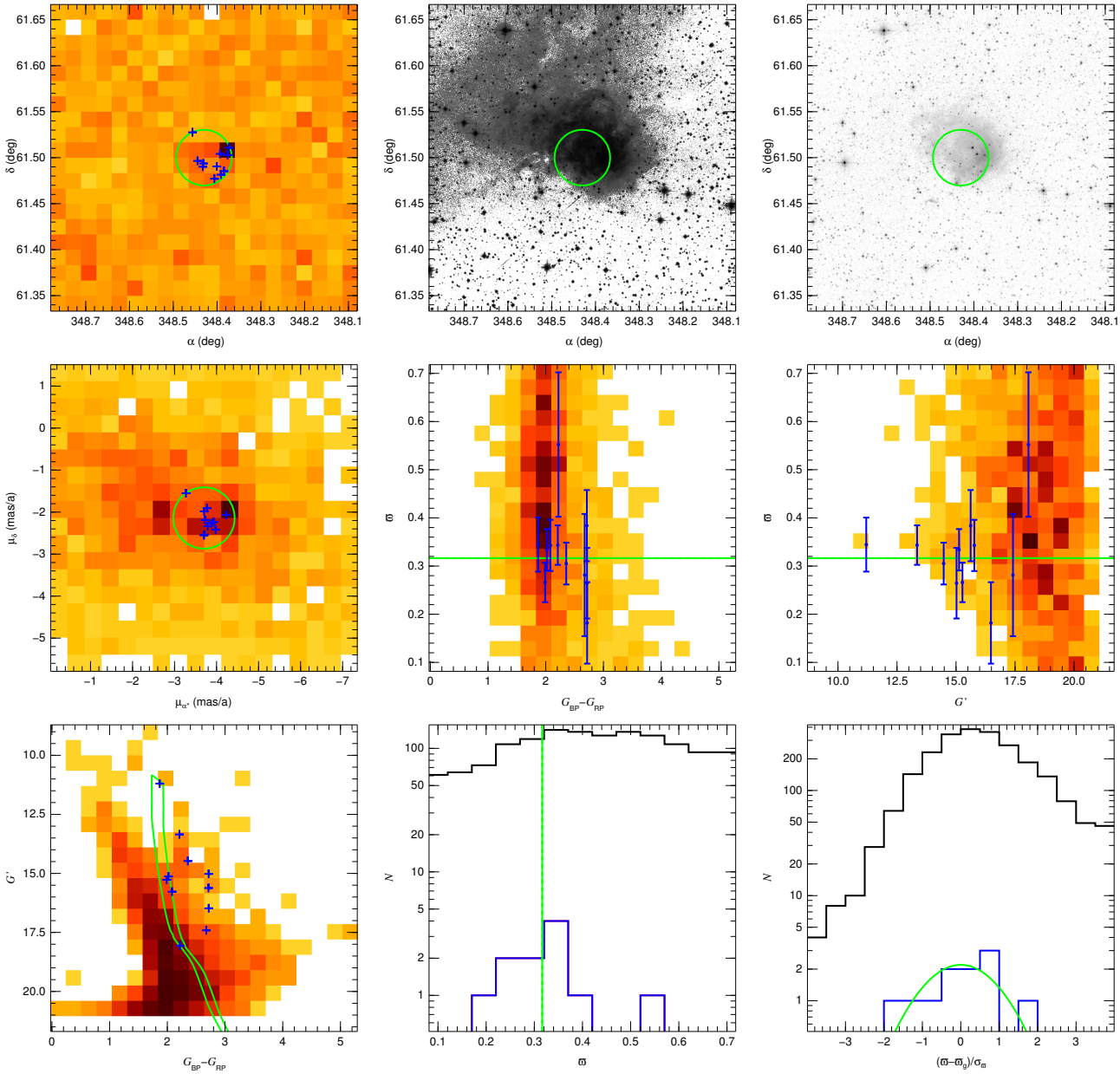

Fig. A.13. Same as Fig. A.1 for Villafranca O-013.

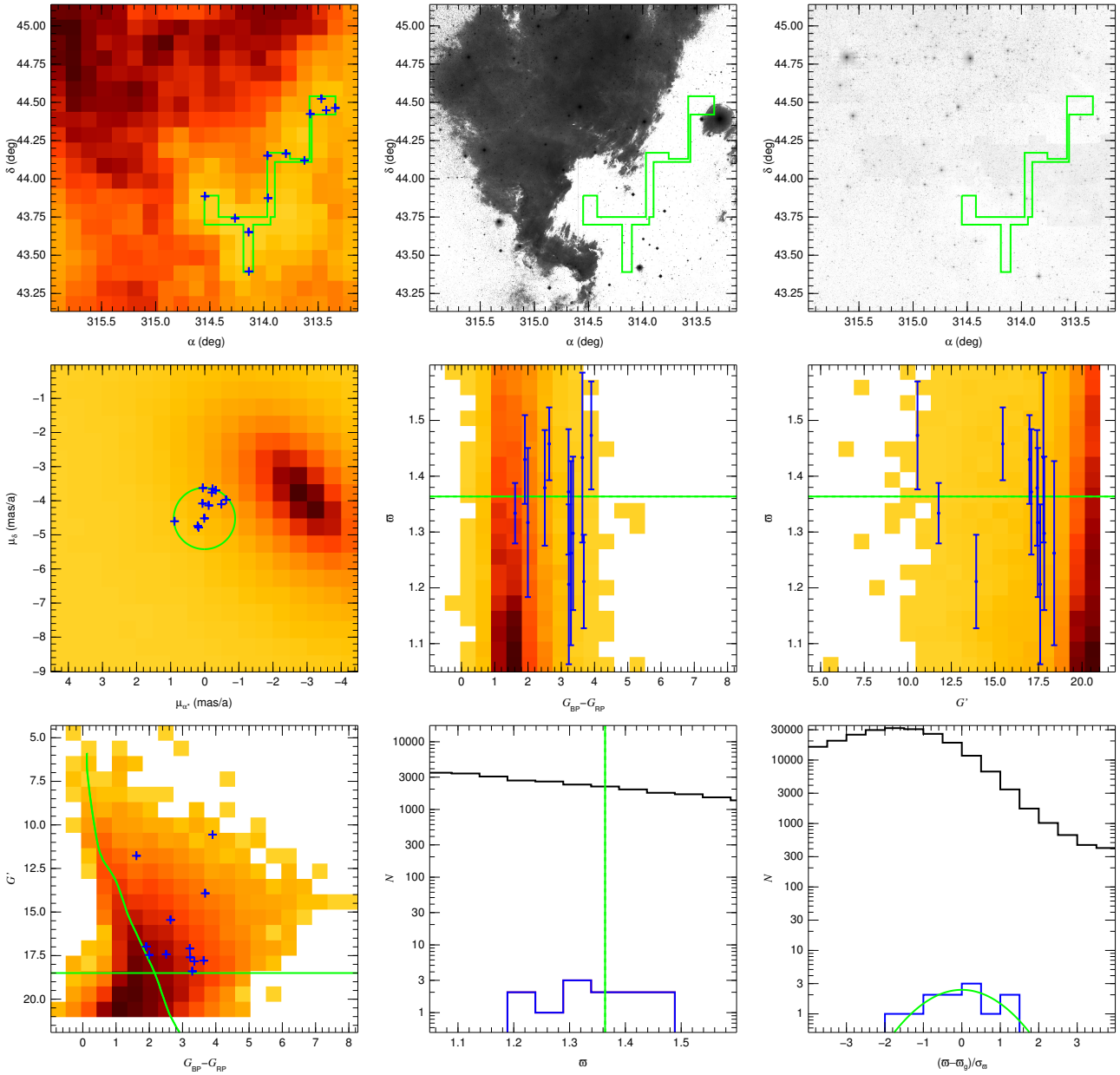

Fig. A.14. Same as Fig. A.1 for Villafranca O-014. The polygon is the ad-hoc selection criterion used to select the stars in the foreground and vicinity of the Atlantic Ocean + Gulf of Mexico molecular cloud.

Table A.2. Possible runaway stars.

Group ID	*Gaia* DR2 ID	Other ID	ϖ (mas)	G	$G_{BP}-G_{RP}$
O-001	5 337 424 376 393 813 632	2MASS J11142369−6106042	0.1690 ± 0.0601	12.4749	2.9503
	5 337 422 447 912 267 008	2MASS J11135811−6109421	0.1542 ± 0.0641	12.8501	2.9031
	5 337 234 538 836 917 248	2MASS J11134605−6112487	0.1899 ± 0.0319	13.5301	2.2358
	5 337 046 316 178 212 864	2MASS J11134629−6116011	0.0878 ± 0.0275	13.7263	1.7215
	5 337 043 739 197 624 064	2MASS J11135770−6124267	0.0122 ± 0.0407	13.9993	2.5442
	5 337 418 088 561 807 872	2MASS J11150238−6115077	0.2157 ± 0.0840	16.4556	2.0834
O-002	5 350 377 447 993 712 896	HDE 303 313	0.3995 ± 0.0544	10.2248	0.2503
	5 350 400 022 343 131 008	ALS 16 078	0.3709 ± 0.0526	12.4273	0.4198
	5 350 399 811 863 167 744	2MASS J10432367−5925594	0.4049 ± 0.0515	12.4363	0.4084
O-003	5 350 358 545 816 438 272	Trumpler 16-201	0.3592 ± 0.0712	12.6082	2.7149
O-004	5 351 703 390 282 380 800	THA 35-II-42	0.1819 ± 0.0529	11.6903	2.2842
	5 255 667 681 036 173 568	SS 215	0.1177 ± 0.0542	11.8627	1.9798
O-005	5 976 057 078 081 522 048	Pismis 24-18	0.7387 ± 0.2707	13.0083	2.3063
	5 976 155 007 639 115 264	2MASS J17252943−3424044	0.6617 ± 0.0645	13.5357	3.1500
	5 976 064 057 399 569 408	2MASS J17250098−3358378	0.6234 ± 0.0558	14.5181	2.7384
	5 976 046 808 810 701 056	2MASS J17252444−3358157	0.5355 ± 0.0415	14.5611	1.9811
	5 976 154 762 809 358 848	2MASS J17235197−3412298	0.6627 ± 0.0441	14.5998	2.3270
	5 976 033 339 793 078 272	2MASS J17252376−3359548	0.7444 ± 0.1110	15.0023	3.2382
	5 976 153 908 127 437 568	2MASS J17251438−3358077	0.6100 ± 0.0513	15.2246	2.0040
	5 976 054 093 074 786 048	2MASS J17254496−3406488	0.5698 ± 0.0878	15.2442	2.8499
O-006	5 337 977 980 510 724 480	2MASS J10584671−6105512	0.0729 ± 0.0556	12.1401	2.1680
	5 337 971 688 334 583 680	2MASS J10592362−6114575	0.1982 ± 0.0530	12.6812	2.0841
O-007	2 067 783 799 613 328 128	Cyg OB2-24	0.5413 ± 0.0616	10.9932	2.1264
O-008	2 067 926 564 325 711 872	[MT91] 453	0.6022 ± 0.0309	13.7738	1.7636
O-009	4 098 005 975 631 742 720	BD −16 4826	0.5681 ± 0.0636	9.4999	1.2675
	4 097 817 409 389 450 624	ALS 4943	0.6086 ± 0.0643	10.4758	0.9175
	4 097 816 275 518 137 216	2MASS J18210951−1608186	0.7550 ± 0.0665	11.2572	1.5734
	4 097 803 596 774 515 584	Tyc 6265-01474-1	0.6954 ± 0.0679	11.5804	0.6549
	4 097 808 024 877 708 160	NGC 6618 B-373	0.4797 ± 0.0917	11.8704	3.0881
	4 098 007 895 470 142 080	2MASS J18200299−1602068	0.5604 ± 0.0616	11.9439	2.5256
	4 097 817 924 785 524 864	2MASS J18211029−1603505	0.6448 ± 0.0384	13.8902	1.7953
O-010	5 940 956 341 923 632 896	2MASS J16403254−4846296	0.7897 ± 0.0348	13.2440	1.1712
O-011	2 071 525 987 444 459 904	2MASS J20354794+4655566	0.3251 ± 0.0190	13.2255	1.2004
	2 071 522 242 233 085 824	2MASS J20351422+4650118	0.2333 ± 0.0319	13.5376	1.8256
	2 071 530 041 893 546 240	2MASS J20351898+4659543	0.2994 ± 0.0196	13.8215	0.9733
	2 071 516 882 113 611 776	2MASS J20351160+4642344	0.2999 ± 0.0283	14.0482	2.4964
	2 071 330 136 937 555 328	2MASS J20354818+4643174	0.3770 ± 0.0265	14.3933	2.2597
O-012	5 602 025 904 044 961 536	HD 64 315 AB (†)	−0.0539 ± 0.0892	9.1365	0.4058
	5 602 033 390 154 015 744	HD 64 568	0.1367 ± 0.0599	9.3061	0.1610
	5 602 048 542 798 630 784	CPD −25 5194	0.2484 ± 0.0994	11.0859	0.1442
	5 601 982 473 333 181 184	2MASS J07532352−2626112	0.2533 ± 0.0605	11.3573	2.3334
	5 602 234 016 670 302 848	Tyc 6557-03393-1	0.2250 ± 0.0544	12.4050	0.1545
	5 602 002 741 267 436 288	2MASS J07513825−2628576	0.3530 ± 0.0617	12.7415	1.4881
	5 602 033 291 388 495 616	2MASS J07533255−2614513	0.1431 ± 0.0588	12.8183	2.0944
O-013	2 014 962 779 980 826 240	2MASS J23141320+6138397	0.3382 ± 0.0499	13.1733	3.1796
	2 014 867 191 189 025 920	2MASS J23122869+6127057	0.4154 ± 0.0419	14.5214	2.1011
	2 014 866 808 933 891 584	[MO2001] 77	0.3424 ± 0.0343	14.7460	1.5634
	2 014 961 852 267 620 608	2MASS J23133905+6133222	0.3191 ± 0.0379	15.1941	1.5426
	2 014 915 569 700 615 296	2MASS J23122004+6132246	0.3595 ± 0.0417	15.4022	1.1392
O-014	2 162 214 599 862 429 056	V354 Cyg	1.2783 ± 0.1033	7.7724	4.1208
	2 162 063 898 039 698 816	Tyc 3179-00416-1	1.3422 ± 0.0581	9.4345	1.9894
	2 162 048 058 200 239 616	Tyc 3179-00023-1	1.4521 ± 0.0541	10.0277	0.3824
	2 162 872 004 724 035 456	[SKV93] 2-72	1.3890 ± 0.0521	11.7749	1.5588
O-015	2 068 356 950 109 724 288	2MASS J20191747+4057512	0.9501 ± 0.0528	12.2638	2.0731
	2 068 352 659 441 818 368	2MASS J20192974+4051474	0.9808 ± 0.0520	12.4495	0.8636
	2 068 362 791 265 246 464	2MASS J20192209+4058234	0.9418 ± 0.0540	12.5043	2.1756
	2 068 369 633 152 677 760	2MASS J20184783+4101193	0.8784 ± 0.0293	13.5034	1.2614
	2 068 357 194 927 339 136	2MASS J20191645+4059011	0.9434 ± 0.0288	13.6283	1.5131
O-016	3 326 734 332 924 414 976	2MASS J06423798+0958062	1.2625 ± 0.0693	12.9885	0.7344
	3 326 951 215 889 632 128	2MASS J06395491+1010070	1.3160 ± 0.0334	13.1739	0.9582

Notes. (†)Target with bad RUWE.